Spring 5-19-2017

Design and Fabrication of Nanostructures for the Enhancement of Photovoltaic Devices

Richard M. Prevost III
University of New Orleans, rprevost@uno.edu

Design and Fabrication of Nanostructures for the Enhancement of Photovoltaic Devices

A Dissertation

Submitted to the Graduate Faculty of the
University of New Orleans
In partial fulfillment of the
Requirements for the degree of

Doctor of Philosophy
In
Chemistry

By

Richie Prevost

B.S. Indiana University-Purdue University Indianapolis, 2006

May 2017

Acknowledgements

I would like to first thank my friends and family. Without your continued support, I would never have gotten this far. To Léa Gustin, Elisha Josepha, and Maria and Kent Lindsay I will forever cherish our impromptu adventures. You are my comrades in arms. Brian Lewis, thank you for always taking my calls when I needed to vent. For becoming one of my dearest friends and confidants. To my loving mother. You are my rock and my idol. I couldn't have gotten here without you.

Dr. Tarr, thank you for all your guidance through my degree. I have enjoyed our conversations, about research and otherwise. You have taught me a great deal. I would also like to thank my committee members Dr. Wiley, Dr. Zhou, and Dr. Poltavets. Every time I have had a question I've found your door open. To my group members, past and present, thank you for all your help and the wonderful memories.

Table of Contents

Table of Figures

Abstract

In 2012 the net world electricity generation was 21.56 trillion kilowatt hours. Photovoltaics only accounted for only 0.1 trillion kilowatt hours, less than 1 % of the total power. Recently there has been a push to convert more energy production to renewable sources. In recent years, a great deal of interest has been shown for dye sensitized solar cells. These devices use inexpensive materials and have reported efficiencies approaching 12% in the lab. Here methods have been studied to improve upon these, and other, devices. Different approaches for the addition of gold nanoparticles to TiO_2 films were studied. These additions acted as plasmonic and light scattering enhancements to reported dye sensitized devices. These nanoparticle enhancements generated a 10% efficiency in device performance for dye sensitized devices. Quantum dot (QD) sensitized solar cells were prepared by successive ionic layer adsorption and reaction (SILAR) synthesis of QDs in mesoporous films as well as the chemical attachment of colloidal quantum dots using 3-mercaptopropionic acid (3-MPA). Methods of synthesizing a copper sulfide (Cu_2S) counter electrode were investigated to improve the device performance. By using a mesoporous film of indium tin oxide nanoparticles as a substrate for SILAR growth of Cu_2S catalyst, an increase in device performance was seen over that of devices using platinum. These devices did suffer from construction drawbacks. This lead to the development of 3D nanostructures for use in Schottky photovoltaics. These high surface area devices were designed to overcome the recombination problems of thin film Schottky devices. The need to deposit a transparent top electrode limited the success of these devices, but did lead to the development of highly ordered metal nanotube arrays. To further explore these nanostructures depleted heterojunction devices were produced. Along with these devices a new approach to depositing lead sulfide quantum dots was developed. This electrophoretic deposition technique uses an applied electric field to deposit nanoparticles onto a substrate. This creates the possibility for a low waste method for depositing nanocrystals onto nanostructured substrates.

Keywords: quantum dots; solar cells; gold nanowire arrays; electrophoretic deposition; SILAR

Chapter 1 Introduction and background

1.1 Energy

With an increasing demand for power, there is an increasing demand to produce it. In 2012 the global energy consumption was 549.28 quadrillion British thermal units (qBtu). Of this 63.77 qBtu came from renewable sources such as hydrothermal, solar, and wind.[1] Of the renewables, solar is less than 1% of the power produced.[2] Renewable energies are defined as those coming from naturally replenishing resources on a human timescale.[3] The source with the highest potential for growth of these sources is solar. The sun produces 120,000 terawatts of energy, or 6000 times the amount currently consumed globally.[4] An alternative to utilizing renewable energies would be to sequester the approximate 25 billion metric tons of CO_2 emissions annually, or the equivalent to the volume of Lake Superior.[5]

1.2 Solar devices

While solar devices currently supply less than 1% of renewable energy, they receive 53% of the investments.[2-3] Solar cells, also known as photovoltaics, absorb light and convert it into electricity. The commercial costs for these devices are higher upfront than traditional methods, but have lower long-term operating costs.[6] Solar cells are currently divided into four generations.[7]

The first generation are the crystalline silicon (c-Si) photovoltaics.[8] These devices are based on high purity silicon doped to create pn-junctions. These are the devices currently being used in solar farms and on the roofs of homes. While these commercial cells have efficiencies of 15-21% depending on quality, they require a large amount of energy to produce. These are the most widely studied.[3, 8-9]

The second-generation devices are the thin film technologies. These include hydrogenated amorphous silicon (a-Si:H)[10-11], cadmium telluride (CdTe)[12-14], and copper indium gallium diselenide (CIGS)[15-17] With better light absorption abilities than c-Si devices, this generation requires less material for similar results and therefore costs less. These devices have reported efficiencies of 12-15%[7] but suffer from high sensitive to water and oxygen. They also contain toxic and scarce materials.

The third-generation devices are multi-junction devices. These devices are very costly and complex. There are no commercial cells available, but are studied for applications where cost is less of a factor than performance. Such as in space. Laboratory efficiencies are reported to reach 46%.[3, 7, 18]

The final, and current, generation are the "emerging photovoltaics". These are devices that utilize nanostructures and lower cost materials.[9] The most widely known of these devices are the dye sensitized solar cells (DSSC).[4, 19-39] Also included are quantum dot (QD) solar cells,[6, 40-51], perovskite devices,[3, 52] and organic polymer devices.[53] According to the National Renewable Energies Laboratory (NREL) best research-cell efficiencies chart, these newer devices have efficiencies from 10-12%.[18]

1.3 Fundamentals of device testing

To test devices in the lab they are connected to a variable voltage source, illuminated under A.M. 1.5 light (1000 W/m^2)[35], and the photo induced current is measured. The current per area is then graphed against the applied bias. This is known as a J-V curve. Figure 1.1 is a sample curve with important points labeled.

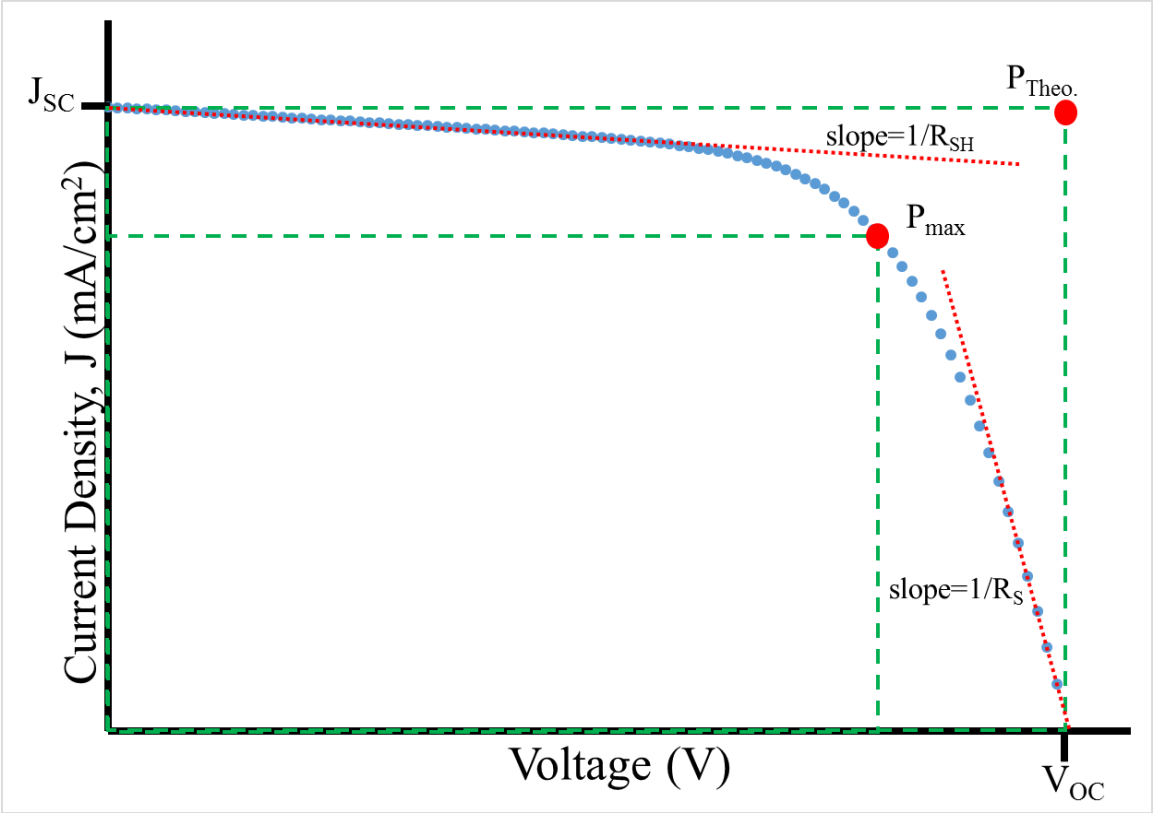

Figure 1.1 Sample J-V curve labeled with shunt resistance (R_{SH}), series resistance (R_S), maximum power (P_{max}), theoretical power ($P_{Theo.}$), short-circuit current density (J_{SC}), and open circuit voltage (V_{OC})

From the curve the first data point is the open circuit current density or J_{sc}. This is the maximum current output for the device per area. The point the curve crosses the x-axis is the open circuit voltage or V_{oc}. This is the maximum voltage of the device. Together these are the theoretical maximum power of the device (P_{Theo}). The inverse slope of the top part of the graph is the device's short circuit or shunt resistance (R_{SH}). The inverse slope of the side of the graph is the transport or series resistance of the device (R_S) or the resistance of the electron's pathway in the device. The maximum power (P_{max}) is found using a power vs voltage curve (Figure 1.2).

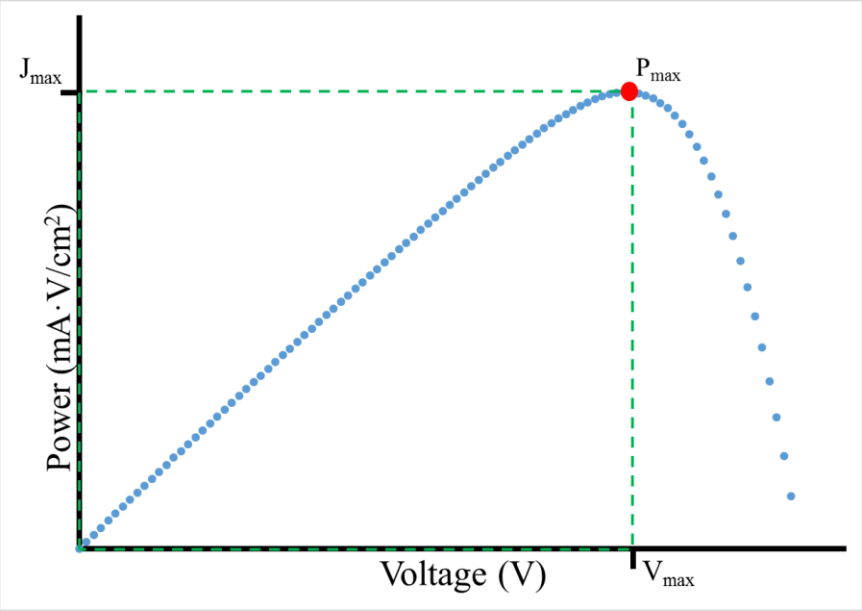

Figure 1.2 Graph of device power as a function of applied voltage with maximum device power (P_{max}) labeled

The efficiency of the device is the ratio of P_{max}/P_{in} where P_{in} is the power input. The last piece of information obtained using a J-V curve is the fill factor (FF). This is the ratio of P_{max}/P_{Theo} and is used as a measure of the "squareness" or how close a curve is to ideal.

1.4 Dye sensitized solar cell fundamentals

Dye sensitized solar cells begin as a transparent conductive oxide (TCO). This is a piece of glass coated on one side with indium tin oxide (ITO) or fluorine tin oxide (FTO) to make it conductive. To this a film of titanium dioxide (TiO_2) particles is deposited and sintered to create a pathway for injected electrons and adhere it to the TCO. This film then has a dye attached to the surface. This dye can be a naturally occurring dye like those found in berries,[38] or one specifically designed for this purpose.[35, 54-56] The sensitized substrate is then sealed to the catalytic cathode using a thermoplastic, or held together with binder clips. This cathode is often a thin layer of platinum, but can also be carbon[57-59], or copper zinc tin sulfide (CZTS).[3, 60] The gap between the contacts is then filled with a redox mediator. This is most commonly an I^-/I_3^- electrolyte,[20, 22, 25-28, 30-31] but can also be a cobalt complex,[4, 35] or a solid hole transporter.[19]

As a photon of light enters the device an electron in the dye is excited. This electron is then injected into the conduction band of the TiO_2 film and out of the device to do work. The dye

is then returned to the ground state by redox mediator, which is then in turn recovered by the catalytic cathode.

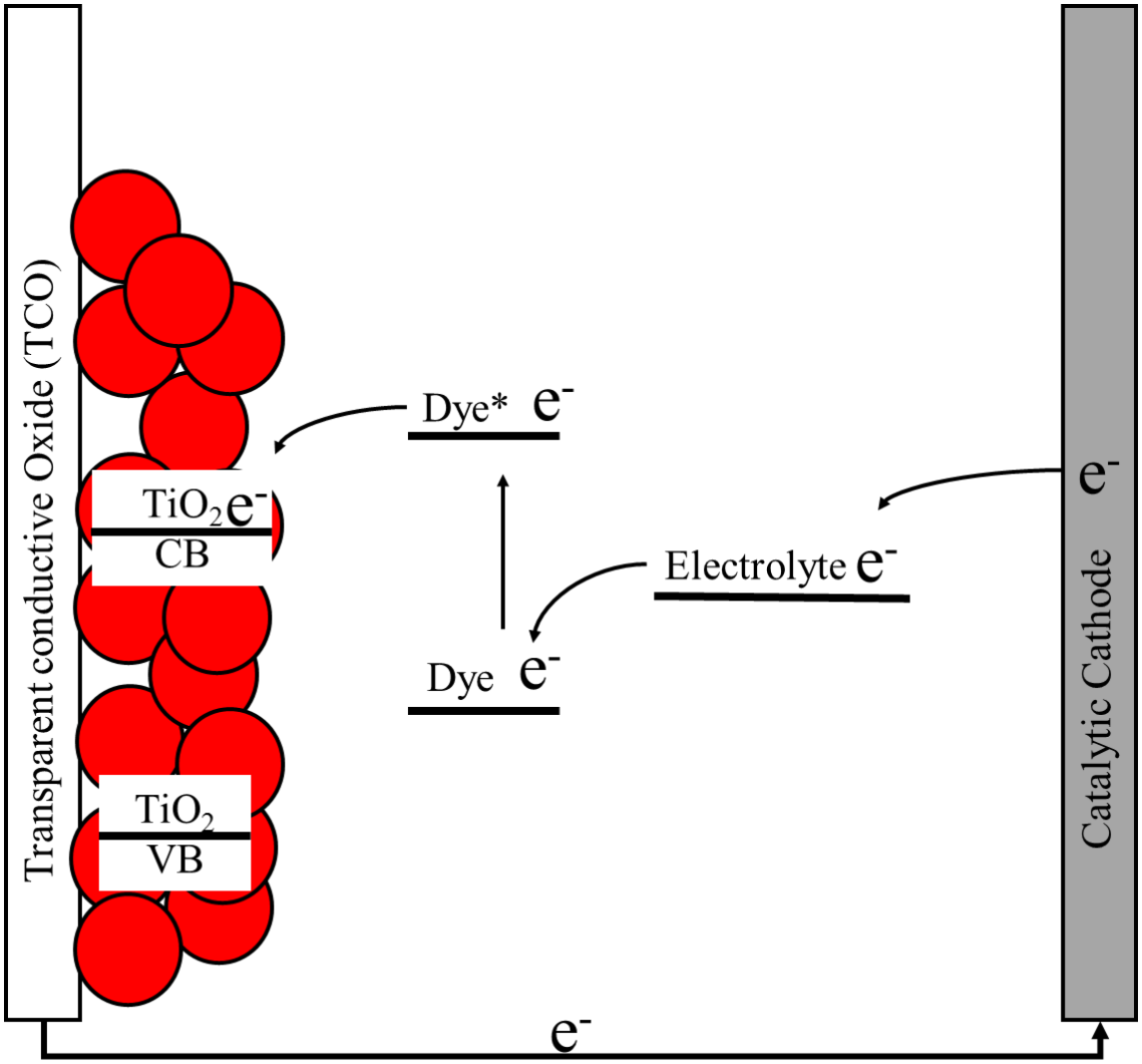

Figure 1.3 Cartoon of DSSC band diagram showing electron path started excitation in the dye, injection into the TiO_2 film, through a circuit to the catalyst, reduction of the electrolyte, ending with regeneration of the dye

Yella et. al reported dye sensitized devices of 12.1% using a cobalt based electrolyte and porphyrin dye.[35] The authors designed zinc based porphyrin dyes to increase the spectrum of absorbance to better match the solar spectrum. The use of the cobalt based dye also increased their device performance from 7.6% to 11.9%. The champion performance was reached by using this electrolyte and two sensitizers in tandem.

1.5 Quantum Dots

Quantum dots (QDs) are semiconductor nanocrystals whose electrons are confined in three dimensions.[61] This confinement is when the dimensions are smaller than the Bohr exciton radius, or average distance of electron-hole pairs. This confinement gives them characteristics between the bulk material, and a discrete molecule. Because of these properties the band gap of the QDs is dependent on the size. As the diameter of the QD decreases the bandgap increases. By choosing an appropriate material and diameter the band gap energy can be tuned to absorb the full solar spectrum.

1.6 Schottky barrier devices

A Schottky barrier is formed at the interface of a semiconductor and a metal with a shallow work function. As a solar cell the inherent bias of the system causes the photo-generated electrons to travel towards the metal and the holes towards the ohmic contact.[40, 62]

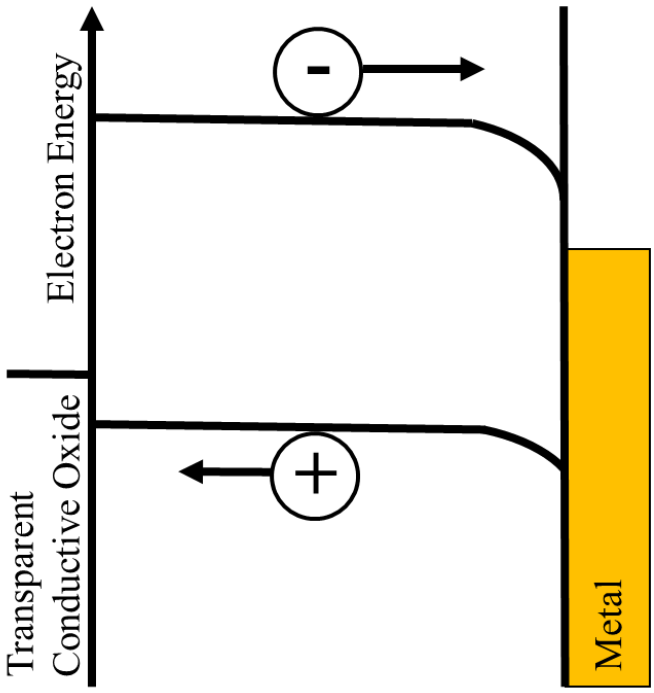

Figure 1.4 Creation of exciton in the semiconductor material of a Schottky barrier device with the positive exciton traveling towards the ohmic contact and the negative exciton traveling towards metal contact.

Devices of these design suffer from high recombination. Since the exciton is generated at the ohmic contact then travels via the semiconductor to the Schottky contact, there is a high probability of recombination. This is reduced by making thinner devices.[40] While the thinner device have lower recombination they have a reduced ability to trap light if too thin.

Tang et. al[48] studied Schottky devices produced by depositing thin films of lead sulfide QDs onto a TCO using a dip coating approach and measured device performance with different metals. They reported that devices with aluminum contacts had a current density twice as high as devices with silver contacts. These devices had lifetimes that were significantly shorter than those with silver lasting 4 hours before declining to 80% of the original measured photon to current efficiency. In contrast silver devices lasted a full 50 hours before reaching the same level of degradation. This loss of efficiency is due to the higher reactivity of aluminum compared to silver. While that reactivity creates a superior Schottky contact, it also increases the rate of degradation of the semiconductor film. The authors solved this degradation by introducing a lithium fluoride layer between the semiconductor and metal. This stabilizing layer increased aluminum device lifetime to 24 hours and an efficiency of 2%. This increased performance comes at the cost of higher device toxicity. Devices that are dangerous to produce are less likely to have significant commercial applications.

A similar study was performed by Luther et. al using lead selenide quantum dots.[49] These authors reported an champion efficiency of 2.1%. The devices were tested using metal contacts made from gold, silver, aluminum, magnesium, or calcium and particles of varying size to measure their impact on V_{oc}.

1.7 Depleted heterojunction device

A depleted heterojunction device is a combination of the structure for a Schottky barrier device and DSSC.[40] In this case both the dye and redox mediator of the DSSC are replaced by the semiconductor absorber of the Schottky device. As the electrons are excited to the conduction band of the absorber they are injected into the TiO_2 film. The electron then travels through the TCO and out of the device to do work. The hole is transported through the absorber material to the metal contact where it recombines with an electron. This cycle constantly regenerates the absorber under illumination preventing degradation and photo bleaching.

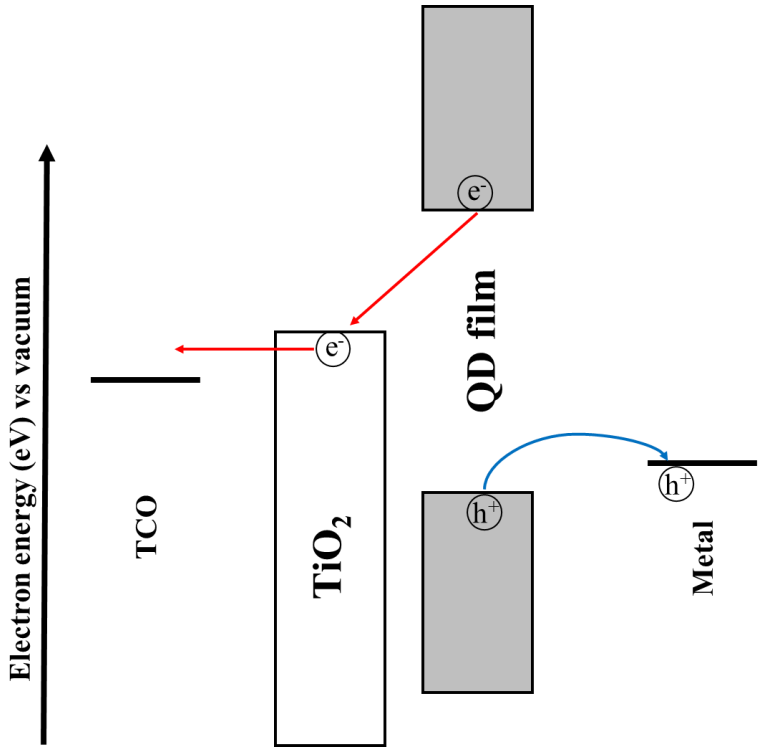

Figure 1.5 Exciton generation in QD film of a depleted heterojunction device with the negative exciton injecting into the conduction band of the TiO_2 and the positive exciton traveling into the metal contact

Pattantyus-Abraham et. al performed a study of performance for depleted heterojunction devices using varying PbS QD sizes. The authors reported a champion efficiency of 5.1% for a device fabricated using 3.7 nm QDs. By using a mesoporous film of TiO_2 the authors were able to create an insulating barrier to short circuits that was an electron acceptor and hole-blocking layer.

1.8 Overview of this dissertation

This dissertation is presented in two halves. Chapters 2 and 3 focus on improving the efficiency of sensitized solar cells. Chapters 4 and 5 focus on new approaches to making solid state photovoltaics. A short abstract for each chapter is presented below.

Chapter 2 will discuss plasmonic enhancements to dye sensitized solar cells. Gold nanoparticles were integrated into mesoporous TiO_2 films. Different techniques for preparing this film and adding the gold particles were studied. The enhancements to light absorbance and device performance were characterized and discussed.

In **Chapter 3** the techniques used with dye cells was applied to quantum dot sensitized cells. Quantum dots were both synthesized directly in the film using SILAR methods, and colloidal QDs were attached using small organic ligands. Methods of preparing a copper sulfide cathode were also investigated. The device performance using these difference conditions was analyzed.

Chapter 4 focused on integrating nanostructures into Schottky barrier devices. A method of growing gold nanowire and nanotube arrays was studied. Different methods for depositing quantum dots onto wire arrays and flat substrates were studied. Methods for making transparent conductive contacts on the top of devices using solution and physical based deposition techniques of indium tin oxide were explored. These devices were characterized by device performance and imaged using scanning electron microscopy.

Chapter 5 focused on improving devices from the previous chapter using depleted heterojunction techniques. The use of titanium dioxide and zinc oxide as hole blocking layers was studied. A new method for depositing ultra-small PbS QDs using an applied electric field was analyzed. While still in development, this technique could reduce waste of material significantly.

1.9 References

1. World energy demand and economic outlook. http://www.eia.gov/outlooks/ieo/world.cfm (accessed 11-23-2016).
2. Janet L. Sawin, F. S., *Renewables 2014 Global Satus Report*. REN21: 2014.
3. Wozny, S. From Copper Zinc Tin Sulfur to Perovskites: Fabrication and Characterization of New Generation Solar Cells. University of New Orleans Theses and Dissertations, 2015.
4. Grätzel, M., Recent Advances in Sensitized Mesoscopic Solar Cells. *Accounts of Chemical Research* **2009,** *42* (11), 1788-1798.
5. Kamat, P. V., Meeting the Clean Energy Demand: Nanostructure Architectures for Solar Energy Conversion. *The Journal of Physical Chemistry C* **2007,** *111* (7), 2834-2860.
6. Sargent, E. H., Colloidal quantum dot solar cells. *Nat Photon* **2012,** *6* (3), 133-135.
7. Green, M. A.; Emery, K.; Hishikawa, Y.; Warta, W.; Dunlop, E. D., Solar cell efficiency tables (Version 45). *Progress in Photovoltaics: Research and Applications* **2015,** *23* (1), 1-9.
8. Descoeudres, A.; Allebé, C.; Badel, N.; Barraud, L.; Jonathan Champliaud; Debrot, F.; Faes, A.; Lachowicz, A.; Levrat, J.; Nicolay, S.; Sansonnens, L.; Despeisse, M.; Ballif, C., Silicon Heterojunction Solar Cells: Towards Low-cost High-Efficiency Industrial Devices and Application to Low-concentration PV. *Energy Procedia* **2015,** *77*, 508-514.
9. Kalyanasundaram, K., Photochemical and Photoelectrochemical Approaches to Energy Conversion. In *Dye-Sensitized Solar Cells*, EPFL Press: 2010; pp 1-43.
10. Carlson, D. E.; Wronski, C. R., Amorphous silicon solar cell. *Applied Physics Letters* **1976,** *28* (11), 671-673.
11. Spear, W. E.; Le Comber, P. G., Substitutional doping of amorphous silicon. *Solid State Communications* **1975,** *17* (9), 1193-1196.
12. Chu, T. L.; Chu, S. S.; Britt, J.; Ferekides, C.; Wang, C.; Wu, C. Q.; Ullal, H. S., 14.6% efficient thin-film cadmium telluride heterojunction solar cells. *IEEE Electron Device Letters* **1992,** *13* (5), 303-304.
13. Nobuo, N.; Hitoshi, M.; Akihiko, N.; Seiji, I.; Hiroshi, U.; Toshio, Y., Screen Printed Thin Film CdS/CdTe Solar Cell. *Japanese Journal of Applied Physics* **1980,** *19* (4), 703.
14. Morales-Acevedo, A., Solar Renewable Energy News International Conference (SREN-2005). *Solar Energy* **2006,** *80* (6), 627-628.
15. Chia-Hua, H.; Chun-Ping, L.; Yueh-Lin, J., Characteristics of CIGS photovoltaic devices co-evaporated with various Se flux rates at low temperatures. *Semiconductor Science and Technology* **2016,** *31* (8), 085004.
16. Jackson, P.; Wuerz, R.; Hariskos, D.; Lotter, E.; Witte, W.; Powalla, M., Effects of heavy alkali elements in Cu(In,Ga)Se2 solar cells with efficiencies up to 22.6%. *physica status solidi (RRL) – Rapid Research Letters* **2016,** *10* (8), 583-586.
17. Yukiko, K.; Jiro, N.; Shogo, I.; Hajime, S.; Shigeru, N., Effects of Mo surface oxidation on Cu(In,Ga)Se 2 solar cells fabricated by three-stage process with. *Japanese Journal of Applied Physics* **2016,** *55* (2), 022304.
18. Photovoltaic Research. http://www.nrel.gov/pv/ (accessed 11-28-2016).
19. Chung, I.; Lee, B.; He, J.; Chang, R. P. H.; Kanatzidis, M. G., All-solid-state dye-sensitized solar cells with high efficiency. *Nature* **2012,** *485* (7399), 486-489.
20. Sahu, G.; Wang, K.; Gordon, S. W.; Zhou, W.; Tarr, M. A., Core-shell Au-TiO2 nanoarchitectures formed by pulsed laser deposition for enhanced efficiency in dye sensitized solar cells. *RSC Advances* **2012,** *2* (9), 3791-3800.

21. Grätzel, M., Dye-sensitized solar cells. *Journal of Photochemistry and Photobiology C: Photochemistry Reviews* **2003,** *4* (2), 145-153.
22. Yasuo, C.; Ashraful, I.; Yuki, W.; Ryoichi, K.; Naoki, K.; Liyuan, H., Dye-Sensitized Solar Cells with Conversion Efficiency of 11.1%. *Japanese Journal of Applied Physics* **2006,** *45* (7L), L638.
23. Dingwen, Z.; Milton, W.; Alexandre, G. B.; Jie, S.; Xiaodong, L.; Sumei, H., Enhanced performance of dye-sensitized solar cells using gold nanoparticles modified fluorine tin oxide electrodes. *Journal of Physics D: Applied Physics* **2013,** *46* (2), 024005.
24. Jung, H.; Koo, B.; Kim, J.-Y.; Kim, T.; Son, H. J.; Kim, B.; Kim, J. Y.; Lee, D.-K.; Kim, H.; Cho, J.; Ko, M. J., Enhanced Photovoltaic Properties and Long-Term Stability in Plasmonic Dye-Sensitized Solar Cells via Noncorrosive Redox Mediator. *ACS Applied Materials & Interfaces* **2014,** *6* (21), 19191-19200.
25. Ito, S.; Murakami, T. N.; Comte, P.; Liska, P.; Grätzel, C.; Nazeeruddin, M. K.; Grätzel, M., Fabrication of thin film dye sensitized solar cells with solar to electric power conversion efficiency over 10%. *Thin Solid Films* **2008,** *516* (14), 4613-4619.
26. Qi, J.; Dang, X.; Hammond, P. T.; Belcher, A. M., Highly Efficient Plasmon-Enhanced Dye-Sensitized Solar Cells through Metal@Oxide Core–Shell Nanostructure. *ACS Nano* **2011,** *5* (9), 7108-7116.
27. Desilvestro, J.; Graetzel, M.; Kavan, L.; Moser, J.; Augustynski, J., Highly efficient sensitization of titanium dioxide. *Journal of the American Chemical Society* **1985,** *107* (10), 2988-2990.
28. Choi, H.; Chen, W. T.; Kamat, P. V., Know Thy Nano Neighbor. Plasmonic versus Electron Charging Effects of Metal Nanoparticles in Dye-Sensitized Solar Cells. *ACS Nano* **2012,** *6* (5), 4418-4427.
29. Hammond, J.; Bhalla, N.; Rafiee, S.; Estrela, P., Localized Surface Plasmon Resonance as a Biosensing Platform for Developing Countries. *Biosensors* **2014,** *4* (2), 172.
30. O'Regan, B.; Gratzel, M., A low-cost, high-efficiency solar cell based on dye-sensitized colloidal TiO2 films. *Nature* **1991,** *353* (6346), 737-740.
31. Law, M.; Greene, L. E.; Johnson, J. C.; Saykally, R.; Yang, P., Nanowire dye-sensitized solar cells. *Nat Mater* **2005,** *4* (6), 455-459.
32. Cheng, W.-Y.; Deka, J. R.; Chiang, Y.-C.; Rogeau, A.; Lu, S.-Y., One-Step, Surfactant-Free Hydrothermal Method for Syntheses of Mesoporous TiO2 Nanoparticle Aggregates and Their Applications in High Efficiency Dye-Sensitized Solar Cells. *Chemistry of Materials* **2012,** *24* (16), 3255-3262.
33. Jeong, N. C.; Prasittichai, C.; Hupp, J. T., Photocurrent Enhancement by Surface Plasmon Resonance of Silver Nanoparticles in Highly Porous Dye-Sensitized Solar Cells. *Langmuir* **2011,** *27* (23), 14609-14614.
34. Sheehan, S. W.; Noh, H.; Brudvig, G. W.; Cao, H.; Schmuttenmaer, C. A., Plasmonic Enhancement of Dye-Sensitized Solar Cells Using Core–Shell–Shell Nanostructures. *The Journal of Physical Chemistry C* **2013,** *117* (2), 927-934.
35. Yella, A.; Lee, H.-W.; Tsao, H. N.; Yi, C.; Chandiran, A. K.; Nazeeruddin, M. K.; Diau, E. W.-G.; Yeh, C.-Y.; Zakeeruddin, S. M.; Grätzel, M., Porphyrin-Sensitized Solar Cells with Cobalt (II/III)–Based Redox Electrolyte Exceed 12 Percent Efficiency. *Science* **2011,** *334* (6056), 629-634.
36. Chandiran, A. K.; Tetreault, N.; Humphry-Baker, R.; Kessler, F.; Baranoff, E.; Yi, C.; Nazeeruddin, M. K.; Grätzel, M., Subnanometer Ga2O3 Tunnelling Layer by Atomic Layer

Deposition to Achieve 1.1 V Open-Circuit Potential in Dye-Sensitized Solar Cells. *Nano Letters* **2012,** *12* (8), 3941-3947.
37. Sahu, G.; Gordon, S. W.; Tarr, M. A., Synthesis and application of core-shell Au-TiO2 nanowire photoanode materials for dye sensitized solar cells. *RSC Advances* **2012,** *2* (2), 573-582.
38. Karna, H. E. C. M. H. G. S. P., Synthesis, Characterization, and Application of Gold Nanoparticles in Green Nanochemistry Dye-Sensitized Solar Cells. Laboratory, A. R., Ed. 2012.
39. Vlachopoulos, N.; Liska, P.; Augustynski, J.; Graetzel, M., Very efficient visible light energy harvesting and conversion by spectral sensitization of high surface area polycrystalline titanium dioxide films. *Journal of the American Chemical Society* **1988,** *110* (4), 1216-1220.
40. Pattantyus-Abraham, A. G.; Kramer, I. J.; Barkhouse, A. R.; Wang, X.; Konstantatos, G.; Debnath, R.; Levina, L.; Raabe, I.; Nazeeruddin, M. K.; Grätzel, M.; Sargent, E. H., Depleted-Heterojunction Colloidal Quantum Dot Solar Cells. *ACS Nano* **2010,** *4* (6), 3374-3380.
41. Brabec, C. J.; Shaheen, S. E.; Winder, C.; Sariciftci, N. S.; Denk, P., Effect of LiF/metal electrodes on the performance of plastic solar cells. *Applied Physics Letters* **2002,** *80* (7), 1288-1290.
42. Wang, X.; Koleilat, G. I.; Fischer, A.; Tang, J.; Debnath, R.; Levina, L.; Sargent, E. H., Enhanced Open-Circuit Voltage in Visible Quantum Dot Photovoltaics by Engineering of Carrier-Collecting Electrodes. *ACS Applied Materials & Interfaces* **2011,** *3* (10), 3792-3795.
43. Huang, X.; Huang, S.; Zhang, Q.; Guo, X.; Li, D.; Luo, Y.; Shen, Q.; Toyoda, T.; Meng, Q., A flexible photoelectrode for CdS/CdSe quantum dot-sensitized solar cells (QDSSCs). *Chemical Communications* **2011,** *47* (9), 2664-2666.
44. Etgar, L.; Moehl, T.; Gabriel, S.; Hickey, S. G.; Eychmüller, A.; Grätzel, M., Light Energy Conversion by Mesoscopic PbS Quantum Dots/TiO2 Heterojunction Solar Cells. *ACS Nano* **2012,** *6* (4), 3092-3099.
45. Chang, L.-Y.; Lunt, R. R.; Brown, P. R.; Bulović, V.; Bawendi, M. G., Low-Temperature Solution-Processed Solar Cells Based on PbS Colloidal Quantum Dot/CdS Heterojunctions. *Nano Letters* **2013,** *13* (3), 994-999.
46. Braga, A.; Giménez, S.; Concina, I.; Vomiero, A.; Mora-Seró, I., Panchromatic Sensitized Solar Cells Based on Metal Sulfide Quantum Dots Grown Directly on Nanostructured TiO2 Electrodes. *The Journal of Physical Chemistry Letters* **2011,** *2* (5), 454-460.
47. Toyoda, T.; Shen, Q., Quantum-Dot-Sensitized Solar Cells: Effect of Nanostructured TiO2 Morphologies on Photovoltaic Properties. *The Journal of Physical Chemistry Letters* **2012,** *3* (14), 1885-1893.
48. Tang, J.; Wang, X.; Brzozowski, L.; Barkhouse, D. A. R.; Debnath, R.; Levina, L.; Sargent, E. H., Schottky Quantum Dot Solar Cells Stable in Air under Solar Illumination. *Advanced Materials* **2010,** *22* (12), 1398-1402.
49. Luther, J. M.; Law, M.; Beard, M. C.; Song, Q.; Reese, M. O.; Ellingson, R. J.; Nozik, A. J., Schottky Solar Cells Based on Colloidal Nanocrystal Films. *Nano Letters* **2008,** *8* (10), 3488-3492.
50. Chung, C.-H.; Song, T.-B.; Bob, B.; Zhu, R.; Duan, H.-S.; Yang, Y., Silver Nanowire Composite Window Layers for Fully Solution-Deposited Thin-Film Photovoltaic Devices. *Advanced Materials* **2012,** *24* (40), 5499-5504.
51. Reilly, N.; Wehrung, M.; O'Dell, R. A.; Sun, L., Ultrasmall colloidal PbS quantum dots. *Materials Chemistry and Physics* **2014,** *147* (1–2), 1-4.

52. Etgar, L.; Gao, P.; Qin, P.; Graetzel, M.; Nazeeruddin, M. K., A hybrid lead iodide perovskite and lead sulfide QD heterojunction solar cell to obtain a panchromatic response. *Journal of Materials Chemistry A* **2014,** *2* (30), 11586-11590.
53. Mor, G. K.; Shankar, K.; Paulose, M.; Varghese, O. K.; Grimes, C. A., High efficiency double heterojunction polymer photovoltaic cells using highly ordered TiO2 nanotube arrays. *Applied Physics Letters* **2007,** *91* (15), 152111.
54. Nazeeruddin, M. K.; Péchy, P.; Renouard, T.; Zakeeruddin, S. M.; Humphry-Baker, R.; Comte, P.; Liska, P.; Cevey, L.; Costa, E.; Shklover, V.; Spiccia, L.; Deacon, G. B.; Bignozzi, C. A.; Grätzel, M., Engineering of Efficient Panchromatic Sensitizers for Nanocrystalline TiO2-Based Solar Cells. *Journal of the American Chemical Society* **2001,** *123* (8), 1613-1624.
55. Chen, C.-Y.; Wang, M.; Li, J.-Y.; Pootrakulchote, N.; Alibabaei, L.; Ngoc-le, C.-h.; Decoppet, J.-D.; Tsai, J.-H.; Grätzel, C.; Wu, C.-G.; Zakeeruddin, S. M.; Grätzel, M., Highly Efficient Light-Harvesting Ruthenium Sensitizer for Thin-Film Dye-Sensitized Solar Cells. *ACS Nano* **2009,** *3* (10), 3103-3109.
56. Hagberg, D. P.; Edvinsson, T.; Marinado, T.; Boschloo, G.; Hagfeldt, A.; Sun, L., A novel organic chromophore for dye-sensitized nanostructured solar cells. *Chemical Communications* **2006,** (21), 2245-2247.
57. Zhang, Q.; Zhang, Y.; Huang, S.; Huang, X.; Luo, Y.; Meng, Q.; Li, D., Application of carbon counterelectrode on CdS quantum dot-sensitized solar cells (QDSSCs). *Electrochemistry Communications* **2010,** *12* (2), 327-330.
58. Fan, S.-Q.; Fang, B.; Kim, J. H.; Kim, J.-J.; Yu, J.-S.; Ko, J., Hierarchical nanostructured spherical carbon with hollow core/mesoporous shell as a highly efficient counter electrode in CdSe quantum-dot-sensitized solar cells. *Applied Physics Letters* **2010,** *96* (6), 063501.
59. Deng, M.; Zhang, Q.; Huang, S.; Li, D.; Luo, Y.; Shen, Q.; Toyoda, T.; Meng, Q., Low-Cost Flexible Nano-Sulfide/Carbon Composite Counter Electrode for Quantum-Dot-Sensitized Solar Cell. *Nanoscale Research Letters* **2010,** *5* (6), 986.
60. Wozny, S.; Wang, K.; Zhou, W., Cu2ZnSnS4 nanoplate arrays synthesized by pulsed laser deposition with high catalytic activity as counter electrodes for dye-sensitized solar cell applications. *Journal of Materials Chemistry A* **2013,** *1* (48), 15517-15523.
61. *Optics of Quantum Dots and Wires*. Artech House, INC.: 2005.
62. Landsberg, P. T.; Klimpke, C., Theory of the Schottky Barrier Solar Cell. *Proceedings of the Royal Society of London. Series A, Mathematical and Physical Sciences* **1977,** *354* (1676), 101-118.

Chapter 2 Plasmonic Solar Cells

2.1 Introduction

Current energy needs are met primarily by the consumption of fossil fuels. These processes release large amounts of greenhouse gasses that in turn cause global climate change. The U.S. energy information administration reported 549 quadrillion British thermal units (Btu) of energy consumed in 2012 and projects an increase to 629 quadrillion Btu by 2020.[1] In an effort to reduce carbon emissions some governments have begun the shift to all renewable energy sources. For example, Germany has implemented an energy transition policy to transition to all renewable sources. With a goal to reduce greenhouse gas emissions by 95% of 1990 levels by 2050 and a phase out of nuclear power by 2022.[2]

Dye sensitized solar cells (DSSCs) are an active area of interest for inexpensive solar energy. With costs of less than $1/peak watt, DSSCs have the potential to meet the global demand of over 14 terawatts.[3] Current DSSCs report conversion efficiencies of 10% or higher at AM 1.5 irradiation.[4-10] Most DSSCs are composed of a transparent conducting oxide (TCO), a mesoporous semi-conductor layer, dye sensitizer, electrolyte, and a platinum counter-electrode. In these systems, a dye sensitizer is excited and injects an electron into the mesoporous film. The dye is then regenerated by the electrolyte, which is then regenerated in turn by the counter-electrode. To maximize photon to current efficiency, each component has been studied for optimize their effect. Some studies replace the rigid fluorine doped tin oxide (FTO) TCO with a flexible conductive polymer.[11] Other studies have been done on the mesoporous oxide replacing the commonly used titanium dioxide (TiO_2) with zinc oxide (ZnO)[12], or substituting a nanostructured anode for the mesoporous film.[12-16] Different electrolyte systems[6, 17] and replacements for the platinum counter-electrode have also been studied.[18] Arguably the most studied aspect of DSSCs is the dye. Modifying these structures allows for broader absorption range, enhanced extinction coefficient, greater electron injection speed, and many other factors.[4-5, 10, 19-23]

The efficacy of solar devices is measured using a current density vs. applied voltage plot also known as a J-V curve. At the y-axis, the short-circuit current (J_{sc}) is the maximum current of the device. As a voltage is applied the curve creates a rounded box shape. The inverse slope of

the top of this box is controlled by the recombination or shunt resistance (R_{sh}). Ideally this resistance is infinite, preventing the recombination of electrons. The inverse slope of the side of the curve is the series resistance (R_s). This is the resistance to the electron passing through the system. Ideally this would be zero and electrons would travel freely. Where the curve intersects the x-axis is the open-circuit voltage (V_{oc}). This is the point where no more current can pass through the device. Ideally a J-V curve would be perfectly rectangle. To measure how rectangular a curve is, the ratio of the maximum power over the theoretical power is used and called the fill factor (FF). The biggest measure of performance is cell efficiency. This is ratio of the power output over the power input. This input is standardized at 1000 W/m^2 and referred to as AM 1.5 or air mass 1.5. This represents the path length of solar light in the atmosphere over the corresponding vertical. At AM 1.5 the sun is at 48.19° from the vertical.[10] A reference J-V curve with relevant labels can be seen in Figure 2.1

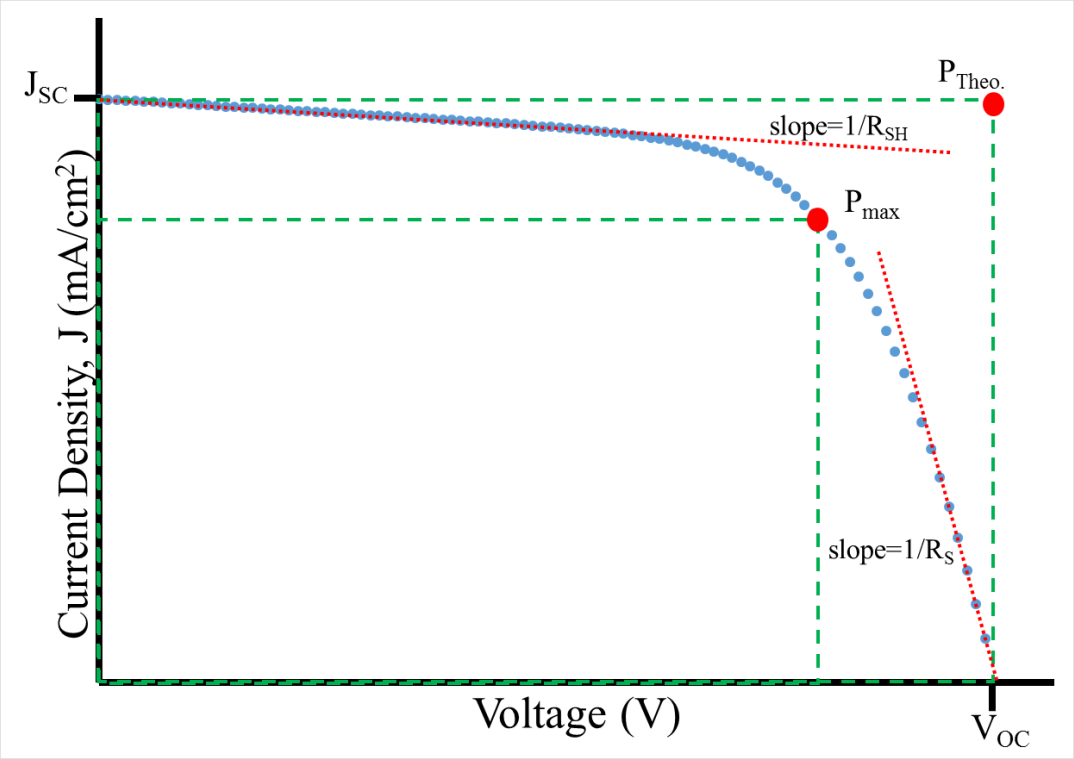

Figure 2.1 Sample J-V curve labeled with shunt resistance (R_{SH}), series resistance (R_s), maximum power (P_{max}), theoretical power ($P_{Theo.}$), short-circuit current density (J_{SC}), and open circuit voltage (V_{OC})

In an attempt to increase the absorption of light by DSSCs, plasmonic nanostructures have been studied.[8, 10, 14-15, 17, 24-28] Plasmonic structures have already been shown to aid in imaging[29-30], nano-lithography[31], and other techniques.[32-34] The local surface plasmon resonance (LSPR) of metal nanoparticles is dependent on the refractive index of the surrounding medium.[15, 35-37] With the optimization of these conditions, the LSPR can be tuned to complement the absorption of the dye in a DSSC.

In a study performed by Jeong et. al[27] TiO_2 films were decorated with silver nanoparticles via photoreduction. This was achieved by drop casting a silver nitrate solution on the mesoporous TiO_2 substrates and exposing them to UV light. Due to the reactive environment presented by the I^-/I_3^- electrolyte, they protected their particles by refluxing in a titanium isopropoxide solution followed by calcining. This process is similar to the $TiCl_4$ treatment of traditional dye-sensitized solar cells to generate a higher surface area for dye adsorption. Devices made with these silver nanoparticles showed an overall increase in current density and a 25% improvement in overall performance. Increases in current density are attributed to increases in light absorption. To compare enhanced dye loading to plasmonic enhancements dye desorption studies were performed. The reported increase in dye concentration was attributed to half of the efficiency increase in silver enhanced devices. This extra loading is caused primarily by the added surface area generated by titanium isopropoxide treatment. While this was not studied by Jeong et. al, similar studies[14] have shown that increased surface area from nanoparticle addition does not significantly increase dye loading. This approach to plasmonic enhancement provides well bound particles distributed throughout the mesoporous film. However, the technique is not easily scalable to larger devices.

A similar study was performed by Cramer et. al at the Army Research Laboratory.[28] These devices were prepared by soaking anthocyanin dyed mesoporous TiO_2 films in gold nanoparticle suspensions. The devices were assembled by clamping on a platinized counter electrode with binder clips and filling the gap with I^-/I_3^- electrolyte by capillary action. This open-air style device is very unstable and only viable for a few minutes before the volatile electrolyte solvents evaporate. Reported devices all showed efficiencies less than 1%. While anthocyanin is a natural dye obtained from blackberry juice, dyes with better absorption capabilities are available. The use of inferior dye and assemble techniques are responsible for

these comparatively low efficiencies. Additionally, gold particles are not strongly bound to the mesoporous film. Despite these pitfalls, Cramer et. al did see an increase in J_{SC} with increased gold loading. Even with an unexplained loss of $V_{oc,}$ an increase in efficiency can be seen. With enhanced technique, these trends would likely be more obvious.

To this end, the inclusion of purchased gold nanoparticles into a TiO_2 paste was studied. These plasmonic films showed an enhanced absorbance versus bare and dyed TiO_2 films. DSSCs fabricated using these plasmonic films showed enhanced efficiency compared to reference devices.

2.2 Experimental

2.2.1 Preparation of TiO_2 paste.

The unmodified paste was made by dissolving 100 µL Triton X-100 (Sigma) and 0.2 g 20,000 MW PEG (Fluka) in 3.0 mL 0.1 M aqueous acetic acid in a 15 mL centrifuge tube. Once the PEG had dissolved completely, 0.5 g TiO_2 nanopowder (Sigma, anatase nanopowder) was mixed in to make a thick paste. The tube was then sealed and left in an ultrasonic bath for approximately 60 minutes. A citric acid paste was also made replacing the acetic acid with $2.23x10^{-3}$ M aqueous citric acid. Gold modified pastes were made by substituting 1.5 mL 10 nm gold nanoparticles in pH 7.4 citrate buffer (Ted Pella) for 1.5 mL of the acetic acid total volume.

2.2.2 Preparation of Mesoporous Film.

Pieces of FTO glass (Sigma, 8 Ω/sq) were cut into approximately 3x2 cm pieces. They were cleaned by submersion in a 1% Alconox solution and sonicating for 60 minutes. They were then washed with Nanopure (deionized 18 Ω/sq, 0.02 µm filtered) water and sonicated for another 60 minutes in Nanopure water to remove any remaining Alconox. Finally, the substrates were sonicated for 60 minutes in isopropyl alcohol and stored in alcohol until use. After drying, the glass was placed in a petri dish conductive side up and covered with 0.04 M $TiCl_4$ solution that was prepared by diluting pure $TiCl_4$ (Sigma) with Nanopure water at 0°C. The substrates were then heated at 60°C for 1 hour, rinsed with Nanopure water, dried, and annealed at 500°C for 30 minutes. The cooled substrates were taped to the bench, conductive side up, using Scotch™ brand tape leaving a 6 mm wide strip of exposed glass. The tape acted to immobilize the glass and as a spacer for uniform film deposition. A small amount of prepared TiO_2 paste was

deposited along the top edge of the glass, and pulled across the surface by a microscope slide edge held flush to the substrate. This is often referred to as the doctor blade method. After drying the films their thickness was measured with a profilimeter (Dektak). Films less than 12 µm had a second layer of TiO_2 deposited. Films were sintered at 450°C for 30 minutes then allowed to cool to room temperature. Once cooled the films were soaked in a 0.6 mM solution of N719 dye (Solaronix) dissolved in a 1:1 ratio of methanol:tert-butanol (both Fisher, HPLC grade).

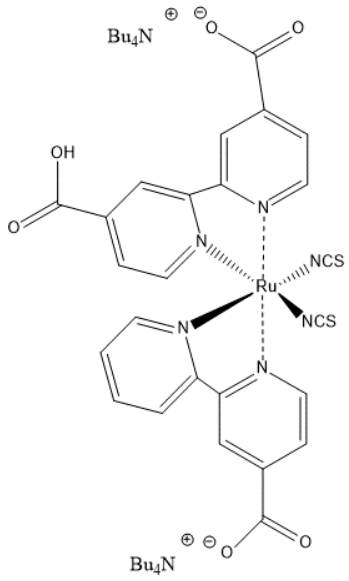

Figure 2.2 Structure of N719 dye

2.2.3 Assembly of Solar Cells.

Cleaned pieces of FTO glass had a thin layer of organo-metallic platinum precursor, Platisol (Solaronix), applied with a cotton applicator and were annealed at 400°C for 30 minutes. The cooled platinized glass had a 0.4 mm diameter hole drilled through for later electrolyte filling. The dyed TiO_2 films were rinsed with methanol, then scraped down to a 6 x 8 mm area. The two pieces of FTO were sealed together with a 60 µm thick Surlyn thermoplastic (Solaronix) gasket. The two electrodes were offset to allow easy electrode attachment for testing. The I^-/I_3^- electrolyte was prepared in an 85:15 v/v acetonitrile:valeronitrile containing 0.6 M butylmethylimidazolium iodide, 0.3 M I_2, 0.1 M guanidinium thiocyanate, and 0.5 M 4-tert-butylpyridine (Solvents Fisher HPLC grade, all others Sigma). The devices were placed in a

vacuum desiccator with a drop of electrolyte over the hole. The desiccator was pumped down pulling the air out of the void space of the devices. Once the atmosphere was returned to the desiccator, the electrolyte was pulled into the void. The devices were sealed using a small square of Surlyn and square of microscope slide, and the edges painted with silver paint (Ted Pella) for better testing electrode contact.

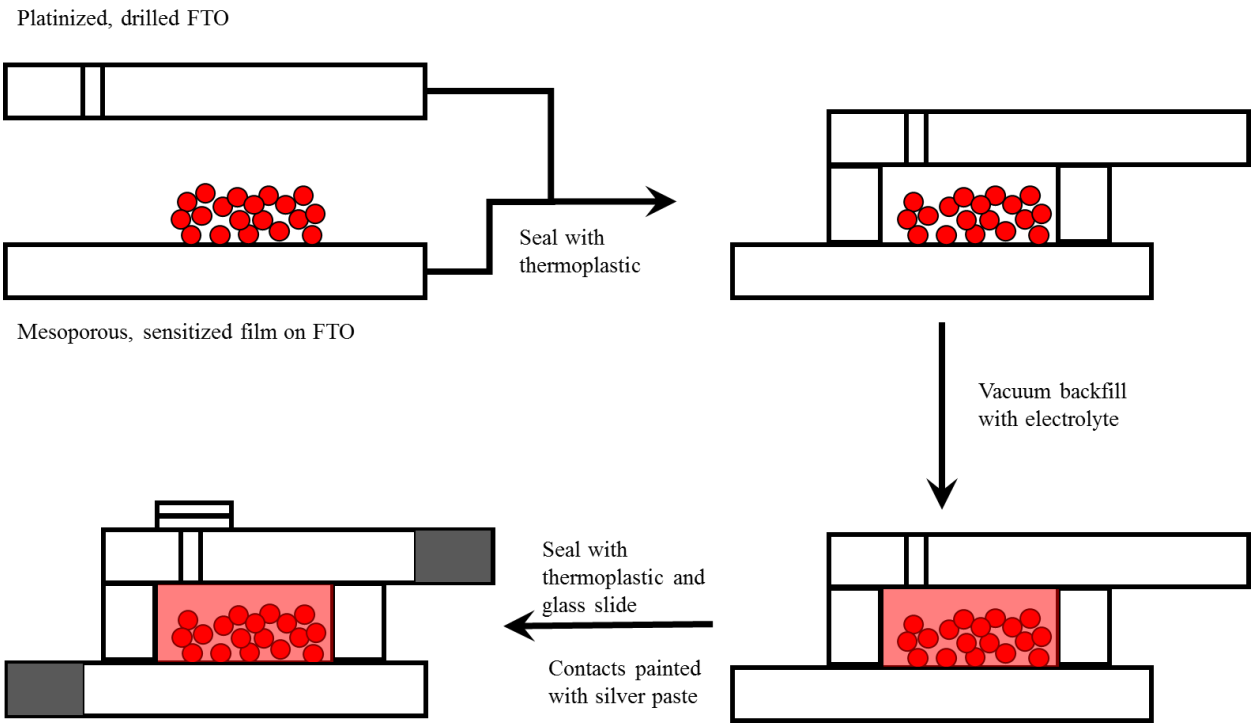

Figure 2.3 Schematic for the assembly of dye sensitized solar cells

2.2.4 Characterization

Film thickness was measured with a Sloan Dektak IIA profilimeter. Particle addition was confirmed using a JOEL 2010 transmission electron microscope (TEM). Diffuse reflectance was measured with a Cary 500 UV-Vis spectrometer with a diffuse reflectance stage attached. Photovoltaic measurements were performed using a Newport® 50-500 W 67005 solar simulator set at 100 mW/cm^2. The light intensity of the xenon lamp was calibrated using a National Renewable Energy Laboratory (NREL) calibrated silicon photodiode (Hamamatsu S1787-08 for visible to IR range). Current density-voltage (J-V) curves were measured with a Keithley 2400 source meter.

2.3 Results and discussion

2.3.1 Effects of paste composition

Films made using pastes containing either acetic acid or citric acid were compared for their mechanical and photovoltaic properties. Mechanical properties were assessed by the ability of the films to stay intact during thickness measuring and dye adsorption. Films with poor adhesion are readily removed by the probe of the profilimeter generating a measurement at or near zero micrometers for thickness and a visible line through the film. Poor adhesion can also be seen by flaking during the overnight soaking in dye solution. Films made with both acids showed excellent adhesion to the TCO substrates during both measurement and soaking phases.

To compare the effects of paste composition on final devices, comparable films were made using both acids. Typical current density-voltage (J-V) curves can be seen in Figure 2.4. Both devices had an efficiency of 4.31%. The acetic acid device had a J_{sc} of 7.39 mA/cm^2, V_{oc} of 0.8205 V, and a FF of 0.71. In comparison the citric acid device had a J_{sc} of 8.84 mA/cm^2, a V_{oc} of 0.78 V, and a FF of 0.62. These differences can be attributed to variance is device fabrication between cells. Even devices considered identical have been shown variances similar to these.

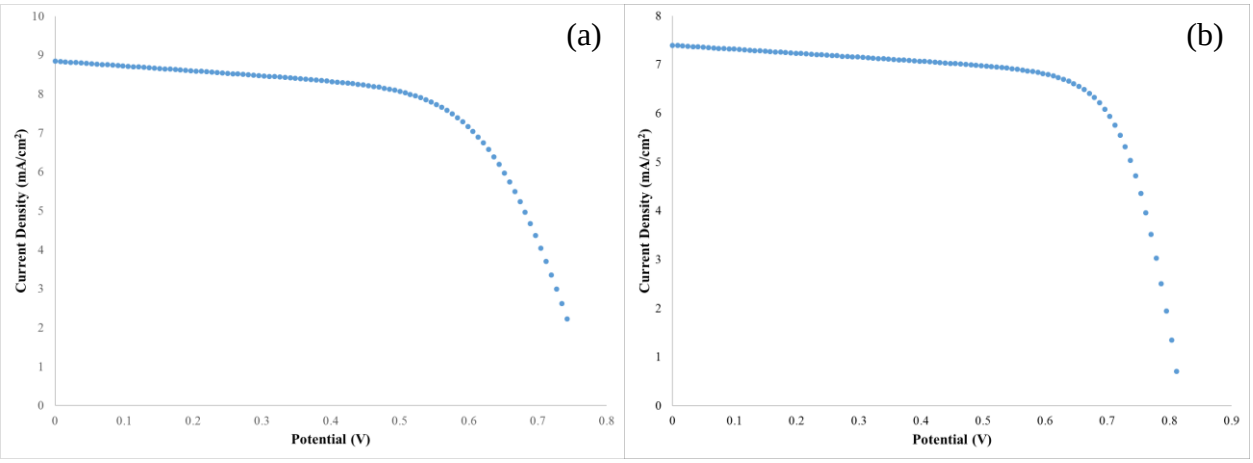

Figure 2.4 Characteristic photocurrent density-voltage curves for (a) devices made with citric acid and (b) devices made with acetic acid both showing similar results

2.3.2 Plasmonic enhancement effects

Suspensions of the 10 nm gold particles from Ted Pella are a red color as purchased. When mixed into a TiO_2 paste the mixture is a light purple color. To study the enhancement to light absorption diffuse reflectance was performed on bare TiO_2 films, TiO_2-gold films, dyed TiO_2 films, and dyed TiO_2-gold films. As can be seen in Figure 2.5(a) bare TiO_2 reflects 100% of the light until it begins absorbing in the UV. Addition of the gold sees a decrease in the reflectance over range of the scan with a peak around 550 nm. This peak corresponds to the characteristic absorbance maximum for gold nanoparticles of this size. This LSPR peak overlaps well with the absorbance of the free dye in solution as seen in Figure 2.5 (b). Such overlap is desirable to maximize the dye absorbance, and hopefully allow for thinner films with higher efficiency. Thinner films mean shorter path lengths for excited electron transport, increasing recombination resistance, and decreasing series resistance. These changes would then lead to potentially higher device efficiencies.

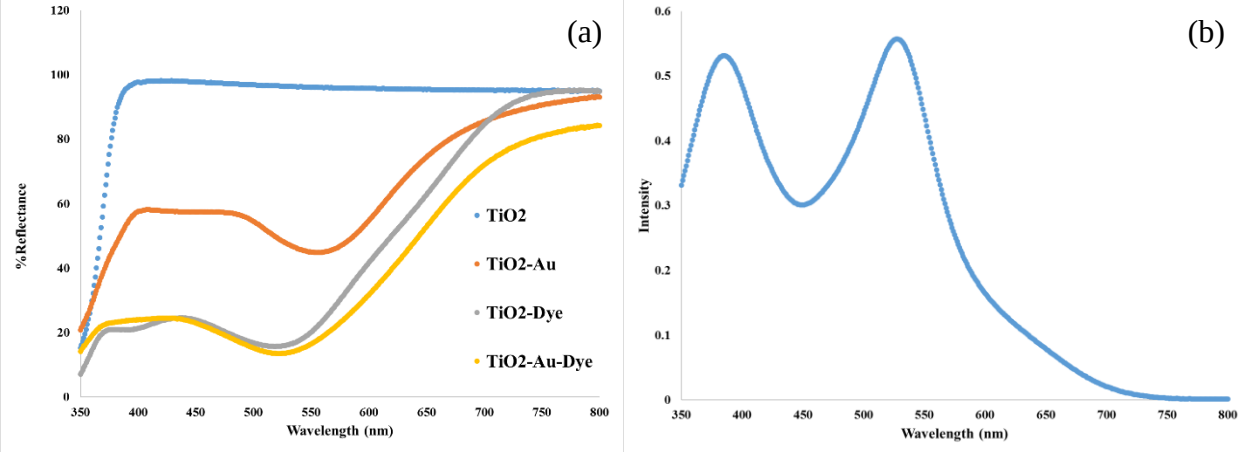

Figure 2.5 (a) Diffuse reflectance of films composed of bare TiO2 (blue), bare TiO2 mixed with 10 nm Au nanoparticles (red), N719 dyed TiO2 (grey), and N719 dyed TiO2 with 10 nm Au nanoparticles. (b) Absorbance of N719 in ethanolic solution.

Figure 2.5 (a) shows a distinct decrease in reflectance over the measured spectrum for films mixed with gold nanoparticles. To confirm the presence of the gold nanoparticles in the film, TEM images were taken. Both samples were prepared from film scrapings taken during shaping of the anodes for cell assembly. Figure 2.6 (b) shows the spherical gold nanospheres absent from

(a). The higher density particles gold particles appear darker than the TiO_2 due to the increased electron deflection.

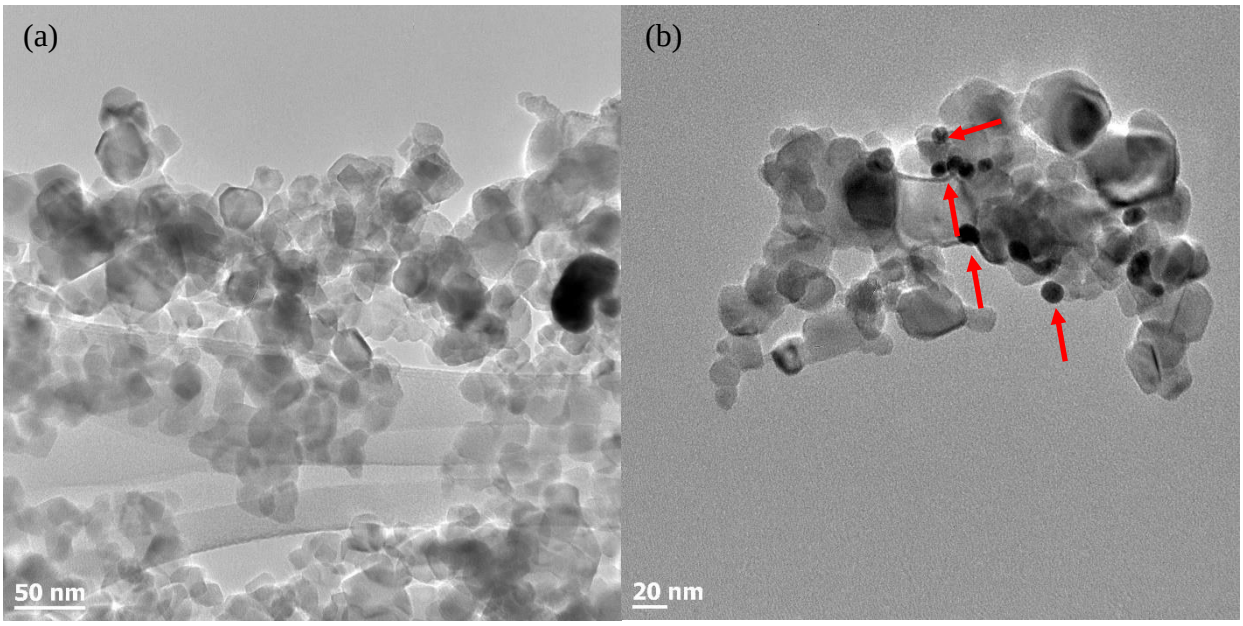

Figure 2.6 TEM images of (a) bare TiO_2 nanoparticles with an average size of 20 nm compared to (b) with the addition of 10 nm Au nanoparticles (red arrows)

Dye-sensitized solar cells were created using both types of films. The average device efficiency for TiO_2 only devices was 4.5% (15 devices +/- 0.2%). The representative J-V curve in Figure 2.7 for TiO_2 only devices has an efficiency of 4.5%, J_{sc} of 8.02 mA/cm^2, a V_{OC} of 0.794 V, and a FF of 0.701. In comparison, the average efficiency for Au nanoparticle modified films was 5.0% (10 devices +/- 0.4%). The representative cell in Figure 2.7 has an efficiency of 5.13%, J_{sc} of 10.54 mA/cm^2, V_{oc} of 0.752 V, and FF of 0.648. This change corresponds to an 11% increase in overall device efficiency by adding plasmonic Au nanoparticles. There is a clear increase in current density for devices containing Au nanoparticles. This effect was observed in all cases when comparing Au modified devices with unmodified devices of the same thickness. There is also a drop in V_{oc} in modified devices compared to the unmodified. These findings are in agreement with those published by Choi et al..[8] This increase in photo current is the expected

result from plasmonic enhancement of the devices. The loss in potential can be explained as a charging effect in the gold.[8]

Gold modified solar cells did suffer from a loss of efficiency over time. This is thought to be caused by dissolving of the gold by the I^-/I_3^- electrolyte and forming AuI_2^- as can be seen in equation (1).[8, 38]

$$2Au + I_3^- + I^- \leftrightarrow 2AuI_2^- \quad (1)$$

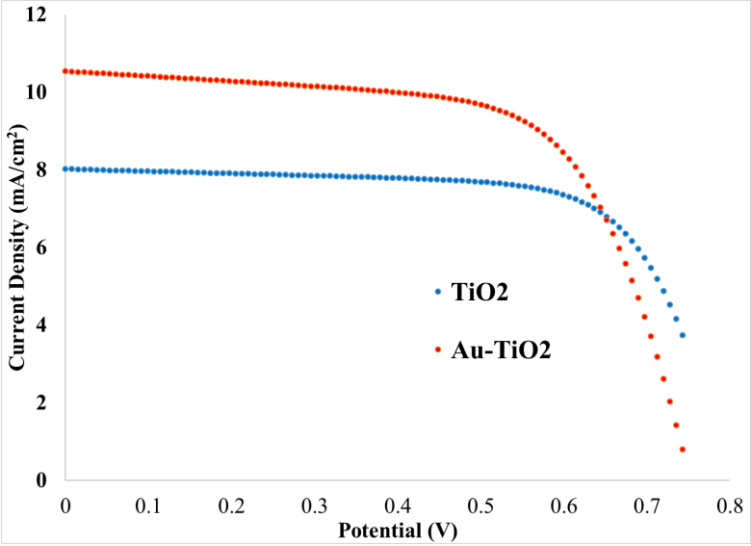

Figure 2.7 Representative J-V curves for cells made with TiO2 (blue) and TiO2 mixed with 10 nm gold nanoparticles (red) showing an increase in current density and corresponding loss in potential

To prevent this loss of gold over time, the particles could be protected with a thin oxide layer. Films would have to be exceedingly thin as plasmonic effects are diminished significantly as the dye moves away from the metal particles. This protection was studied by Choi et al., who found that shells of TiO_2 around 2 nm maintained stability and the 11% plasmonic efficiency enhancement.[8] Another approach would to be to use a non-corrosive electrolyte. Jung et al. replaced the corrosive I^-/I_3^- electrolyte with non-corrosive cobalt(II/III) tris(2,2'-bipyridine) ($[Co(bpy)_3]^{2+/3+}$) system. Their devices also showed an 11% increase in efficiency.[17]

These systems could be maximized with the use of enhanced engineering techniques published by Gratzel et al. Devices using these techniques have been shown to have efficiencies exceeding 10%.[7] In theory these techniques, combined with the newest dyes and electrolyte systems, could allow dye-sensitized devices to reach 15% efficiency or higher. According to the National Renewable Energies Laboratory independently confirmed results, the highest laboratory tested single crystal silicon solar cell has an efficiency of 25%.[39] These devices are widely studied and similar to current commercial devices. This efficiency comes at the high cost of refining high quality, single crystal silicon. As silicon quality decreases, and devices become polycrystalline, efficiencies decrease to 18.5%.[40] Reducing the silicon for these polycrystalline cells is still more energy intensive than the oxidation of titanium into particles for mesoporous devices as this process is energetically favorable. Additionally, mesoporous devices lend themselves well to existing reel-to-reel mass production techniques.

2.4 Conclusions

By creating devices using metal nanoparticles in the starting TiO_2 paste a balance was reached between colloidal synthesis size control, and intimate particle contact between oxide and metal. This approach allows for possible scaling to industrial fabrication. While the gold particles in these devices are unstable in the current system, suspensions of oxide coated particles are commercially available. The use of such particles could prevent device degradation, and increase enhancements further.

2.5 References

1. World energy demand and economic outlook. http://www.eia.gov/outlooks/ieo/world.cfm (accessed 11-23-2016).
2. Hoff, S. Germany's renewables electricity generation grows in 2015, but coal still dominant. http://www.eia.gov/todayinenergy/detail.php?id=26372 (accessed 11-23-2016).
3. Grätzel, M., Recent Advances in Sensitized Mesoscopic Solar Cells. *Accounts of Chemical Research* **2009,** *42* (11), 1788-1798.
4. Zeng, W.; Cao, Y.; Bai, Y.; Wang, Y.; Shi, Y.; Zhang, M.; Wang, F.; Pan, C.; Wang, P., Efficient Dye-Sensitized Solar Cells with an Organic Photosensitizer Featuring Orderly Conjugated Ethylenedioxythiophene and Dithienosilole Blocks. *Chemistry of Materials* **2010,** *22* (5), 1915-1925.
5. Yasuo, C.; Ashraful, I.; Yuki, W.; Ryoichi, K.; Naoki, K.; Liyuan, H., Dye-Sensitized Solar Cells with Conversion Efficiency of 11.1%. *Japanese Journal of Applied Physics* **2006,** *45* (7L), L638.
6. Chung, I.; Lee, B.; He, J.; Chang, R. P. H.; Kanatzidis, M. G., All-solid-state dye-sensitized solar cells with high efficiency. *Nature* **2012,** *485* (7399), 486-489.
7. Ito, S.; Murakami, T. N.; Comte, P.; Liska, P.; Grätzel, C.; Nazeeruddin, M. K.; Grätzel, M., Fabrication of thin film dye sensitized solar cells with solar to electric power conversion efficiency over 10%. *Thin Solid Films* **2008,** *516* (14), 4613-4619.
8. Choi, H.; Chen, W. T.; Kamat, P. V., Know Thy Nano Neighbor. Plasmonic versus Electron Charging Effects of Metal Nanoparticles in Dye-Sensitized Solar Cells. *ACS Nano* **2012,** *6* (5), 4418-4427.
9. O'Regan, B.; Gratzel, M., A low-cost, high-efficiency solar cell based on dye-sensitized colloidal TiO2 films. *Nature* **1991,** *353* (6346), 737-740.
10. Yella, A.; Lee, H.-W.; Tsao, H. N.; Yi, C.; Chandiran, A. K.; Nazeeruddin, M. K.; Diau, E. W.-G.; Yeh, C.-Y.; Zakeeruddin, S. M.; Grätzel, M., Porphyrin-Sensitized Solar Cells with Cobalt (II/III)–Based Redox Electrolyte Exceed 12 Percent Efficiency. *Science* **2011,** *334* (6056), 629-634.
11. Huang, X.; Huang, S.; Zhang, Q.; Guo, X.; Li, D.; Luo, Y.; Shen, Q.; Toyoda, T.; Meng, Q., A flexible photoelectrode for CdS/CdSe quantum dot-sensitized solar cells (QDSSCs). *Chemical Communications* **2011,** *47* (9), 2664-2666.
12. Law, M.; Greene, L. E.; Johnson, J. C.; Saykally, R.; Yang, P., Nanowire dye-sensitized solar cells. *Nat Mater* **2005,** *4* (6), 455-459.
13. Sahu, G.; Wang, K.; Gordon, S. W.; Zhou, W.; Tarr, M. A., Core-shell Au-TiO2 nanoarchitectures formed by pulsed laser deposition for enhanced efficiency in dye sensitized solar cells. *RSC Advances* **2012,** *2* (9), 3791-3800.
14. Qi, J.; Dang, X.; Hammond, P. T.; Belcher, A. M., Highly Efficient Plasmon-Enhanced Dye-Sensitized Solar Cells through Metal@Oxide Core–Shell Nanostructure. *ACS Nano* **2011,** *5* (9), 7108-7116.
15. Sheehan, S. W.; Noh, H.; Brudvig, G. W.; Cao, H.; Schmuttenmaer, C. A., Plasmonic Enhancement of Dye-Sensitized Solar Cells Using Core–Shell–Shell Nanostructures. *The Journal of Physical Chemistry C* **2013,** *117* (2), 927-934.
16. Sahu, G.; Gordon, S. W.; Tarr, M. A., Synthesis and application of core-shell Au-TiO2 nanowire photoanode materials for dye sensitized solar cells. *RSC Advances* **2012,** *2* (2), 573-582.

17. Jung, H.; Koo, B.; Kim, J.-Y.; Kim, T.; Son, H. J.; Kim, B.; Kim, J. Y.; Lee, D.-K.; Kim, H.; Cho, J.; Ko, M. J., Enhanced Photovoltaic Properties and Long-Term Stability in Plasmonic Dye-Sensitized Solar Cells via Noncorrosive Redox Mediator. *ACS Applied Materials & Interfaces* **2014,** *6* (21), 19191-19200.
18. Wozny, S.; Wang, K.; Zhou, W., Cu2ZnSnS4 nanoplate arrays synthesized by pulsed laser deposition with high catalytic activity as counter electrodes for dye-sensitized solar cell applications. *Journal of Materials Chemistry A* **2013,** *1* (48), 15517-15523.
19. Kwon, T.-H.; Armel, V.; Nattestad, A.; MacFarlane, D. R.; Bach, U.; Lind, S. J.; Gordon, K. C.; Tang, W.; Jones, D. J.; Holmes, A. B., Dithienothiophene (DTT)-Based Dyes for Dye-Sensitized Solar Cells: Synthesis of 2,6-Dibromo-DTT. *The Journal of Organic Chemistry* **2011,** *76* (10), 4088-4093.
20. Nazeeruddin, M. K.; Péchy, P.; Renouard, T.; Zakeeruddin, S. M.; Humphry-Baker, R.; Comte, P.; Liska, P.; Cevey, L.; Costa, E.; Shklover, V.; Spiccia, L.; Deacon, G. B.; Bignozzi, C. A.; Grätzel, M., Engineering of Efficient Panchromatic Sensitizers for Nanocrystalline TiO2-Based Solar Cells. *Journal of the American Chemical Society* **2001,** *123* (8), 1613-1624.
21. Chen, C.-Y.; Wang, M.; Li, J.-Y.; Pootrakulchote, N.; Alibabaei, L.; Ngoc-le, C.-h.; Decoppet, J.-D.; Tsai, J.-H.; Grätzel, C.; Wu, C.-G.; Zakeeruddin, S. M.; Grätzel, M., Highly Efficient Light-Harvesting Ruthenium Sensitizer for Thin-Film Dye-Sensitized Solar Cells. *ACS Nano* **2009,** *3* (10), 3103-3109.
22. Mai, C.-L.; Huang, W.-K.; Lu, H.-P.; Lee, C.-W.; Chiu, C.-L.; Liang, Y.-R.; Diau, E. W.-G.; Yeh, C.-Y., Synthesis and characterization of diporphyrin sensitizers for dye-sensitized solar cells. *Chemical Communications* **2010,** *46* (5), 809-811.
23. Hsieh, C.-P.; Lu, H.-P.; Chiu, C.-L.; Lee, C.-W.; Chuang, S.-H.; Mai, C.-L.; Yen, W.-N.; Hsu, S.-J.; Diau, E. W.-G.; Yeh, C.-Y., Synthesis and characterization of porphyrin sensitizers with various electron-donating substituents for highly efficient dye-sensitized solar cells. *Journal of Materials Chemistry* **2010,** *20* (6), 1127-1134.
24. Dingwen, Z.; Milton, W.; Alexandre, G. B.; Jie, S.; Xiaodong, L.; Sumei, H., Enhanced performance of dye-sensitized solar cells using gold nanoparticles modified fluorine tin oxide electrodes. *Journal of Physics D: Applied Physics* **2013,** *46* (2), 024005.
25. Hammond, J.; Bhalla, N.; Rafiee, S.; Estrela, P., Localized Surface Plasmon Resonance as a Biosensing Platform for Developing Countries. *Biosensors* **2014,** *4* (2), 172.
26. Cheng, W.-Y.; Deka, J. R.; Chiang, Y.-C.; Rogeau, A.; Lu, S.-Y., One-Step, Surfactant-Free Hydrothermal Method for Syntheses of Mesoporous TiO2 Nanoparticle Aggregates and Their Applications in High Efficiency Dye-Sensitized Solar Cells. *Chemistry of Materials* **2012,** *24* (16), 3255-3262.
27. Jeong, N. C.; Prasittichai, C.; Hupp, J. T., Photocurrent Enhancement by Surface Plasmon Resonance of Silver Nanoparticles in Highly Porous Dye-Sensitized Solar Cells. *Langmuir* **2011,** *27* (23), 14609-14614.
28. Karna, H. E. C. M. H. G. S. P., Synthesis, Characterization, and Application of Gold Nanoparticles in Green Nanochemistry Dye-Sensitized Solar Cells. Laboratory, A. R., Ed. 2012.
29. Jung, L. S.; Campbell, C. T.; Chinowsky, T. M.; Mar, M. N.; Yee, S. S., Quantitative Interpretation of the Response of Surface Plasmon Resonance Sensors to Adsorbed Films. *Langmuir* **1998,** *14* (19), 5636-5648.
30. Jennifer M. Brockman; Bryce P. Nelson, a.; Corn, R. M., SURFACE PLASMON RESONANCE IMAGING MEASUREMENTS OF ULTRATHIN ORGANIC FILMS. *Annual Review of Physical Chemistry* **2000,** *51* (1), 41-63.

31. Srituravanich, W.; Fang, N.; Sun, C.; Luo, Q.; Zhang, X., Plasmonic Nanolithography. *Nano Letters* **2004,** *4* (6), 1085-1088.
32. Willets, K. A.; Duyne, R. P. V., Localized Surface Plasmon Resonance Spectroscopy and Sensing. *Annual Review of Physical Chemistry* **2007,** *58* (1), 267-297.
33. Kelly, K. L.; Coronado, E.; Zhao, L. L.; Schatz, G. C., The Optical Properties of Metal Nanoparticles: The Influence of Size, Shape, and Dielectric Environment. *The Journal of Physical Chemistry B* **2003,** *107* (3), 668-677.
34. Nie, S.; Emory, S. R., Probing Single Molecules and Single Nanoparticles by Surface-Enhanced Raman Scattering. *Science* **1997,** *275* (5303), 1102.
35. Underwood, S.; Mulvaney, P., Effect of the Solution Refractive Index on the Color of Gold Colloids. *Langmuir* **1994,** *10* (10), 3427-3430.
36. Chen, H.; Kou, X.; Yang, Z.; Ni, W.; Wang, J., Shape- and Size-Dependent Refractive Index Sensitivity of Gold Nanoparticles. *Langmuir* **2008,** *24* (10), 5233-5237.
37. Liz-Marzán, L. M.; Giersig, M.; Mulvaney, P., Synthesis of Nanosized Gold−Silica Core−Shell Particles. *Langmuir* **1996,** *12* (18), 4329-4335.
38. Konyratbekova, S. S.; Baikonurova, A.; Ussoltseva, G. A.; Erust, C.; Akcil, A., Thermodynamic and kinetic of iodine–iodide leaching in gold hydrometallurgy. *Transactions of Nonferrous Metals Society of China* **2015,** *25* (11), 3774-3783.
39. Photovoltaic Research. http://www.nrel.gov/pv/ (accessed 11-28-2016).
40. Green, M. A.; Emery, K.; Hishikawa, Y.; Warta, W.; Dunlop, E. D., Solar cell efficiency tables (Version 45). *Progress in Photovoltaics: Research and Applications* **2015,** *23* (1), 1-9.

Chapter 3 Quantum dot sensitized solar cells

3.1 Introduction

Dye sensitized solar cells have been a major focus of research in recent years for their stability, lost cost of production, and overall efficiency.[1] These devices employ a mesoporous titanium dioxide (TiO_2) film attached to a fluorine doped tin oxide glass substrate. These mesoporous films are then sensitized with organo-metallic dye molecules that absorbs photons and injects their excited electrons into the TiO_2 network. The dye is then brought back to the ground state with an electron from a redox shuttle, which is then in turn regenerated by a platinum counter-electrode. [1-6]

There have been multiple studies on improving this system to increase overall cell efficiency. New dyes with improved absorbance ranges, less toxic metals, or higher stability are all commonly studied.[3, 7-15] There have also been studies on the redox shuttle used. Both changing the composition of the liquid electrolyte[13, 16], or using a solid material.[17] The platinum catalyzed counter electrode is not only expensive, but also a fairly rare metal. Because of this there have also been studies to replace it with cheaper and more abundant alternatives.[18-21]

To measure the efficiency of a solar cell, a J-V curve is recorded at A.M. 1.5 light or 1000 W/m^2. This is the current density (J, mA/cm^2) graphed against the applied voltage (V). Figure 3.1 shows a typical J-V curve with the important details highlighted. With an applied back-voltage of 0 V the maximum current of the cell is the short-circuit current density (J_{SC}) of the device. At the other extreme of the data is the point where the applied back-voltage is equal to the voltage of the device, this is known as the open-circuit voltage (V_{OC}). This maximum current density and voltage together equal the theoretical maximum power (P_{Theo}) whereas P_{max} is the actual maximum power output. When analyzing the slope of the line that intersects J_{SC}, the inverse is equal to the short circuit or shunt resistance (R_{SH}). This is how resistant the device is to having electrons traveling in the wrong direction. Ideally this resistance is infinite and the slope is zero. The inverse of the slope of the line intercepting V_{OC} is the transport or series resistance (R_S). This is the resistance the electrons encounter traveling through the device. Ideally this resistance is zero, and the line is perpendicular to the x-axis. The ratio of the P_{max}/P_{Theo} is known as the fill factor (FF) is a measure of the "squareness" of the graph or how close to the ideal

shape it is. The final, and most important, piece of information obtained from this graph is the device efficiency. This is the ratio of the maximum power over the power of the input or P_{max}/P_{in}.

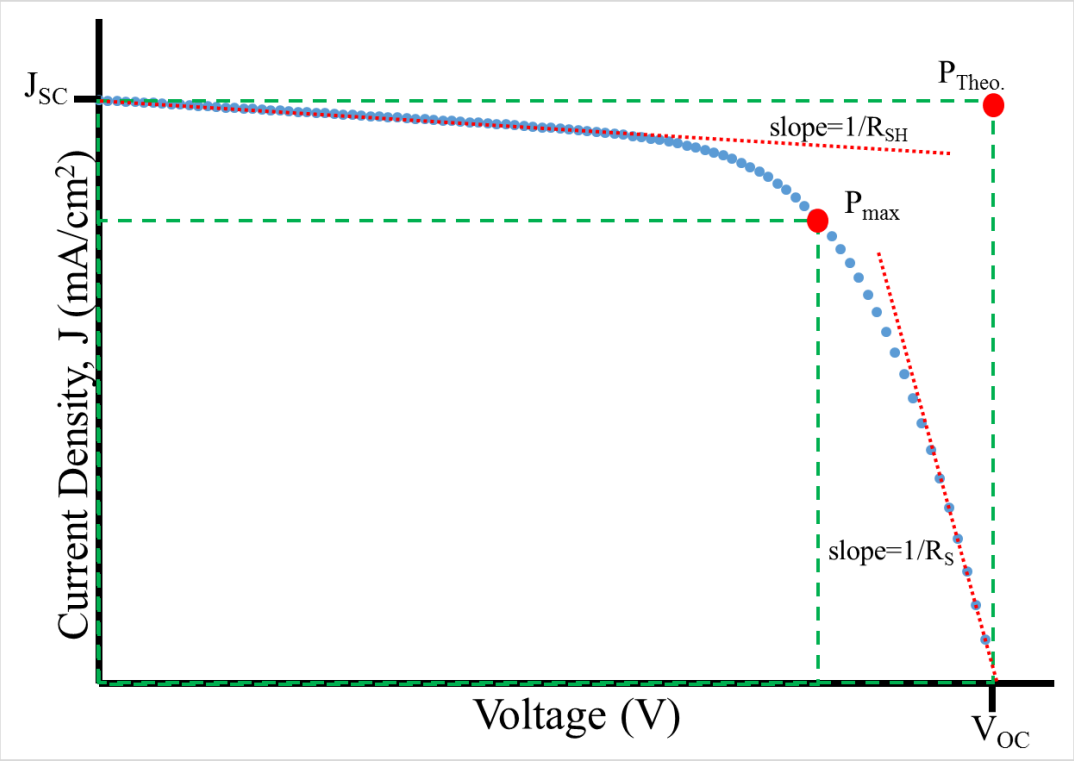

Figure 3.1 Sample J-V curve labeled with shunt resistance (R_{SH}), series resistance (R_s), maximum power (P_{max}), theoretical power ($P_{Theo.}$), short-circuit current density (J_{SC}), and open circuit voltage (V_{OC})

Not surprisingly, the mesoporous film has also received attention[22-32]. The serpentine pathway presented electrons by a mesoporous film creates an extended path length. This increases the likelihood for recombination of the electrons with defect sites. The grain boundaries created by sintering nanoparticles creates an increased series resistance to the system as well. To reduce the resistance due to grain boundaries Wijnhoven et al. proposed the use of their "air sphere" reverse opal system as a suitable substrate, although they did not actually prepare devices.[27] Despite this, a highly porous network created around a sacrificial support via a chemical deposition method would have fewer grain boundaries and therefore less transport resistance. Ohsaki et al. proposed using a solution synthesized nanotube paste to replace the traditional nanoparticles.[23] Others have reported highly ordered arrays of vertically aligned TiO_2 nanotubes as cathodes.[22, 24, 30-31]

As an alternative to organometallic dyes semiconductor nanocrystals with tunable bandgaps, known as quantum dots (QDs), could be employed. As these particles decrease in size approaching their Bohr exciton radius, their bandgaps begin changing from that of bulk material. As the particle size decreases, the bandgap of the particle increases.[33] With careful size control and composition these nanoparticles can be tuned to absorb more of the solar spectrum. These materials are also well studied with protocols for varying sizes and compositions available.[10, 34-44] These materials do have some drawbacks. Since the majority of QDs are produced with a combination of elements from groups II-VI of the periodic table, they often contain elements that are either rare, toxic, or both. This balance between control, cost, and toxicity all should be considered when choosing a material.

Considering these variables, zinc sulfide coated cadmium selenide (CdSe/ZnS) and PbS quantum dots (QDs) were used independently to sensitize TiO_2 mesoporous substrates. In addition, different counter electrode architectures and materials were studied to explore optimization routes.

3.2 Experimental

3.2.1 Preparation of TiO_2 paste.

The unmodified paste was made by dissolving 100 µL Triton X-100 (Sigma) and 0.2 g 20,000 MW PEG (Fluka) in 3.0 mL 0.1 M aqueous acetic acid in a 15 mL centrifuge tube. Once the PEG had dissolved completely, 0.5 g TiO_2 nanopowder (Sigma, anatase nanopowder) was mixed in to make a thick paste. The tube was then sealed and left in an ultrasonic bath for approximately 60 minutes.

3.2.2 Preparation of Mesoporous Film.

Pieces of FTO glass (Sigma, 8 Ω/sq) were cut into approximately 3x2 cm pieces. They were cleaned by submersion in a 1% Alconox solution and sonicating for 60 minutes. They were then washed with Nanopure (deionized 18 Ω/sq, 0.02 µm filtered) water and sonicated for another 60 minutes in Nanopure water to remove any remaining Alconox. Finally, the substrates were sonicated for 60 minutes in isopropyl alcohol and stored in alcohol until use. After drying, the glass was placed in a petri dish conductive side up and covered with 0.04 M $TiCl_4$ solution that was prepared by diluting pure $TiCl_4$ (Sigma) with Nanopure water at 0°C. The substrates were

then heated at 60°C for 1 hour, rinsed with Nanopure water, dried, and annealed at 500°C for 30 minutes. The cooled substrates were taped to the bench, conductive side up, using Scotch™ brand tape leaving a 6 mm wide strip of exposed glass. The tape acted to immobilize the glass and as a spacer for uniform film deposition. A small amount of prepared TiO_2 paste was deposited along the top edge of the glass, and pulled across the surface by a microscope slide edge held flush to the substrate. This is often referred to as the doctor blade method. After drying the films their thickness was measured with a profilimeter (Dektak). Films less than 12 µm had a second layer of TiO_2 deposited. Films were sintered at 450°C for 30 minutes then allowed to cool to room temperature.

3.2.3 Successive ionic layer adsorption and reaction (SILAR)

3.2.3.1 Lead sulfide SILAR

Solutions of 0.01 M lead nitrate ($Pb(NO_3)_2$) (Fisher, certified ACS) in methanol (Fisher, ACS grade) and 0.01M sodium sulfide (Na_2S) (Alfa Aesar, anhydrous) in 1:1 (v/v) methanol: Nanopure water were prepared. FTO substrates with mesoporous TiO_2 films were first submerged in the lead solution for 1 minute, rinsed, then dried with nitrogen. These dried films were then submerged in the sulfur solution for 1 minute, rinsed, and dried with nitrogen. This was one SILAR cycle.

3.2.3.2 Cadmium sulfide SILAR

A solution of 0.05 M cadmium sulfate (Fisher, ACS) in a 1:1 (v/v) ratio of ethanol (200 proof, Aaper Alcohol) to Nanopure water and a solution of 0.05M Na_2S in 1:1 (v/v) ratio of methanol: Nanopure water. Substrates were soaked in the cadmium solution for 1 minute, rinsed with 200 proof ethanol, then dried with nitrogen. The substrates were then soaked in the sulfur precursor for 1 minute, rinsed with methanol, then dried with nitrogen. This was one SILAR cycle.

3.2.3.3 Zinc sulfide SILAR

Solutions of 0.1 M zinc acetate (Fisher, certified) solution in water and 0.1 M Na_2S in 1:1 (v/v) methanol: water were prepared. Previously sensitized substrates were soaked first in the zinc solution, rinsed with water, and dried with nitrogen. The substrates were then soaked in the

sulfur precursor, rinsed with methanol, and dried with nitrogen. This was a full SILAR cycle for the ZnS capping layer.

3.2.4 QD synthesis

3.2.4.1 CdSe/ZnS QD synthesis

CdSe/ZnS QDs were prepared using a modified version of a previously published method.[45] In a 100 mL 3-neck flask 30 mg cadmium oxide (CdO, Sigma) and 180 mg lauric acid(Sigma). The system was connected to a condenser, the other two necks closed with septa, and the flask was evacuated for 10 minutes. The flask was then flushed with ultra-high purity argon (UHP Ar), and the flow was adjusted so a very small flow remained (approximately 1 bubble per second). The system was heated to 80°C and 2 g hexadecylamine (Sigma, Tech. grade 90% pure) and 2 g trioctylphosphine oxide (TOPO, Sigma, Tech. grade 90% pure) were added. The system was then purged and flushed with UHP Ar three times to remove any oxygen and returned to a slow flow of blanket UHP Ar. The system was heated to 280°C over 1 hour and stirred until the solution turned clear. While the Cd solution was heating, 80 mg selenium (Se) was dissolved in 2 mL trioctylphosphine (TOP, Sigma, Tech. grade 90% pure) and stored under flowing UHP Ar until use. Once the Cd solution was clear it was cooled to 225°C and stirred vigorously. The Se solution was then rapidly injected under the surface of the Cd solution. The mixture quickly changes color as the crystals grow. The solution was immediately quenched in an ice bath after the color began appearing (approximately 30 seconds from injection). The solution was then brought back up to 180°C for the shell growth. A solution containing 2 mL TOP, 250 µL hexamethyldisilathiane, and 1 mL diethyl zinc (Sigma, 1.0 M solution in heptane) was then dripped into the CdSe QD solution. The system was held at 180°C for 1 hour to allow for shell growth. The CdSe/ZnS QDs were allowed to cool to room temperature. The QDs were precipitated using methanol and centrifuged at 4000 rpm for 10 minutes. This was repeated 3 more times for a total of 4 washes. The QDs were then suspended in hexanes at 25 mg QDs per mL chloroform. This QD solution was then used in some cases to replace the chloroform used in TiO_2 shell growth.

3.2.4.2 PbS QD synthesis

PbS QDs were prepared using a modified version of a published method.[44] In a 100 mL 3-neck flask 18.8 mmol octadecene (Acros, 90% Technical grade), 28.5 mmol oleic acid (Acros,

97%), and 12 mmol lead oxide (Acros, 99.9+%) were heated to 100 °C under vacuum and vigorous stirring. After 1 hour the solution became clear, and ultra-high purity argon (UHP Ar) was flushed over the reaction at a low rate (1 bubble/sec in the bubbler). The temperature was decreased to 80°C. As the solution was heating, 4 g octadecene and 6 mmol hexamethyldisilathiane (Sigma, synthesis grade) were sealed into a conical 10 mL flask and purged with UHP Ar. After the lead solution had stabilized at 80°C the sulfur solution was rapidly injected. The mixture quickly turned from clear to black and was allowed to stir for 2 minutes. The reaction was then quenched in an ice bath to bring it to room temperature. The particles were then precipitated with acetone and separated by centrifugation at 3000 rpm for 5 minutes. The pellets were then suspended using minimal hexanes and ultra-sonication to break up larger agglomerates. These suspensions were then precipitated with acetone and centrifuged. This was done three times to remove any unreacted precursors. QDs were suspended in hexanes at 25 mg/mL. After depositing onto TiO_2 substrates, films were treated with one cycle of ZnS SILAR to protect QDs from the electrolyte.

3.2.5 Chemical binding of colloidal QDs to TiO_2 films

A 10% (v/v) solution of 3-mercaptopropionic acid (3-MPA, Sigma) was prepared in methanol. The substrate had a drop of 3-MPA added, reacted for 1 minutes, then it was rinsed with methanol and dried with a nitrogen stream. A drop of QD solution was added, allowed to react for 1 minute, then excess rinsed with hexanes and dried with nitrogen.

Alternatively, substrates were submerged in the 3-MPA solution overnight to ensure maximum surface modification. The substrates were then rinsed with methanol and nitrogen dried. They were then submerged in QD solutions up to 24 hours in a sealed container in the refrigerator.

3.2.6 Copper sulfide counter electrodes

3.2.6.1 Sputtered copper electrode

Cleaned and dried pieces of FTO glass were arranged in the sputtering instrument (Denton Vacuum Desk V), and it was set to 40 amps and 600 s. Copper was sputtered onto FTO glass. These substrates were then soaked in a portion of electrolyte solution for 30 minutes.

3.2.6.2 Mesoporous ITO Film electrode

A paste identical to the TiO_2 substrate precursor for the QDs was made using indium tin oxide (ITO) nanoparticles (Alfa Aesar, NanoTek 99.5%, product # 44927). After sintering and cooling these films were deposited with copper sulfide (Cu_2S) using a SILAR process. The copper precursor was aqueous 0.1 M copper nitrate (Fisher, certified ACS), and the sulfur precursor was an aqueous 0.1 M Na_2S solution. For each element the substrate was soaked in the precursor for 1 minute, rinsed then nitrogen dried. Each film was deposited for 12 cycles.

3.2.6.3 Brass electrode

Following published protocols[39-40] pieces of brass from the local hardware store were cut to approximately 3x2 cm sizes. These metal substrates then were then exposed to a 30% HCl (Fisher, certified ACS Plus) aqueous solution for 10 minutes. The substrates were then rinsed with Nanopure water, dried with nitrogen, and soaked in a portion of electrolyte for 30 minutes. The substrates were again rinsed, and dried, then immediately used to prevent possible oxidation.

3.2.7 Device assembly

Cleaned pieces of FTO glass had a thin layer of organo-metallic platinum precursor, Platisol (Solaronix), applied with a cotton applicator and were annealed at 400°C for 30 minutes. The cooled platinized glass had a 0.4 mm diameter hole drilled through for later electrolyte filling. The sensitized TiO_2 films were scraped down to a 6 x 8 mm area. The two pieces of FTO were sealed together with a 60 μm thick Surlyn thermoplastic (Solaronix) gasket. The two electrodes were offset to allow easy electrode attachment for testing. The polysulfide electrolyte was prepared in water, and contained 1.0 M Na_2S, 1.0 M sulfur (EM Science, sublimed), and 0.1 M NaOH (Fisher, ACS pellets). The devices were placed in a vacuum desiccator with a drop of electrolyte over the hole. The desiccator was pumped down pulling the air out of the void space of the devices. Once the atmosphere was returned to the desiccator, the electrolyte was pulled into the void. The devices were sealed using a small square of Surlyn and square of microscope slide, and the edges painted with silver paint (Ted Pella) for better testing electrode contact.

3.2.8 Characterization

Film thickness was measured with a Sloan Dektak IIA profilimeter. Absorbance measurements were performed using a Cary 500 UV-Vis spectrometer. Photovoltaic

measurements were performed using a Newport® 50-500 W 67005 solar simulator set at 100 mW/cm^2. The light intensity of the xenon lamp was calibrated using a National Renewable Energy Laboratory (NREL) calibrated silicon photodiode (Hamamatsu S1787-08 for visible to IR range). Current density-voltage (J-V) curves were measured with a Keithley 2400 source meter.

3.3 Results and discussion

The first cell design to be tested were the SILAR sensitized devices. These devices had 2 cycles of PbS, 7 of CdS, and 3 of ZnS as a protective layer. Since the SILAR process creates a thin film of material across the entire area of the substrate, instead of individual particles like colloidal synthesis, an incident photon to current efficiency analysis was performed. This is the efficiency of a device at each wavelength to convert incident light to power. In Figure 3.2 a representative cell can be seen to extend the range of effect for a device well outside the range of the bare TiO_2 reference device. The reference device was assembled identically, only the film was not sensitized.

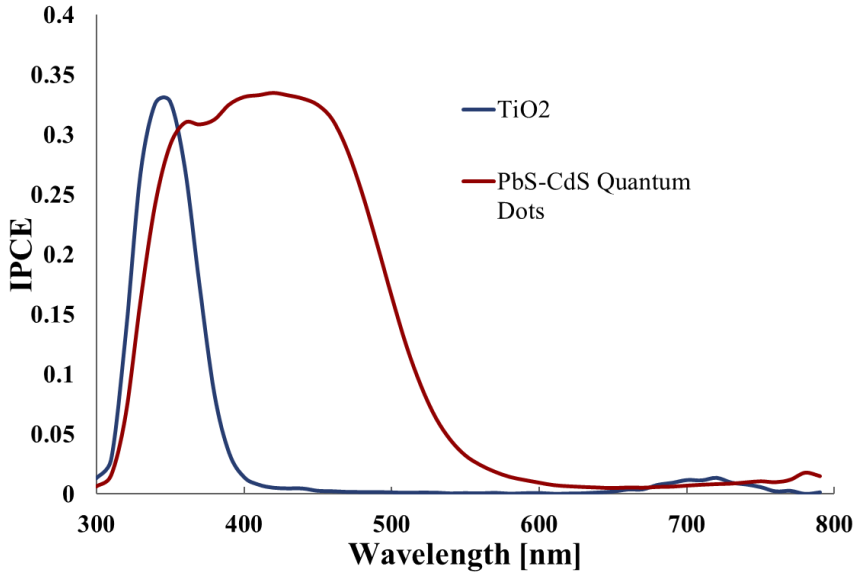

Figure 3.2 Incident photon to current efficiency vs wavelength for a device with only TiO_2 (blue) and a device coated in PbS-CdS quantum dots (red)

While these devices showed an improvement in light harvesting, the efficiencies were low. The J-V curve for the champion cell can be seen in Figure 3.3.

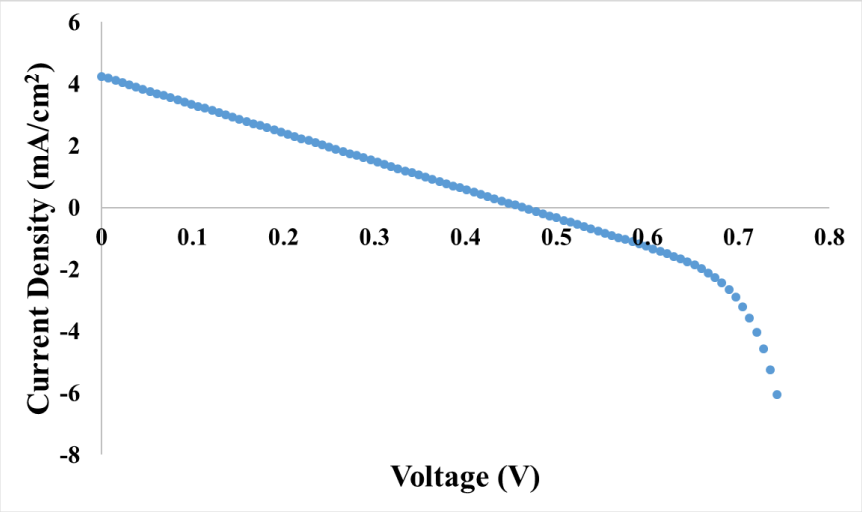

Figure 3.3 Photocurrent density as a function of applied voltage for a champion SILAR device

This champion cell had an efficiency of 0.49%. While the low short-circuit current was a factor, the low recombination resistance is also a major contributor. The band gaps of the semiconductors in a photovoltaic are tuned to reduce recombination. As can be seen in Figure 3.4 the conduction band align so the electrons flow towards the TiO_2 film. They are also aligned so the holes travel to the electrolyte.

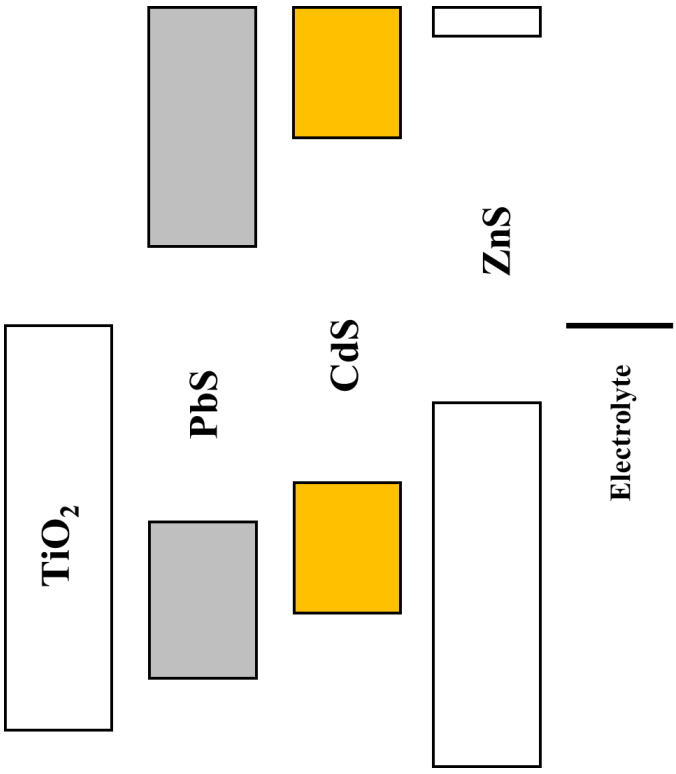

Figure 3.4 Representative cartoon of band-gap alignment for layered semiconductor sensitizer on TiO_2 substrate

While this cartoon is an ideal case, in practice the bandgaps are dependent on the size and shape of the material. As the semiconductors become smaller than their Bohr exciton radius, their bandgap increases in energy and shifts. As an example PbS shifts from the bulk value of 0.40 eV with the conduction band at -4.50 eV vs vacuum[46] to 1.4 eV with the conduction band at -3.7 eV vs vacuum for 2 nm quantum dots.[41] In comparison bulk TiO_2 has a bandgap of 3.2 eV and a conduction band at -4.1 eV vs vacuum. The smaller PbS QDs will readily give up their electrons, while the bulk PbS would be unable.

With this in mind, an approach was devised to have better control of this gap alignment. To do this, colloidal CdSe/ZnS QDs were synthesized to sensitize fabricated mesoporous films. These QDs were found to have a first absorption maximum at 500 nm as can be seen in Figure 3.5. Using Planck's constant in eV·s and the speed of light in nm/s, the bandgap was calculated to be 2.48 eV with a conduction band at -3.22 eV vs vacuum.

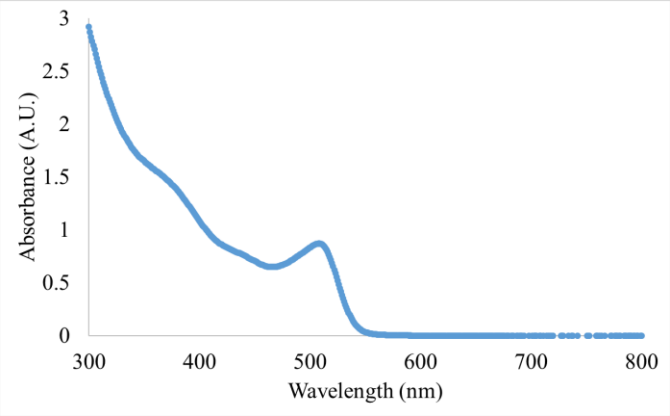

Figure 3.5 Absorbance of CdSe/ZnS QDs suspended in hexanes

The champion cell for of this type had an efficiency of only 0.0145% which is very low for a device of this type. Like the SILAR device, these devices had a V_{oc} of 0.5 V. However, the J_{sc} for these devices were lower by a factor of nearly 100. As can be seen in Figure 3.6, the device has improved recombination resistance compared to SILAR devices. The low current density can be contributed to low light absorbance, or poor catalytic activity at the counter electrode. To increase light absorbance films were soaked for longer periods of time in the QD solution. However, any soaking longer than overnight, and some even overnight, caused the TiO_2 films to flake off the FTO. To increase loading, improved adhesion of the TiO_2 film will needed to be studied.

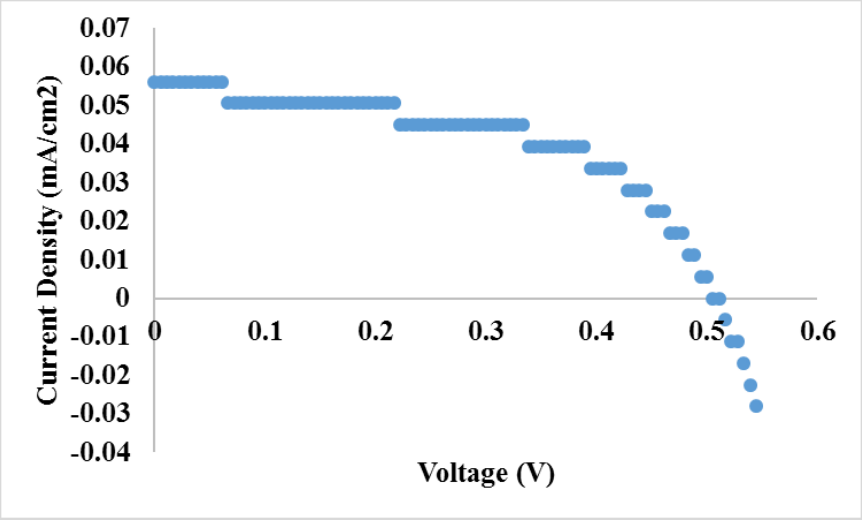

Figure 3.6 Photocurrent density vs voltage curve for champion CdSe/ZnS device

Gimenez et. al studied the effect of the catalytic electrode composition on device performance. Their studies found a 3-fold increase in efficiency from platinum to copper sulfide (Cu_2S). Their studies also support a theory of low J_{sc} due to poor QD loading into the mesoporous film.[40] To make this Cu_2S electrode, published results used a piece of brass soaked in HCl then soaked in a batch of electrolyte.[39-40] Since brass is an alloy of copper and zinc with trace other metals, the HCl removes the zinc leaving behind a high surface area copper substrate. While these have been shown to work, a transparent alternative was desired.

The first attempt to reproduce this was to sputter copper onto FTO substrates. This process had poor results. The biggest problem being the sputtering step. While some batches produced a reflective copper colored coating, other produced a matte black and uneven film. Due to this non-reproducible nature, and poor results, other methods were investigated.

To maintain a high surface area, ITO mesoporous films were sensitized using a SILAR process. These films were produced to be approximately 6 μm thick. This was to allow for sufficient catalytic surface area without causing an electron transport problem. After deposition, films presented as a dark gray color but were still optically transparent when held to a light source. To test film resistance, a probe was place on the top of the mesoporous film and another at the edge of the glass. They produced a resistance from 10-15 Ω, meaning the films were not insulating. Devices created in this manner had very low photocurrents. On the order of 0.01 mA/cm^2 in the best-case devices. The J-V curves did show the characteristic diode behavior expected from a device with no shorts. This low photocurrent could be contributed to poor QD or catalyst performance.

To compare the catalytic performance against published results, devices were created using modified brass as the counter electrode. These devices presented a fabrication problem. The thermoplastic used in other devices was unable to bind reliably to the metal surface. Different techniques for improving adhesion were studied, all with little effect. To test these devices, the two halves were instead held together with binder clips. This device assembly process leads to leaking of the electrolyte and is not ideal. Unfortunately, even the best devices showed results well below those previously published. The J-V curve for the highest efficiency brass device can be seen in Figure 3.7.

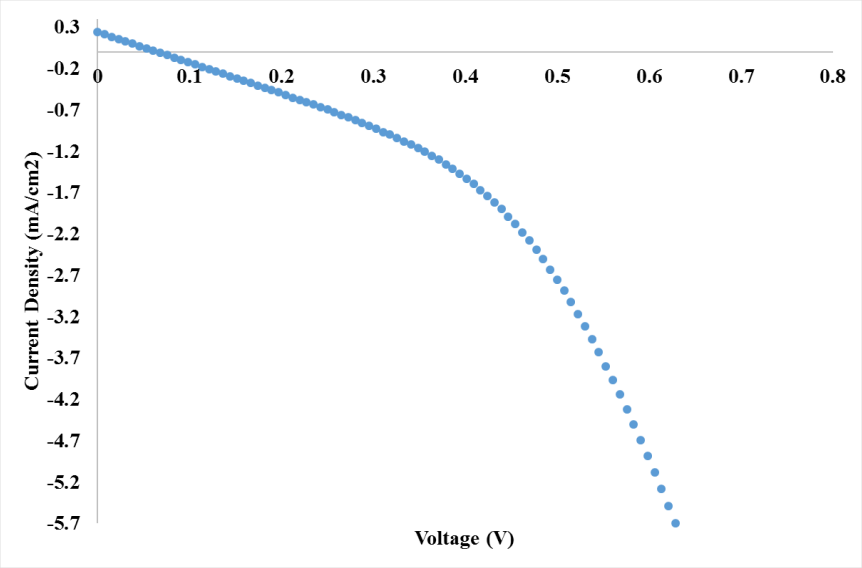

Figure 3.7 Photocurrent density vs voltage curve for device made with modified brass counter electrode

The J_{sc} for this device is 20 times lower than devices reported by Gimenez et. al[40] with a proportional loss of V_{oc} and efficiency. With an optimum efficiency of only 0.01% these devices are far from optimized.

To analyze the effects of QD type on current density, PbS QDs were used as a sensitizer with the ITO mesoporous counter electrodes. Since PbS QDs are reported to be sensitive to the polysulfide electrolyte[46] the sensitized films were treated with one SILAR cycle of ZnS to create a thin protective coating. From Figure 3.8 it can be seen that the best PbS sensitized device had 10 times the current density of the best CdSe device in Figure 3.6.

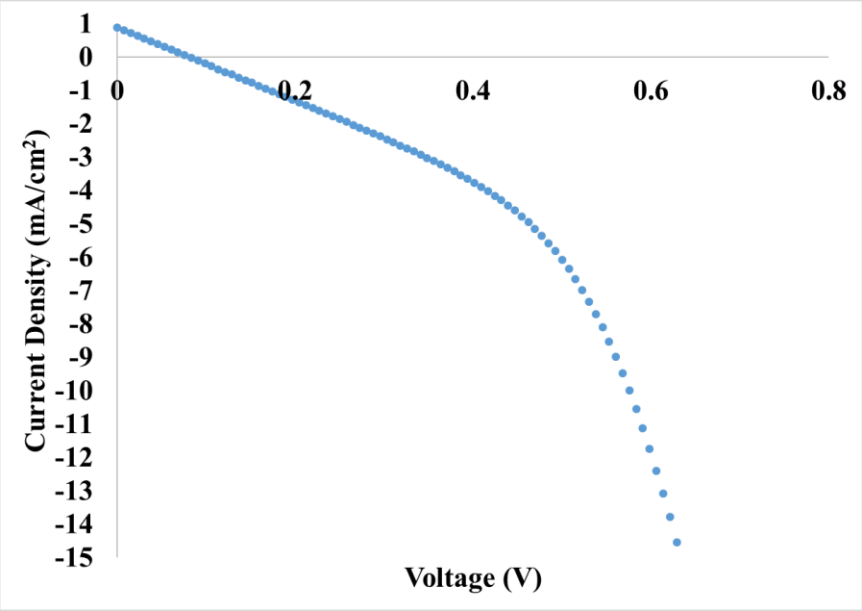

Figure 3.8 Photocurrent density vs voltage curve for PbS sensitized device with ITO counter electrode

This increase in current density can be attributed to higher loading of the smaller PbS QDs and a broader absorption spectrum. From the absorbance spectrum in Figure 3.9 it is clear that the PbS absorbs much more broadly than the CdSe/ZnS QDs that do not begin absorbing until around 550 nm.

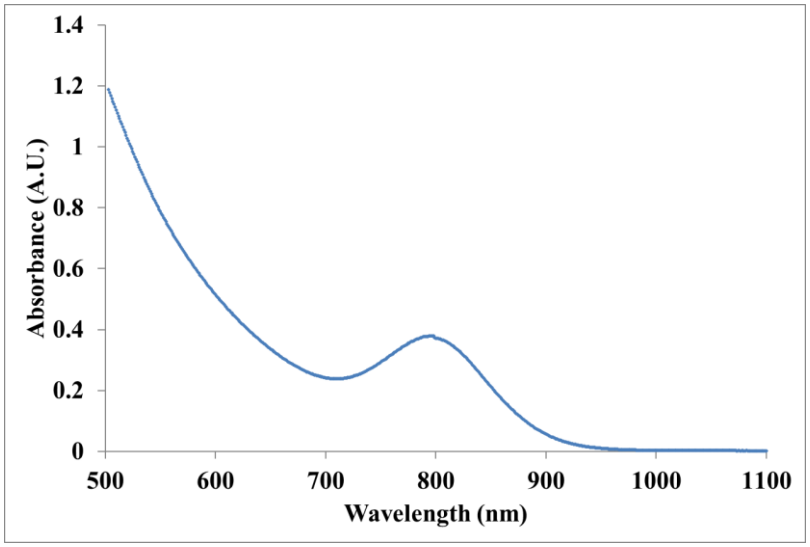

Figure 3.9 Absorbance spectrum for PbS QDs suspended in hexanes with maximum at 800 nm.

While these PbS devices are still not optimized, they show potential to surpass the CdSe/ZnS devices. PbS QDs have their sizes controlled by the molar ratios of the precursors with a number of protocols published for well controlled size production.[42, 44, 47] In contrast CdSe QD size is controlled by reaction time and quenching speed.

3.4 Conclusions

With an understanding of how each component of the solar cell effects the overall performance, future studies can focus on optimizing each. To improve low current density results techniques to improve mesoporous film adhesion and more efficient methods for quantum dot sensitization are under way. It is possible that a new substrate design, such as a core-shell nanowire array, could provide similar surface area while also providing a more direct path for QDs to diffuse during sensitizing and for electrons during device functioning. With an easily controlled bandgap, QDs have a promising future as photovoltaic sensitizers.

3.5 References

1. Grätzel, M., Recent Advances in Sensitized Mesoscopic Solar Cells. *Accounts of Chemical Research* **2009,** *42* (11), 1788-1798.
2. Grätzel, M., Dye-sensitized solar cells. *Journal of Photochemistry and Photobiology C: Photochemistry Reviews* **2003,** *4* (2), 145-153.
3. Yasuo, C.; Ashraful, I.; Yuki, W.; Ryoichi, K.; Naoki, K.; Liyuan, H., Dye-Sensitized Solar Cells with Conversion Efficiency of 11.1%. *Japanese Journal of Applied Physics* **2006,** *45* (7L), L638.
4. Ito, S.; Murakami, T. N.; Comte, P.; Liska, P.; Grätzel, C.; Nazeeruddin, M. K.; Grätzel, M., Fabrication of thin film dye sensitized solar cells with solar to electric power conversion efficiency over 10%. *Thin Solid Films* **2008,** *516* (14), 4613-4619.
5. Desilvestro, J.; Graetzel, M.; Kavan, L.; Moser, J.; Augustynski, J., Highly efficient sensitization of titanium dioxide. *Journal of the American Chemical Society* **1985,** *107* (10), 2988-2990.
6. O'Regan, B.; Gratzel, M., A low-cost, high-efficiency solar cell based on dye-sensitized colloidal TiO2 films. *Nature* **1991,** *353* (6346), 737-740.
7. Kwon, T.-H.; Armel, V.; Nattestad, A.; MacFarlane, D. R.; Bach, U.; Lind, S. J.; Gordon, K. C.; Tang, W.; Jones, D. J.; Holmes, A. B., Dithienothiophene (DTT)-Based Dyes for Dye-Sensitized Solar Cells: Synthesis of 2,6-Dibromo-DTT. *The Journal of Organic Chemistry* **2011,** *76* (10), 4088-4093.
8. Hara, K.; Tachibana, Y.; Ohga, Y.; Shinpo, A.; Suga, S.; Sayama, K.; Sugihara, H.; Arakawa, H., Dye-sensitized nanocrystalline TiO2 solar cells based on novel coumarin dyes. *Solar Energy Materials and Solar Cells* **2003,** *77* (1), 89-103.
9. Zeng, W.; Cao, Y.; Bai, Y.; Wang, Y.; Shi, Y.; Zhang, M.; Wang, F.; Pan, C.; Wang, P., Efficient Dye-Sensitized Solar Cells with an Organic Photosensitizer Featuring Orderly Conjugated Ethylenedioxythiophene and Dithienosilole Blocks. *Chemistry of Materials* **2010,** *22* (5), 1915-1925.
10. Nazeeruddin, M. K.; Péchy, P.; Renouard, T.; Zakeeruddin, S. M.; Humphry-Baker, R.; Comte, P.; Liska, P.; Cevey, L.; Costa, E.; Shklover, V.; Spiccia, L.; Deacon, G. B.; Bignozzi, C. A.; Grätzel, M., Engineering of Efficient Panchromatic Sensitizers for Nanocrystalline TiO2-Based Solar Cells. *Journal of the American Chemical Society* **2001,** *123* (8), 1613-1624.
11. Chen, C.-Y.; Wang, M.; Li, J.-Y.; Pootrakulchote, N.; Alibabaei, L.; Ngoc-le, C.-h.; Decoppet, J.-D.; Tsai, J.-H.; Grätzel, C.; Wu, C.-G.; Zakeeruddin, S. M.; Grätzel, M., Highly Efficient Light-Harvesting Ruthenium Sensitizer for Thin-Film Dye-Sensitized Solar Cells. *ACS Nano* **2009,** *3* (10), 3103-3109.
12. Hagberg, D. P.; Edvinsson, T.; Marinado, T.; Boschloo, G.; Hagfeldt, A.; Sun, L., A novel organic chromophore for dye-sensitized nanostructured solar cells. *Chemical Communications* **2006,** (21), 2245-2247.
13. Yella, A.; Lee, H.-W.; Tsao, H. N.; Yi, C.; Chandiran, A. K.; Nazeeruddin, M. K.; Diau, E. W.-G.; Yeh, C.-Y.; Zakeeruddin, S. M.; Grätzel, M., Porphyrin-Sensitized Solar Cells with Cobalt (II/III)–Based Redox Electrolyte Exceed 12 Percent Efficiency. *Science* **2011,** *334* (6056), 629-634.
14. Mai, C.-L.; Huang, W.-K.; Lu, H.-P.; Lee, C.-W.; Chiu, C.-L.; Liang, Y.-R.; Diau, E. W.-G.; Yeh, C.-Y., Synthesis and characterization of diporphyrin sensitizers for dye-sensitized solar cells. *Chemical Communications* **2010,** *46* (5), 809-811.

15. Hsieh, C.-P.; Lu, H.-P.; Chiu, C.-L.; Lee, C.-W.; Chuang, S.-H.; Mai, C.-L.; Yen, W.-N.; Hsu, S.-J.; Diau, E. W.-G.; Yeh, C.-Y., Synthesis and characterization of porphyrin sensitizers with various electron-donating substituents for highly efficient dye-sensitized solar cells. *Journal of Materials Chemistry* **2010,** *20* (6), 1127-1134.
16. Jung, H.; Koo, B.; Kim, J.-Y.; Kim, T.; Son, H. J.; Kim, B.; Kim, J. Y.; Lee, D.-K.; Kim, H.; Cho, J.; Ko, M. J., Enhanced Photovoltaic Properties and Long-Term Stability in Plasmonic Dye-Sensitized Solar Cells via Noncorrosive Redox Mediator. *ACS Applied Materials & Interfaces* **2014,** *6* (21), 19191-19200.
17. Chung, I.; Lee, B.; He, J.; Chang, R. P. H.; Kanatzidis, M. G., All-solid-state dye-sensitized solar cells with high efficiency. *Nature* **2012,** *485* (7399), 486-489.
18. Wozny, S.; Wang, K.; Zhou, W., Cu2ZnSnS4 nanoplate arrays synthesized by pulsed laser deposition with high catalytic activity as counter electrodes for dye-sensitized solar cell applications. *Journal of Materials Chemistry A* **2013,** *1* (48), 15517-15523.
19. Roy-Mayhew, J. D.; Bozym, D. J.; Punckt, C.; Aksay, I. A., Functionalized Graphene as a Catalytic Counter Electrode in Dye-Sensitized Solar Cells. *ACS Nano* **2010,** *4* (10), 6203-6211.
20. Zhang, X.; Yang, Y.; Guo, S.; Hu, F.; Liu, L., Mesoporous Ni0.85Se Nanospheres Grown in Situ on Graphene with High Performance in Dye-Sensitized Solar Cells. *ACS Applied Materials & Interfaces* **2015,** *7* (16), 8457-8464.
21. Veerappan, G.; Bojan, K.; Rhee, S.-W., Sub-micrometer-sized Graphite As a Conducting and Catalytic Counter Electrode for Dye-sensitized Solar Cells. *ACS Applied Materials & Interfaces* **2011,** *3* (3), 857-862.
22. Sahu, G.; Wang, K.; Gordon, S. W.; Zhou, W.; Tarr, M. A., Core-shell Au-TiO2 nanoarchitectures formed by pulsed laser deposition for enhanced efficiency in dye sensitized solar cells. *RSC Advances* **2012,** *2* (9), 3791-3800.
23. Ohsaki, Y.; Masaki, N.; Kitamura, T.; Wada, Y.; Okamoto, T.; Sekino, T.; Niihara, K.; Yanagida, S., Dye-sensitized TiO2 nanotube solar cells: fabrication and electronic characterization. *Physical Chemistry Chemical Physics* **2005,** *7* (24), 4157-4163.
24. Kang, T.-S.; Smith, A. P.; Taylor, B. E.; Durstock, M. F., Fabrication of Highly-Ordered TiO2 Nanotube Arrays and Their Use in Dye-Sensitized Solar Cells. *Nano Letters* **2009,** *9* (2), 601-606.
25. Martin, C. R., Membrane-Based Synthesis of Nanomaterials. *Chemistry of Materials* **1996,** *8* (8), 1739-1746.
26. Martin, C. R., Nanomaterials: A Membrane-Based Synthetic Approach. *Science* **1994,** *266* (5193), 1961-1966.
27. Wijnhoven, J. E. G. J.; Vos, W. L., Preparation of Photonic Crystals Made of Air Spheres in Titania. *Science* **1998,** *281* (5378), 802-804.
28. Hanaor, D. A. H.; Chironi, I.; Karatchevtseva, I.; Triani, G.; Sorrell, C. C., Single and mixed phase TiO2 powders prepared by excess hydrolysis of titanium alkoxide. *Advances in Applied Ceramics* **2012,** *111* (3), 149-158.
29. Lakshmi, B. B.; Dorhout, P. K.; Martin, C. R., Sol−Gel Template Synthesis of Semiconductor Nanostructures. *Chemistry of Materials* **1997,** *9* (3), 857-862.
30. Sahu, G.; Gordon, S. W.; Tarr, M. A., Synthesis and application of core-shell Au-TiO2 nanowire photoanode materials for dye sensitized solar cells. *RSC Advances* **2012,** *2* (2), 573-582.

31. Chu, S.-Z.; Wada, K.; Inoue, S.; Todoroki, S.-i., Synthesis and Characterization of Titania Nanostructures on Glass by Al Anodization and Sol−Gel Process. *Chemistry of Materials* **2002,** *14* (1), 266-272.
32. Martin, C. R., Template Synthesis of Electronically Conductive Polymer Nanostructures. *Accounts of Chemical Research* **1995,** *28* (2), 61-68.
33. Kethineedi, V. R. Synthesis and Applications of Luminescent Quantum Dots in Bioassays. University of New Orleans, Thesis and Dissertations, 2011.
34. Zhang, Q.; Zhang, Y.; Huang, S.; Huang, X.; Luo, Y.; Meng, Q.; Li, D., Application of carbon counterelectrode on CdS quantum dot-sensitized solar cells (QDSSCs). *Electrochemistry Communications* **2010,** *12* (2), 327-330.
35. Sargent, E. H., Colloidal quantum dot solar cells. *Nat Photon* **2012,** *6* (3), 133-135.
36. Islam, M. A.; Xia, Y.; Telesca, D. A.; Steigerwald, M. L.; Herman, I. P., Controlled Electrophoretic Deposition of Smooth and Robust Films of CdSe Nanocrystals. *Chemistry of Materials* **2004,** *16* (1), 49-54.
37. Song, K. W.; Costi, R.; Bulović, V., Electrophoretic Deposition of CdSe/ZnS Quantum Dots for Light-Emitting Devices. *Advanced Materials* **2013,** *25* (10), 1420-1423.
38. Yu, W. W.; Qu, L.; Guo, W.; Peng, X., Experimental Determination of the Extinction Coefficient of CdTe, CdSe, and CdS Nanocrystals. *Chemistry of Materials* **2003,** *15* (14), 2854-2860.
39. Shuqing, H.; Quanxin, Z.; Xiaoming, H.; Xiaozhi, G.; Minghui, D.; Dongmei, L.; Yanhong, L.; Qing, S.; Taro, T.; Qingbo, M., Fibrous CdS/CdSe quantum dot co-sensitized solar cells based on ordered TiO 2 nanotube arrays. *Nanotechnology* **2010,** *21* (37), 375201.
40. Sixto, G.; Iván, M.-S.; Lorena, M.; Nestor, G.; Teresa, L.-V.; Roberto, G.; Lina, J. D.; Qing, S.; Taro, T.; Juan, B., Improving the performance of colloidal quantum-dot-sensitized solar cells. *Nanotechnology* **2009,** *20* (29), 295204.
41. Etgar, L.; Moehl, T.; Gabriel, S.; Hickey, S. G.; Eychmüller, A.; Grätzel, M., Light Energy Conversion by Mesoscopic PbS Quantum Dots/TiO2 Heterojunction Solar Cells. *ACS Nano* **2012,** *6* (4), 3092-3099.
42. Greben, M.; Fucikova, A.; Valenta, J., Photoluminescence quantum yield of PbS nanocrystals in colloidal suspensions. *Journal of Applied Physics* **2015,** *117* (14), 144306.
43. Toyoda, T.; Shen, Q., Quantum-Dot-Sensitized Solar Cells: Effect of Nanostructured TiO2 Morphologies on Photovoltaic Properties. *The Journal of Physical Chemistry Letters* **2012,** *3* (14), 1885-1893.
44. Reilly, N.; Wehrung, M.; O'Dell, R. A.; Sun, L., Ultrasmall colloidal PbS quantum dots. *Materials Chemistry and Physics* **2014,** *147* (1–2), 1-4.
45. Peng, Z. A.; Peng, X., Formation of High-Quality CdTe, CdSe, and CdS Nanocrystals Using CdO as Precursor. *Journal of the American Chemical Society* **2001,** *123* (1), 183-184.
46. Braga, A.; Giménez, S.; Concina, I.; Vomiero, A.; Mora-Seró, I., Panchromatic Sensitized Solar Cells Based on Metal Sulfide Quantum Dots Grown Directly on Nanostructured TiO2 Electrodes. *The Journal of Physical Chemistry Letters* **2011,** *2* (5), 454-460.
47. Wang, X.; Koleilat, G. I.; Fischer, A.; Tang, J.; Debnath, R.; Levina, L.; Sargent, E. H., Enhanced Open-Circuit Voltage in Visible Quantum Dot Photovoltaics by Engineering of Carrier-Collecting Electrodes. *ACS Applied Materials & Interfaces* **2011,** *3* (10), 3792-3795.

Chapter 4 Schottky Devices

4.1 Introduction

With global energy demands ever increasing, so must green methods of producing it. In 1990 the world energy consumption was 350 quadrillion British thermal units (Btu). This increased to just over 400 quadrillion Btu in 2000, and is projected to exceed 800 quadrillion Btu by 2040.[1] Current power production techniques depend heavily on petroleum. With 84% of the 549.3 quadrillion Btu coming from petroleum sources in 2012 and 83% of the 575.4 quadrillion Btu in 2015.[1] While a meager decline in petroleum consumption, nuclear and other techniques saw a combined growth from 88.3 quadrillion Btu to 96.3 quadrillion Btu.[1] While promising, there is an even cleaner method of energy production that does not produce radioactive waste. Just 1 hour of energy from the sun reaching the Earth is the equivalent of 1 year of global power needs.[2] This means that with efficient solar collection, and energy storage, the global dependence on petroleum based energy could be resolved.

Schottky solar cells are assessed using current density vs. applied voltage graphs, also known as J-V curves. At the y-axis, the short-circuit current (J_{sc}) is the maximum current of the device. As a voltage is applied the curve creates a rounded box shape. The inverse slope of the top of this box is controlled by the recombination or shunt resistance (R_{sh}). Ideally this resistance is infinite preventing the recombination of electrons. The inverse slope of the side of the curve is the series resistance (R_s). This is the resistance to the electron passing through the system. Ideally this would be zero and electrons would travel freely. Where the curve intersects the x-axis is the open-circuit voltage (V_{oc}). This is the point where no more current can pass through the device. Ideally a J-V curve would be perfectly rectangular. To measure how rectangular a curve is, the ratio of the maximum power over the theoretical power is used and called the fill factor (FF). The biggest measure of performance is cell efficiency. This is ratio of the power output (electrical) over the power input (light flux). This input is standardized at 1000 W/m^2 and referred to as AM 1.5 or air mass 1.5. This represents the path length of solar light in the atmosphere over the corresponding vertical. At AM 1.5 the sun is at 48.19° from the vertical.[3] A reference J-V curve with relevant labels can be seen in Figure 4.1.

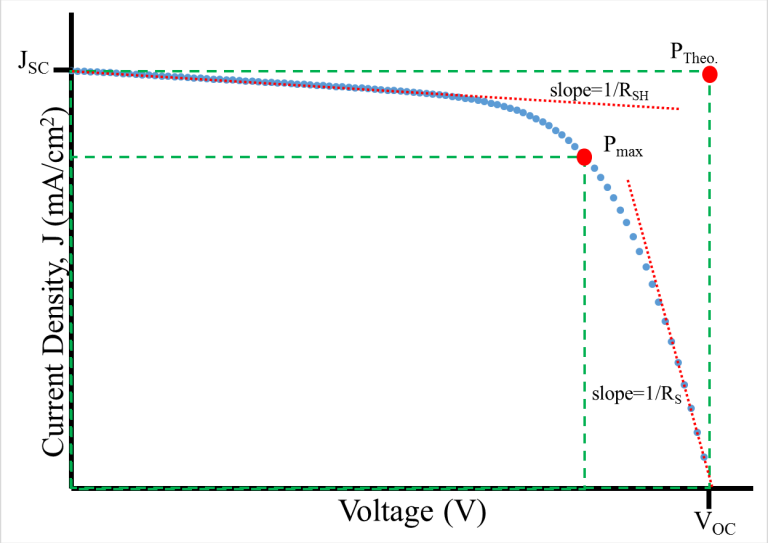

Figure 4.1 Sample J-V curve labeled with shunt resistance (R_{SH}), series resistance (R_s), maximum power (P_{max}), theoretical power ($P_{Theo.}$), short-circuit current density (J_{SC}), and open circuit voltage (V_{OC})

A very simply designed device to collect solar energy is known as a Schottky barrier solar cell. This barrier is found at the interface of a semiconductor and a metal. In a photovoltaic this barrier induces an inherent bias in the cell and causes electron-hole pairs to travel in opposite directions under illumination.[4] Since the electron-hole pairs are generated at the ohmic contact for the device, the electrons must travel the thickness of the semiconductor film to the Schottky contact.[5] This means that the electrons are more susceptible to recombination as the film thickness increases. Conversely, films that are too thin are unable to absorb light efficiently and are more likely to develop shorts during fabrication. Furthermore, the shallow work function metals ideal for these devices are readily oxidized.

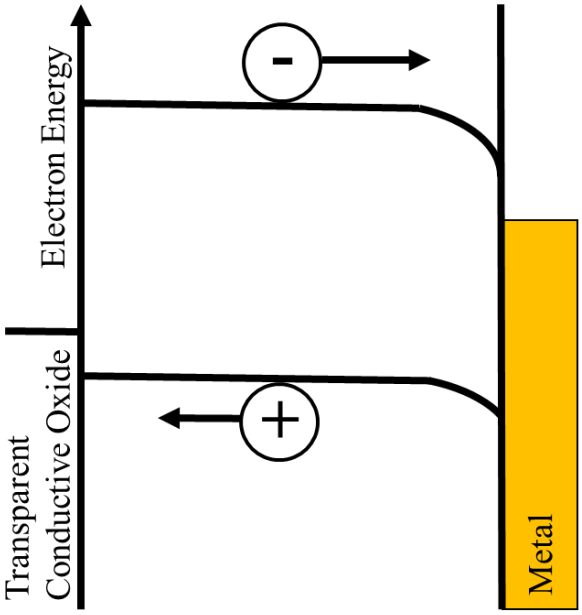

Figure 4.2 Creation of exciton in the semiconductor material of a Schottky barrier device with the positive exciton traveling towards the ohmic contact and the negative exciton traveling towards metal contact

Tang et. al studied these types of devices and ways to improve upon them.[6] While aluminum provides a device with higher V_{oc}, the efficiency of the devices declines at twelve times the rate of silver devices. This decline in cell performance was directly proportional to the rate of oxidation of the Schottky contact. Tang et. al studied the use of a stabilizing layer to prevent the oxidation of the metallic contacts. Their results showed that a thin, less than 1 nm, film of lithium fluoride (LiF), could significantly improve device efficiency and lifetime. This material had already been proposed to work by forming a dipole layer at the electrode interface[7], and shown to block the reaction of Al with an organic film.[7] After applying this technique the researchers found that aluminum contact devices had a 6-fold increase in lifetime. LiF treated devices also showed an increase in R_{SH} and decrease in R_S. While this technique did improve the device stability, the use of a fluorinated compound can be problematic. The safety data sheet (SDS) for LiF lists it as acutely toxic.[8] This ionic compound is readily soluble in water, making it an environmental hazard.

An alternate method to improve device performance would be to provide a shortened path-length for charge carriers without making the film thinner. Yu et. al used nanostructured

zinc oxide with platinum tips as Schottky diodes for gas sensing.[9] While this is not a photovoltaic application, the underlying theory is similar. The nanoscale features provided a different response than a bulk material.

With this in mind, gold nanowire arrays were studied for their potential in Schottky type solar cells using lead sulfide (PbS) quantum dots (QDs) as the semiconductor.

4.2 Experimental

4.2.1 Gold nanowire growth

Anodized aluminum oxide (AAO) membranes (Whatman 6809-7023, 13 mm diameter 200 nm pore size) were inverted onto microscope slides and attached with minimal

Scotch™ tape. Membranes were then sputtered with silver for 600s at 40 amps (Denton Vacuum Desk V). Sputtered membranes were then attached to a piece of microscope slide using double-sided copper tape (TedPella). The tape was cut down so none was exposed to the plating solution and only a small strip for electrical contact remained. Substrates were then immersed in a gold plating solution (Technic, OROTEMP ® 24 RTO RACK, 210927) with a platinum wire as a counter-electrode and a Ag/AgCl reference electrode. Wires were grown at 9 mA for varying lengths of time. After deposition the substrates were rinsed with Nanopure water, dried, and soaked in 3 M NaOH for 30-60 minutes to dissolve the membrane. After soaking, the films were rinsed with Nanopure water and dried for further use. A schematic of this process is shown in Figure 4.3 Schematic .

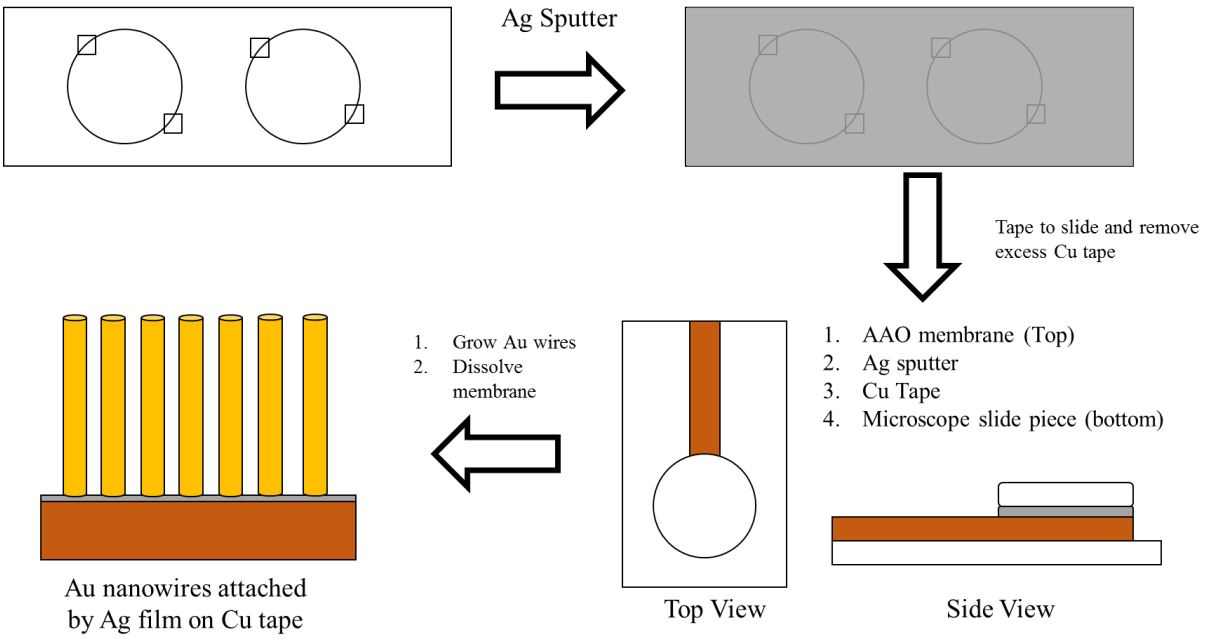

Figure 4.3 Schematic of membrane directed electrophoretic growth of metal nanowires

4.2.2 Lead sulfide quantum dot growth

PbS QDs were prepared using a modified version of a published method.[10] In a 100 mL 3-neck flask 14 g octadecene (Acros, 90% technical grade), 1.3 g oleic acid (Acros, 97%), and 450 mg lead oxide (Acros, 99.9+%) were heated to 100 °C under vacuum and vigorous stirring. After 1 hour the solution became clear and ultra-high purity argon (UHP Ar) was flushed over the reaction at a low rate (1 bubble/sec in the bubbler). The temperature was increased to 180°C. As the solution was heating 4 g octadecene and 210 µL hexamethyldisilathiane (Sigma, synthesis grade) were sealed into a conical 10 mL flask and purged with UHP Ar. After the lead solution had stabilized at 180°C the sulfur solution was rapidly injected. The mixture quickly turned from clear to black and was allowed to stir for 2 minutes. The reaction was then quenched in an ice bath to bring it to room temperature. The particles were then precipitated with acetone and separated by centrifugation at 3000 rpm for 5 minutes. The pellets were then suspended using minimal hexanes and ultra-sonication to break up larger agglomerates. These suspensions were then precipitated with acetone and centrifuged. This was done three times to remove any unreacted precursors. The PbS QDs were then suspended in hexanes at 25 mg QDs/mL.

4.2.3 Depositing QD films

4.2.3.1 Drop casting

A drop of QD suspension was added to the substrate and the hexanes allowed to evaporate. Then a 10% (v/v) solution of 3-mercaptopropionic acid (3-MPA) in methanol was deposited onto the substrate. This was then rinsed off with methanol and dried using nitrogen. This was considered one cycle of deposition. Cycles were repeated until the films were thick enough to not transmit light (approximately 20 cycles) on FTO substrates. For nanowire substrates the same number of cycles was used for uniformity of technique.

4.2.3.2 Dip coating

Clean and dry substrates were first dipped into a 10% (v/v) solution of 3-MPA in methanol. The excess was then rinsed off by pipetting methanol over the surface then drying with nitrogen. The substrates were then dipped into the QD solution. They were then similarly rinsed with hexanes and dried with nitrogen. This was considered one cycle. This was repeated for 20 cycles creating a film that is not optically transparent when deposited on FTO. The dipping angle and speed were not controlled.

4.2.3.3 Spin coating

Clean and dry substrates were placed into a spin coater (Laurell, WS-400A-6NPP/LITE). The surface was covered with a 10% (v/v) 3-MPA in methanol solution and the lid closed. The device was then spun at 2500 rpm for 10 seconds. To rinse, the substrates were spun at 2500 rpm and ~ 2 mL methanol was deposited using a Pasteur pipette then allowed to spin for ~25 seconds to dry. This was done again with QD solution and hexane. This was considered one deposition cycle. This was repeated for 20 cycles.

4.2.4 Conductive films

To produce a conductive top layer for solar devices, two approaches were used. The first was by masking the devices and sputtering (Kurt J. Lesker PVD 75) them with an indium doped tin oxide (ITO) film. For a solution processable approach, silver nanowires dispersed in isopropyl alcohol (Seashell Technologies) were deposited onto the films by drop casting or spin coating followed by an ITO nanoparticle paste. To make the ITO paste 1.0 g ITO (30-50 nm

Sigma) was sonicated in 3 mL isopropyl alcohol. Simultaneously 0.1 g poly-vinyl alcohol (Fisher) was dissolved in 4 mL Nanopure water in a separate container. The two solutions were then mixed and sonicated for 30 minutes prior to use. This produced a 30% (w/v) ITO paste. This layer was drop cast or spin coated (2500 rpm, 30 s) on top of the silver nanowire layer. Unused paste was sealed in a tube and stored in the refrigerator. It was then warmed to room temperature and sonicated for 1 hour prior to use.

4.2.5 Characterization

Absorbance was measured with a Cary 500 UV-Vis spectrometer. FESEM images were taken using a Carl Zeiss 1530 field emission scanning electron microscope (FESEM). Photovoltaic measurements were performed using a Newport® 50-500 W 67005 solar simulator set at 100 mW/cm^2. The light intensity of the xenon lamp was calibrated using a National Renewable Energy Laboratory (NREL) calibrated silicon photodiode (Hamamatsu S1787-08 for visible to IR range). Current density-voltage (J-V) curves were measured with a Keithley 2400 source meter.

4.3 Results and Discussion

Gold nanowires grown using electrodeposition were analyzed by FESEM to assess their length. Figure 4.4 shows FESEM images of two different samples grown under the optimized conditions of 9 mA for 1800 s. This long, slow process allows for uniform wires with a high level of control with respect to length. Depositing at higher current for shorter times results in the growth of weak multi-crystal chains of varied length and crystal size.

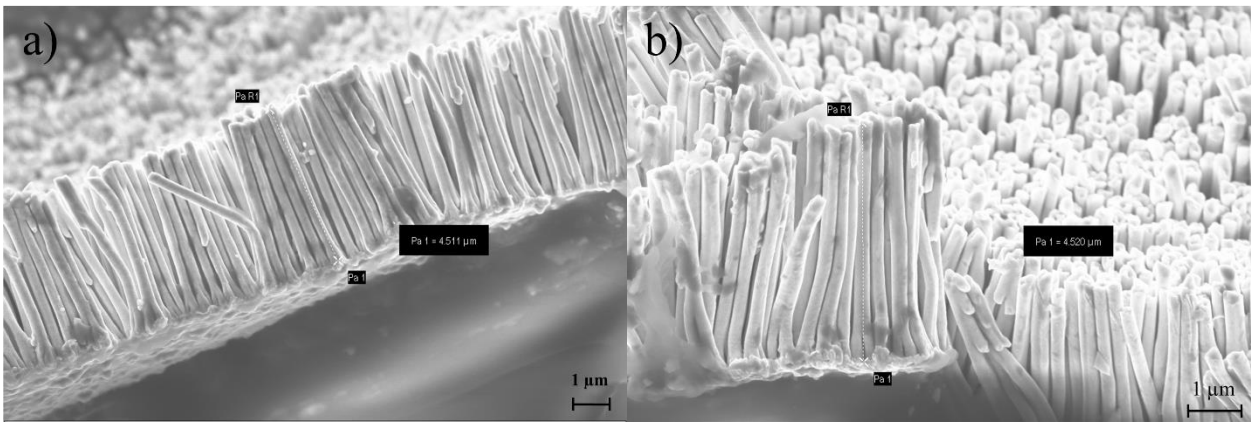

Figure 4.4 FESEM micrographs of two separate 4.5 µm gold nanowires grown under optimized conditions

It was found that if the wires were grown for only 400 seconds, metallic tubes could be grown. Their outer diameters were controlled by the walls of the template, however their inner diameters varied. In Figure 4.5 this difference can be seen within a single sample. While after sufficient deposition all samples become wires, these short deposition times all create tubes. It is thought that even after a long sputtering period the pores of the templates never fully seal with silver. So as the wires grow they begin by plating along the sputtered edges of the template creating a tube. The areas with smaller inner diameters are those with heavier deposition due to their position inside the chamber. This theory was never tested, and template imperfections could also be responsible.

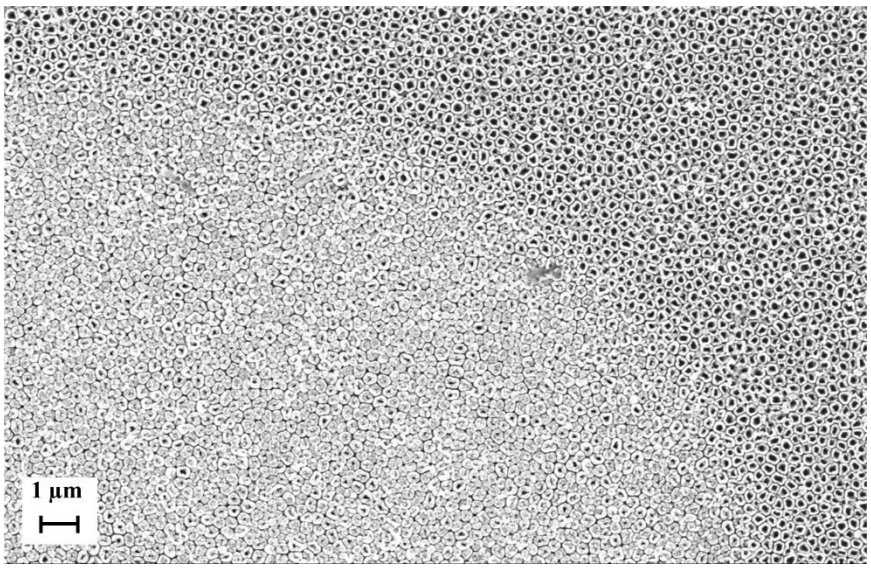

Figure 4.5 FESEM micrograph of Au nanotubes showing two distinct regions within the same sample

This theory is supported however, when comparing images from other samples. As an example, images taken of a second sample can be seen in Figure 4.6. This sample was from the same set of sputtered templates, but a different position in the instrument. The close up of the tubes in Figure 4.6 a) shows that the tubes are shaped like the original membrane all with similarly sized pores in the center. Figure 4.6 b) shows the larger area where a) was observed. All the observed areas of this sample were identically sized. This would seem to support the theory of uneven sputtering effecting the final tube size. Further studies of this phenomenon are needed for any definitive proof.

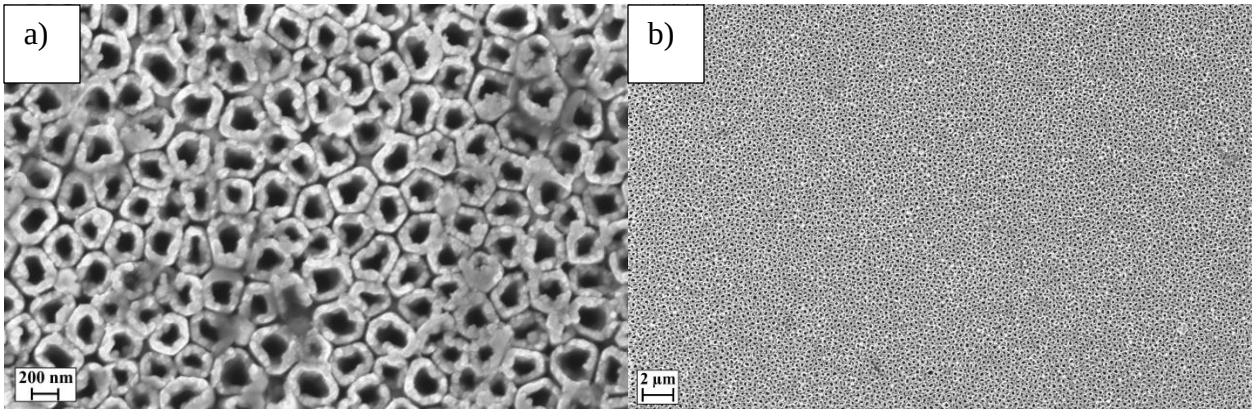

Figure 4.6 FESEM micrograph of gold nanotube (a) high magnification for size and (b) far away to show uniformity across the sample

These high surface area tubes are of interest for photovoltaic applications. The increased surface area could lead to better absorber loading and higher current densities. These do suffer from the inability to reach significant length. Any sample imaged that had reached 1 µm or longer was a fully developed wire.

Initial studies into the fabrication of these Schottky devices was performed by depositing quantum dots directly onto FTO glass. After a full deposition the glass substrates became a matte black and were not transparent to light. Figure 4.7 shows a PbS QD film deposited by spin coating. Layer a), demarked by the red highlighting bars, shows the compact PbS QD that is approximately 1 µm thick and uniform across the length of the sample. The grey area labeled b) is the support soda lime glass, and the bright line between the two areas is the thin layer of fluorine-doped tin oxide.

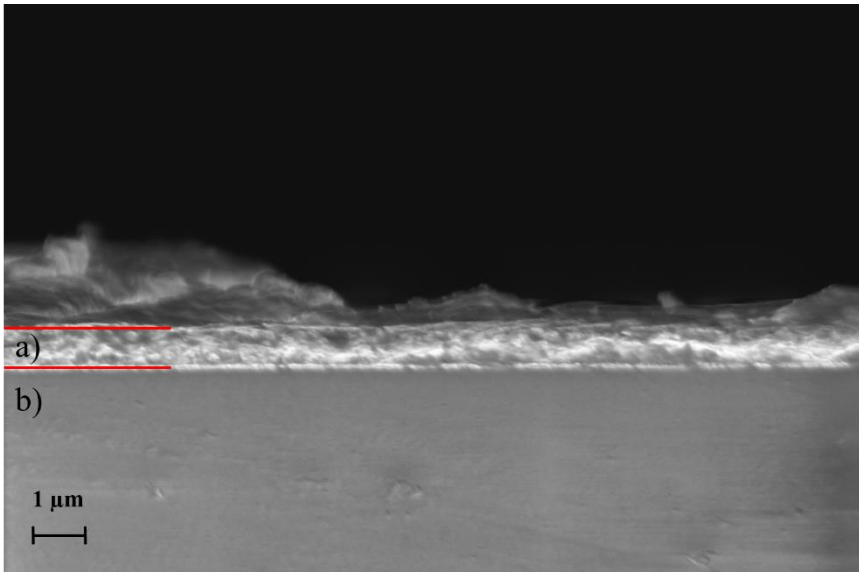

Figure 4.7 FESEM cross section of spin-coated (a) PbS QD film on (b) ITO coated glass

Films formed by dip coating are nearly identical to those formed by spin coating. This is due to the fact that both techniques deposited one layer of particles at a time. The difference is that dip coating covers all sides of the substrate. This results in the absorption of light by the QDs adsorbed to the non-conducting side of the glass. Dip coating also requires much larger volumes of solution, and has a tendency for contamination of the QD solution with 3-MPA. This leads to irreversible flocculation of the particles. However for depositing onto textures substrates, such as nanowire arrays, spin coating can deposit unevenly where dip coating can infiltrate the irregular surface. In contrast to these films, drop casting leads to very thick yet uneven films. This can be seen in Figure 4.8. The darker grey PbS film measures as thick as 10 µm in some areas, and presents holes in other areas. In theory, this technique would penetrate a nanowire array via capillary action and deposit a nice film. In practice all devices created with drop casting, whether on glass or wires, created a shorted device and had no photovoltaic activity.

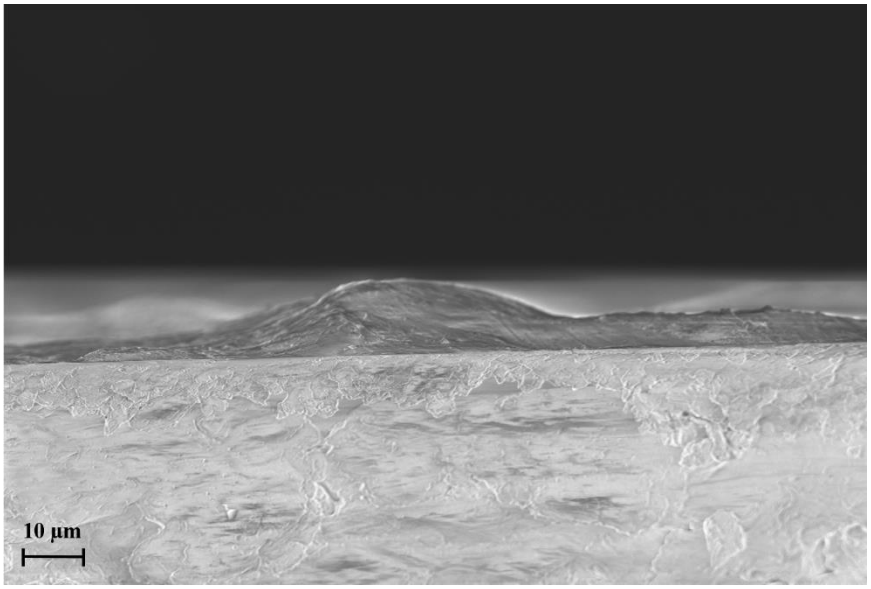

Figure 4.8FESEM cross section of drop cast PbS QD films on ITO coated glass

To test the spin coated devices, pixelated anodes of ITO (Ossila) were used as a baseline device. These substrates, along with the associated accessories, allow for creation and testing of 6 devices on one substrate. After spin coating the films the substrates were loaded into a mask and silver was thermally deposited as a back contact. Under A.M. 1.5 illumination these devices showed low photocurrent. The J-V curve for a representative device with V_{oc} of 0.314 V, J_{sc} of 0.137 mA/cm^2, fill factor of 0.25, and overall efficiency of 0.1% can be seen in Figure 4.9. None of these devices showed the expected diode behavior. The films preferentially deposited on the ITO areas while leaving the bare glass mostly devoid of particles. This uneven deposition likely exposed the edges of the ITO film and allowed for shorts to develop. The poor photovoltaic activity can also be attributed to a high level of recombination. Chang et. al found that their PbS QD/cadmium sulfide heterojunction devices had a loss of current density after the film thickness exceeded 200 nm.[11]

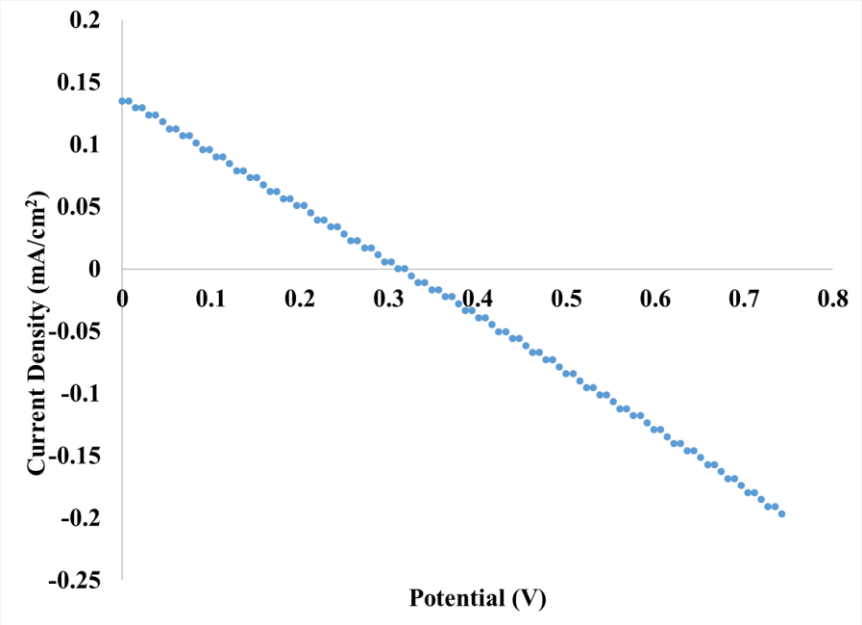

Figure 4.9 Photocurrent density vs voltage curve for representative patterned ITO device

To simulate the cell design for nanowires as a planar device, gold sputtered copper tape on a microscope slide was used. The gold was deposited for 600 s to create a thick gold layer. After deposition of the QD layer, these devices were either sputtered with an ITO layer or the Ag nanowire/ITO nanoparticle layer was deposited. After depositing the QD layer on these devices the resistance was tested in multiples places along the device to test for shorts by piercing the film at one end then touching the other probe to the surface. All films had a resistance in the megohm range before deposition of the conductive top layer. After sputtering or spin coating of the top layer, all the devices had a resistance of ~8 ohms. This loss of resistance was also seen in devices fabricated using nanowire arrays. The source of this shorting may be contact with the edges of the conductive substrate.

4.4 Conclusions

New techniques need to be studied for assembling these devices without the generation of shorts. The use of lower energy physical deposition techniques may prevent penetration of the thin devices. Current studies are underway using the physical attachment of the top contact to devices using compression. While sandwiching the PbS QD layer between the conductive oxide and support for the metal contact does not provide a high level of binding, it does make the

development of shorts nearly impossible. The use of other templates to increase inter-wire distances and possible light harvesting need to also be studied. The use of polycarbonate membranes may allow for the synthesis nanowires using aluminum. Efficiency of Schottky barrier devices could be greatly increased by using nanostructures if a method could be devised for their production.

4.5 References

1. World energy demand and economic outlook. http://www.eia.gov/outlooks/ieo/world.cfm (accessed 11-23-2016).
2. Sargent, E. H., Colloidal quantum dot solar cells. *Nat Photon* **2012,** *6* (3), 133-135.
3. Yella, A.; Lee, H.-W.; Tsao, H. N.; Yi, C.; Chandiran, A. K.; Nazeeruddin, M. K.; Diau, E. W.-G.; Yeh, C.-Y.; Zakeeruddin, S. M.; Grätzel, M., Porphyrin-Sensitized Solar Cells with Cobalt (II/III)–Based Redox Electrolyte Exceed 12 Percent Efficiency. *Science* **2011,** *334* (6056), 629-634.
4. Landsberg, P. T.; Klimpke, C., Theory of the Schottky Barrier Solar Cell. *Proceedings of the Royal Society of London. Series A, Mathematical and Physical Sciences* **1977,** *354* (1676), 101-118.
5. Pattantyus-Abraham, A. G.; Kramer, I. J.; Barkhouse, A. R.; Wang, X.; Konstantatos, G.; Debnath, R.; Levina, L.; Raabe, I.; Nazeeruddin, M. K.; Grätzel, M.; Sargent, E. H., Depleted-Heterojunction Colloidal Quantum Dot Solar Cells. *ACS Nano* **2010,** *4* (6), 3374-3380.
6. Tang, J.; Wang, X.; Brzozowski, L.; Barkhouse, D. A. R.; Debnath, R.; Levina, L.; Sargent, E. H., Schottky Quantum Dot Solar Cells Stable in Air under Solar Illumination. *Advanced Materials* **2010,** *22* (12), 1398-1402.
7. Brabec, C. J.; Shaheen, S. E.; Winder, C.; Sariciftci, N. S.; Denk, P., Effect of LiF/metal electrodes on the performance of plastic solar cells. *Applied Physics Letters* **2002,** *80* (7), 1288-1290.
8. Lithium Fluoride. http://www.sigmaaldrich.com/MSDS/MSDS/DisplayMSDSPage.do?country=US&language=en&productNumber=237965&brand=ALDRICH&PageToGoToURL=http%3A%2F%2Fwww.sigmaaldrich.com%2Fcatalog%2Fproduct%2Faldrich%2F237965%3Flang%3Den (accessed 12-4-16).
9. Yu, J.; Ippolito, S. J.; Wlodarski, W.; Strano, M.; Kalantar-zadeh, K., Nanorod based Schottky contact gas sensors in reversed bias condition. *Nanotechnology* **2010,** *21* (26), 265502.
10. Reilly, N.; Wehrung, M.; O'Dell, R. A.; Sun, L., Ultrasmall colloidal PbS quantum dots. *Materials Chemistry and Physics* **2014,** *147* (1–2), 1-4.
11. Chang, L.-Y.; Lunt, R. R.; Brown, P. R.; Bulović, V.; Bawendi, M. G., Low-Temperature Solution-Processed Solar Cells Based on PbS Colloidal Quantum Dot/CdS Heterojunctions. *Nano Letters* **2013,** *13* (3), 994-999.

Chapter 5 Depleted heterojunction solar cells

5.1 Introduction

As society's dependence on technology increases, so does it's need for electricity. Current production techniques rely heavily on fossil fuels to produce electricity. These techniques burn fuel, primarily coal, to produce steam that then turns turbines and produces electricity. This method then releases large amounts of CO_2, and other greenhouse gasses, into the atmosphere. According to the U.S. Energy Information Administration the world net electricity generation was 21.56 trillion kilowatt hours (tkWh) in 2012. Of this 14.49 tkWh, or 67.2 %, came from liquid petroleum, natural gas, and coal. While 2.34 tkWh (10.88%) came from nuclear and 4.73 tkWh (22%) came from renewables. Of the world generation only 0.1 tkWh (0.48%) came from solar.[1]

Despite the low utilization, solar energy has huge potential as a renewable replacement to petroleum products. The sun produces 120,000 terawatts or 6000 times the amount currently used globally.[2] With improved photovoltaics, and energy storage devices, the transition to fully renewable energy is a certainty. Recently, depleted heterojunction devices have been studied as a source of solar energy.[3] This structure is a sort of hybrid of sensitized solar cells and Schottky barrier devices.

A sensitized solar cell uses a mesoporous titanium dioxide (TiO_2) film and a sensitizer to absorb light. This light absorber can be an organic dye or quantum dot (QD). With both sensitizers, they are excited by a photon of light. The excited electron is then transported into the oxide layer and out of the cell to perform work. The hole is then recovered by a redox species. This redox material can either be a liquid electrolyte like I^-/I_3^-[4-5], or a solid hole transport material such as $CsSnI_3$.[6] These devices then use a catalytic counter electrode such as platinum,[4-9] graphene,[10] or copper sulfide in the case of QD sensitized devices.[11-12] These devices are robust due to the rapid charge separation cause by the injection of electrons into the TiO_2 which reduces recombination potentials

Schottky barrier devices are much simpler. They consist of a semiconductor light absorber, a Schottky contact, and an ohmic contact. At the Schottky contact the absorber and shallow work function metal create a depletion zone. The electrons are then injected into the

metal and the holes travel through the material to the ohmic contact, which is normally a transparent conductive oxide like indium tin oxide (ITO) or fluorine tin oxide (FTO) on glass. This structure does suffer from higher recombination rates since the transport medium is also the light absorbing material. To rectify this, devices are often very thin and do not maximize their light absorbing abilities.[3, 13-16]

Depleted heterojunction devices combine these two architectures. By using QDs with conduction bands above that of the oxide layer, the electrons are injected into the oxide. The holes then travel through the material, like in the Schottky devices, to a metal contact such as gold.[3, 17] By using a high surface area oxide layer, the light absorption can be maximized while using a thin layer of QD material above the film to transport holes and prevent shorting of the metal to the TiO_2. An example of bandgap alignment for a PbS sensitized depleted heterojunction device can be seen in Figure 5.1.

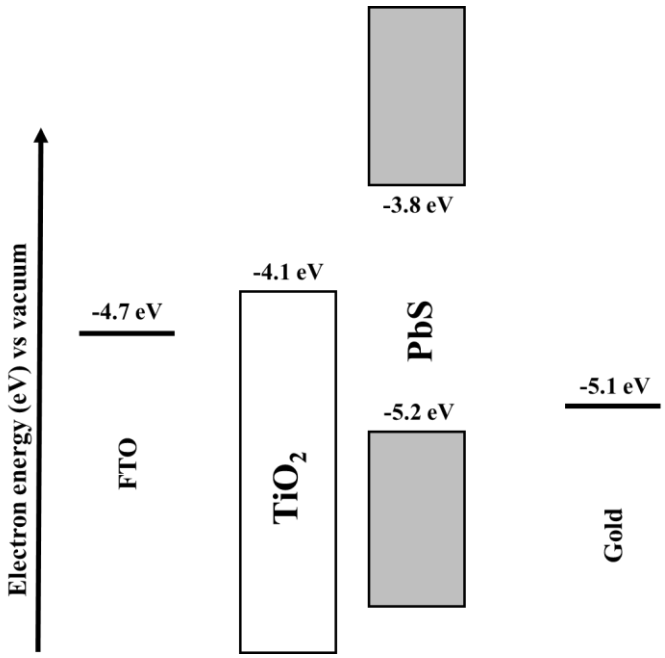

Figure 5.1 Band alignment of PbS QD depleted heterojunction devices vs vacuum.

These devices are assembled primarily using spin coating.[3, 14-18] This technique holds the substrate to a chuck often using vacuum and spins at a variable speed. The resulting thin film thickness is dependent on rotation speed and deposited solution viscosity. These techniques are

reproducible though wasteful as the bulk of the deposited material is removed from the device.[19] While this technique is efficient for flat surfaces, it cannot deposit well on textured surfaces such as nanowire arrays. To do this a technique for depositing nanoparticles using an applied field, known as electrophoretic deposition, was studied for use in these applications. Additionally, as a submersion technique little if any material is wasted. Unused QDs can be recovered, dried, and resuspended in solvent. This would not only decrease cost of fabrication, but also the environmental impact of disposing of heavy metals.

To analyze test devices, they are irradiated with A.M. 1.5 (1000 W/m^2) light and a reverse voltage is applied. The current density (J, mA/cm^2) of the device is plotted as a function of this applied voltage and a graph similar to Figure 5.2 is produced.

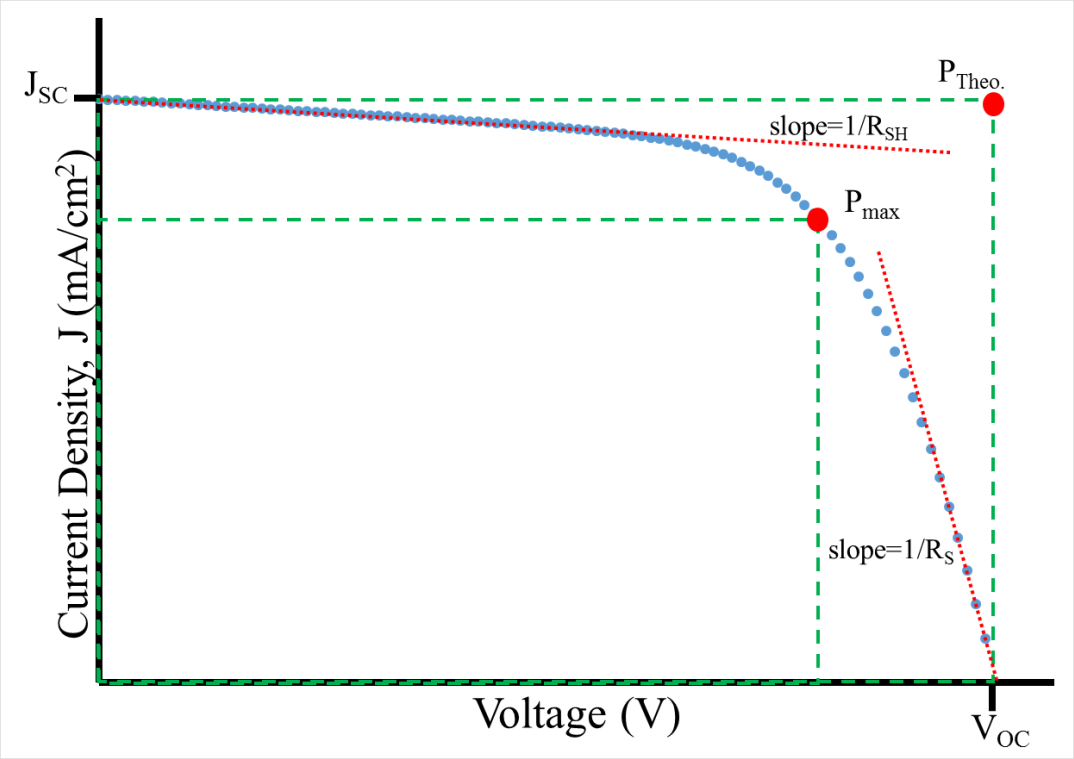

Figure 5.2 Sample J-V curve labeled with shunt resistance (R_{SH}), series resistance (R_S), maximum power (P_{max}), theoretical power ($P_{Theo.}$), short-circuit current density (J_{SC}), and open circuit voltage (V_{OC})

The current density with no applied voltage is known as the short-circuit current density (J_{SC}) and is the maximum current the device can supply. When the applied voltage is equal to the voltage of the device, and the current is therefore zero, this point is known as the open-circuit

voltage (V_{OC}) and is the maximum voltage of the device. The inverse of the slope that intersects the J_{SC} is the recombination or shunt resistance (R_{SH}). This is how resistant the electrons are to recombining with the generated holes. Under ideal conditions this resistance is infinite and the slope of the line is zero. The inverse of the slope of the line intersecting V_{OC} is the series resistance (R_S) or the device. This is the path resistance of electrons in the device. Under ideal conditions this resistance is zero and the line is perpendicular to the x-axis creating a perfect rectangle. The point of this rectangle is the theoretical power ($P_{Theo.}$) of the device. A measure of this "squareness" is known as the fill factor (FF) which is the maximum power output of the device (P_{max}) over the theoretical power. The final, and arguably most important, piece of information obtained from a J-V curve is the device efficiency. This is the P_{max}/P_{in} or the percentage of power produced from energy put in from the light source.

5.2 Experimental

5.2.1 Preparation of substrates

Pieces of either indium tin oxide (ITO, Sigma 8 Ω/sq) or fluorine tin oxide (FTO, sigma 8 Ω/sq) coated glass were cut into 1 x 2.5 cm pieces They were cleaned by submersion in a 1% Alconox solution and sonicating for 60 minutes. They were then washed with Nanopure (deionized 18 Ω/sq, 0.02 μm filtered) water and sonicated for another 60 minutes in Nanopure water to remove any remaining Alconox. Finally, the substrates were sonicated for 60 minutes in isopropyl alcohol and stored in alcohol until use.

After cleaning some substrates were dried and masked with Scotch™ tape. A small amount of zinc powder was added to the area that the ITO/FTO was to be removed and spread with minimal ethanol (195 proof, Aaper Alcohol) and the tip of a microspatula to create a film over the entire area. After the Zn films dried 1-2 drops of 1.0 M aqueous HCl (Fisher, certified ACS Plus) were added. The etching progressed for 5 minutes, was rinsed with water, then the cleaning and storing process was repeated.

For TiO_2 coated substrates, the glass pieces were dried and placed in a petri dish conductive side up. The substrates were then covered with 0.04 M $TiCl_4$ solution that was prepared by diluting pure $TiCl_4$ (Sigma) with Nanopure water at 0°C. The substrates were then

heated at 60°C for 1 hour, rinsed with Nanopure water, dried, and annealed at 500°C for 30 minutes.

ZnO coated substrates were deposited using a Kurt J. Lesker PVD 75 thin film deposition system.

5.2.2 Synthesis of 2 nm PbS QDs

In a 100 mL 3-neck flask 9,960 µL octadecene (Acros, 90% technical grade), 640 µL oleic acid (Acros, 97%) and 0.22 g lead oxide (PbO, Acros, 99,9+%) were stirred and put under vacuum. The system was set to heat from room temperature to 150 °C over 1 hour then maintained at 150 °C until the solution turned clear. As the heating started the system was flushed with ultra-high purity argon (UHP Ar) then purged three times. The system was left under flowing argon at a rate of 1 bubble every 2-3 seconds. After the solution becomes clear the temperature was reduced to 75 °C. After stabilizing 1 mL 1,2-dichloroethane was added and the solution was allowed to stir for 1 hour. During this time 6 mL octadecene was mixed with 126 µL hexamethyldisilathiane (Sigma, synthesis grade) and vacuum purged with UHP Ar then left under slowly flowing Ar for later use. After reacting for 1 hour the lead precursor solution was cooled to 50 °C. After the temperature stabilized, 5 mL of the sulfur solution was rapidly injected below the surface of the lead precursor. The solution slowly changed from clear, to light yellow, the progressively darker red until appearing a deep red or black. The reaction was then quenched in an ice bath to bring it to room temperature. The particles were precipitated with acetone and separated by centrifugation at 3000 rpm for 5 minutes. The pellets were then suspended using minimal hexanes and ultra-sonication to break up larger agglomerates. These suspensions were then precipitated with acetone and centrifuged. This was done three times to remove any unreacted precursors.

5.2.3 Synthesis of CdSe QDs.

CdSe QDs were prepared using a modified version of a previously published method.[20] In a 100 mL 3-neck flask 30 mg cadmium oxide (CdO, Sigma) and 180 mg lauric acid(Sigma). The system was connected to a condenser, the other two necks closed with septa, and the whole thing evacuated for 10 minutes. The flask was then flushed with ultra-high purity argon (UHP Ar) and the flow was adjusted so a very small flow remained (approximately 1 bubble per second). The

system was heated to 80°C and 2 g hexadecylamine (Sigma, Tech. grade 90% pure) and 2 g trioctylphosphine oxide (TOPO, Sigma, Tech. grade 90% pure) were added. The system was then purged and flushed with UHP Ar three times to remove any oxygen and returned to a slow flow of blanket UHP Ar. The system was heated to 280°C over 1 hour and stirred there until the solution turned clear. While the Cd solution was heating 80 mg selenium (Se) was dissolved in 2 mL trioctylphosphine (TOP, Sigma, Tech. grade 90% pure) and stored under flowing UHP Ar until use. Once the Cd solution was clear it was cooled to 225°C and stirred vigorously. The Se solution was then rapidly injected under the surface of the Cd solution. The mixture quickly changes color as the crystals grow. The solution was immediately quenched in an ice bath after the color began appearing (approximately 30 seconds from injection).

5.2.4 QD spin coating

Colloidal PbS QDs were suspended 25 mg/mL in hexanes. Clean and dry substrates were placed into a spin coater (Laurell, WS-400A-6NPP/LITE). The surface was covered with a 10% (v/v) 3-MPA in methanol solution and the lid closed. The device was then spun at 2500 rpm for 10 seconds. To rinse the substrates were spun at 2500 rpm and ~ 2 mL methanol was deposited using a Pasteur pipette then allowed to spin for ~25 seconds to dry. This was done again with QD solution and hexane. This was considered one deposition cycle. This was repeated for 5-20 cycles. After deposition an area of film was removed using a razor to allow for electrode placement.

5.2.5 Electrophoretic deposition of QDs

Quantum dots were suspended at 20 mg/mL in a 14% (v/v) acetonitrile in chloroform solution. This was done by first suspending the particles in the chloroform and sonicating for 5 minutes to break up agglomerated particles. The acetonitrile was then added to reach the desired ratio. Substrates were separated from a copper counter electrode using microscope slides and held together using Scotch™ tape. The area of deposition was defined by aligning the bottom of the counter electrode with the etching line of the substrate and the fill level of the beaker. The assembly was then suspended in a 10 mL beaker using a custom holder pictured in Figure 5.3. Films were deposited for 20 minutes at 400 V (1000 V/cm). After deposition, the films were rinsed with chloroform to remove free quantum dots.

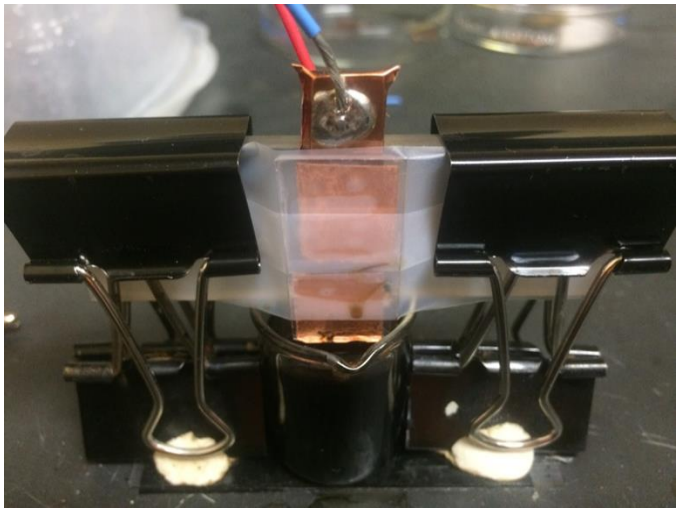

Figure 5.3 Image of custom electrophoretic deposition sample holder

5.2.6 Device assembly and testing

After deposition of the QD layer devices were masked. Silver was thermally deposited (Cressington coating system 308 R) to a thickness of 20 nm. Contacts were made using copper tape with a length of wire soldered to it. One was place on the bare FTO/ITO and the second was attached to the silver/etched area. Both were carefully positioned to avoid touching the QD film. Figure 5.4 is a cartoon diagram showing what a finished device typically looked like and areas labeled for clarity.

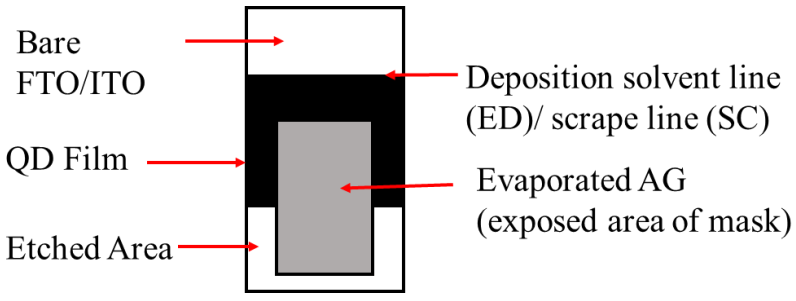

Figure 5.4 Labeled diagram of depleted heterojunction solar device

5.2.7 Characterization

Absorbance was measured with a Cary 500 UV-Vis spectrometer. Photovoltaic measurements were performed using a Newport® 50-500 W 67005 solar simulator set at 100 mW/cm^2. The light intensity of the xenon lamp was calibrated using a National Renewable Energy Laboratory (NREL) calibrated silicon photodiode (Hamamatsu S1787-08 for visible to IR range). Current density-voltage (J-V) curves were measured with a Keithley 2400 source meter.

5.3 Results and discussion

The first cell design tested used FTO substrates with a thin layer of compact TiO_2. Early devices used 5 spin coating cycles. This was to create devices that would have low transport resistance. These early devices had a high failure rate with 1 in 20 showing any photocurrent and all devices showing very low recombination resistance. To ensure that the shorts were not developing from the solution based oxide layer, 10 nm thick ZnO films were obtained from a collaborator. These films were deposited using magnetron sputtering and therefore should be even and hole free. These devices also showed similar behavior to the TiO_2 devices with only 1 in 20 showing any photo current and showing signs of short circuits. The J-V curve for the champion device for 5 cycle devices can be seen in Figure 5.5

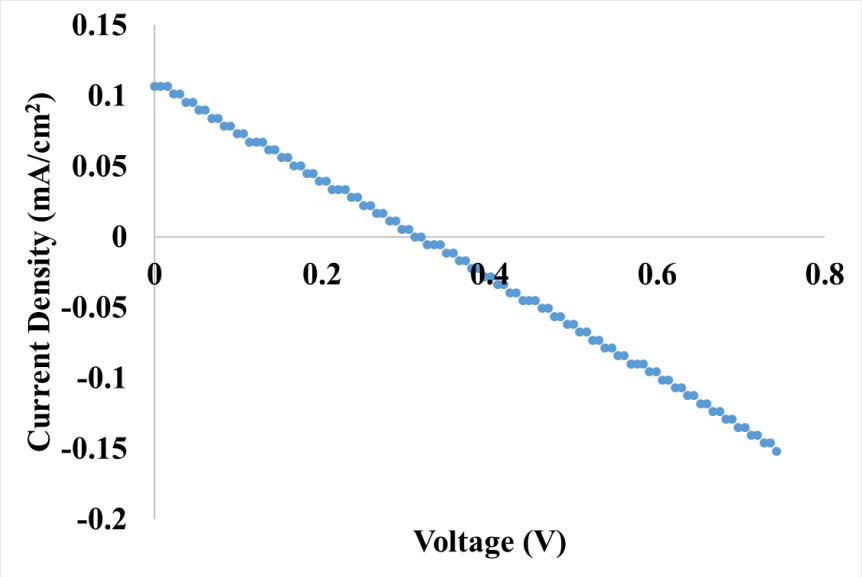

Figure 5.5 Photocurrent density vs voltage curve for best device made using 5 deposition cycles

This device had a J_{sc} of 0.11 mA/cm^2, V_{oc} of 0.32 V, a fill factor of 0.25 and overall efficiency of 0.009%. The recombination resistance in this device is very low at 3 Ω. This device was tested in the dark to see if this low resistance was due to exciton recombination, or shorts in the device and to show the current was caused by illumination. The J-V curve for the measurement can be seen in Figure 5.6

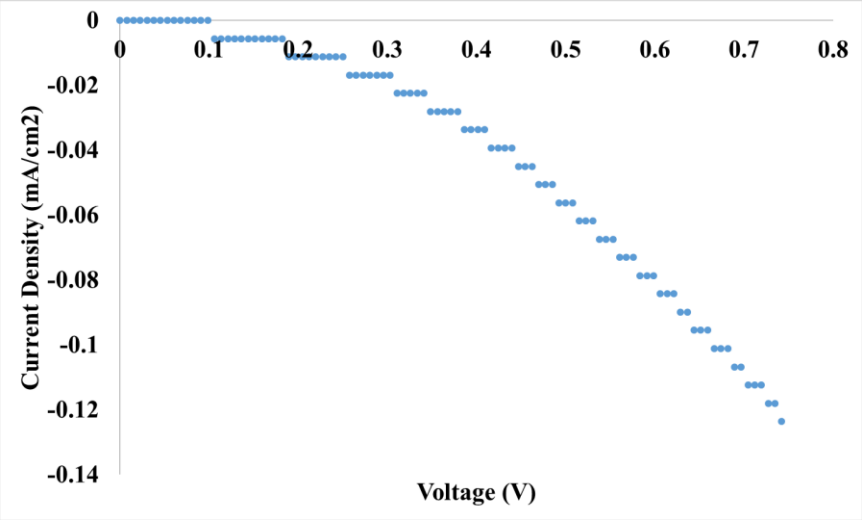

Figure 5.6 Photocurrent density vs voltage curve for 5 cycle QD deposition device in the dark

The stepped appearance is an artifact of the testing software. When the data exports very small changes are lost due to rounding of numbers after 10 decimal places. Despite this, a more diode like shape can be seen. This curve should ideally follow the x-axis until reaching the V_{oc} of the device. What the shape of this curve implies is a mixture of recombination within the film, and shorts within the device.

To correct for this behavior, the number of cycles was increased until the maximum efficiency was achieved using 20 layers. Devices with more cycles began declining in performance. The J-V curve for a device made with 20 cycles can be seen in Figure 5.7. This device had a J_{sc} of 5.54 mA/cm^2, a V_{oc} of 0.17 V, fill factor of 0.25 and efficiency of 0.23%. This is a significant increase over the 5 cycle device.

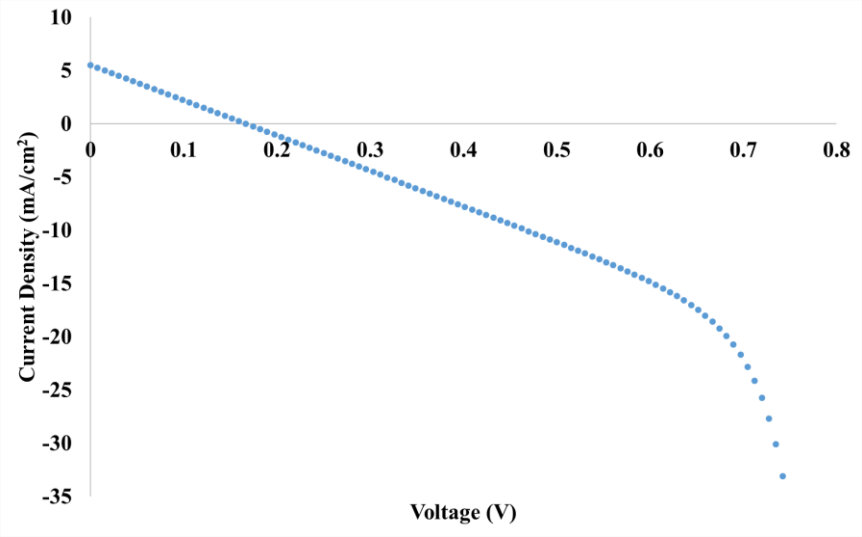

Figure 5.7 Typical photocurrent density vs voltage curve for devices with 20 cycles spin coating

These 20 cycle devices still exhibit a low shunt resistance. For the device analyzed here the R_{SH} is 6 Ω. While double that of the 5 cycle device, this is still far from ideal. To see how this is impacted by recombination, and therefore film thickness, an example device constructed using 15 layers can be seen in Figure 5.8. This device had a J_{sc} of 3.29 mA/cm^2, a V_{oc} of 0.14 V, a FF of 0.25, efficiency of 0.12% and R_{SH} of 4 Ω.

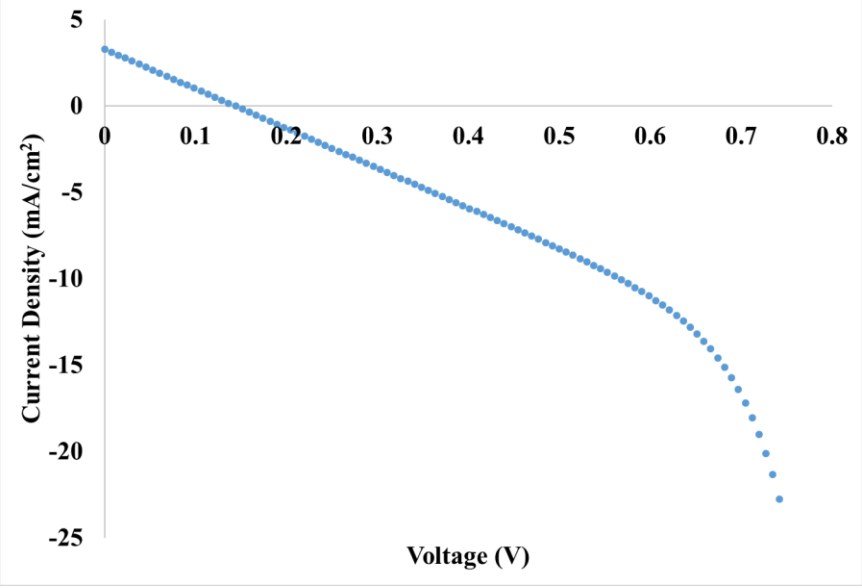

Figure 5.8 Typical photocurrent vs voltage curve for device with 15 cycles spin coating

For a point of comparison, the calibrated silicon cell used to adjust the light source was tested. As can be seen in Figure 5.9, the silicon cell has a similar current density as the QD devices, and it has an effectively infinite recombination resistance. This device had a J_{sc} of 4.4 mA/cm^2, a V_{oc} of 0.56 V, fill factor of 0.66, and efficiency of 1.65%.

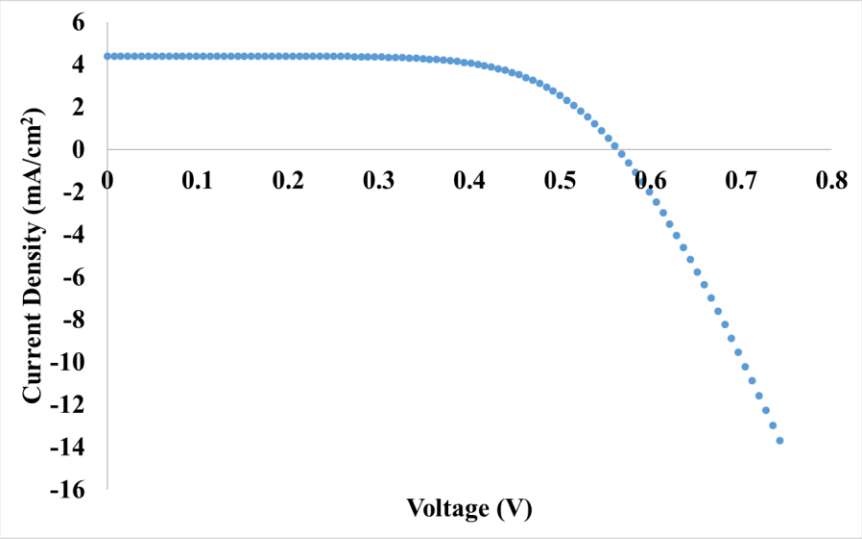

Figure 5.9 Photocurrent density vs voltage curve for calibrated silicon solar cell

These results show that a technique that produces films with no pinholes for shorting during metal deposition is needed. Using published protocols for deposition of nanoparticles into mesoporous films, a protocol was developed to create hole free films.[21-26] This method uses a high voltage to move particles through the solvent and deposit them onto the film. The deposition of the particles was dependent on particle concentration, solvent composition, electrode/substrate spacing, applied voltage, and time.

If a higher concentration of acetonitrile was used the particles flocculated created a very uneven film. Lower concentrations did not remove enough ligands to adequately charge the particles and no films grew. The window for acetonitrile concentration was found to be 14-16% (v/v) with chloroform as the major solvent. As the spacing between the substrates was increased from 1 mm (1 microscope slide) up to 1 cm (10 microscope slides), only 4 mm showed even distribution. 1-3 mm showed deposition along the sides, but the centers were clear or lightly deposited. The spacing between the plates likely slowed diffusion of particles into these smaller

spaces. At each change of distance and solvent composition the voltage was tested at 50 V increments to the maximum of the source at 400 V. No set of conditions showed any deposition below 400 V. Until these factors were set, the time of each deposition was 1 hour. This did cause a problem with evaporation of solvent so a plastic container was fashioned into a lid and a solvent soaked lab wipe was introduced into the environment to saturate the head space and reduce evaporation. After optimization, 20 minutes was used for all subsequent films. Deposition longer than 30 minutes produced rough films. Films deposited for shorter times showed no resistance when tested with a multimeter.

Films made using this technique showed diode behavior during J-V testing, however there was no detectable photocurrent. The electrophoretic deposition was applied to CdSe QDs to see if a different material would have better photovoltaic results. These attempts resulted in no deposition of particles and a darkening of the QD solution.

To begin investigating this, the fluorescence of the pristine and used QDs was measured. In Figure 5.10 the original QD solution showed the characteristic sharp emission of QDs. The additional large peak starting around 600 nm would account for the darkening of the solution after exposure to the high voltage. These changes require further study to understand why they are happening.

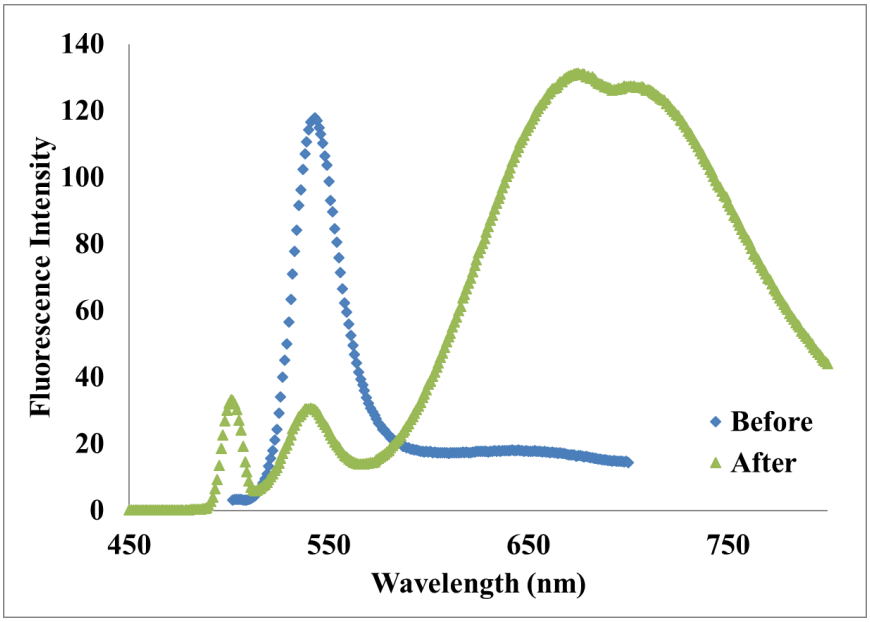

Figure 5.10 Fluorescence spectra for CdSe QD solution before (blue) with major emission at 550 nm and after deposition attempt with decreased peak at 550 nm and broad peak centered around 700 nm

Planned studies of the CdSe particles include elemental analysis of the particles to account for doping of the particles caused by the high voltage. The CdSe particles and PbS films scraped after deposition need to be analyzed by IR to account for damage and/or loss of ligands, as this could create defects in the QDs and therefore trapping sites for excitons. PbS QD films fabricated through dip coating or spin coating need to be compared to electrophoreticly deposited films using diffuse reflectance to assess any changes to absorbance from the applied electric field.

5.4 Conclusion

Depleted heterojunction thin film devices using ultra small PbS QDs have shown great potential as photovoltaic devices. The solution processable techniques presented here need to be characterized further then applied to higher surface area electrodes. These techniques, particularly electrophoretic deposition, could be applied to core-shell nanowire arrays. A substrate with this architecture would present much greater surface area for electron transfer than a thin-film design increasing current density.

5.5 References

1. World energy demand and economic outlook. http://www.eia.gov/outlooks/ieo/world.cfm (accessed 11-23-2016).
2. Grätzel, M., Recent Advances in Sensitized Mesoscopic Solar Cells. *Accounts of Chemical Research* **2009,** *42* (11), 1788-1798.
3. Pattantyus-Abraham, A. G.; Kramer, I. J.; Barkhouse, A. R.; Wang, X.; Konstantatos, G.; Debnath, R.; Levina, L.; Raabe, I.; Nazeeruddin, M. K.; Grätzel, M.; Sargent, E. H., Depleted-Heterojunction Colloidal Quantum Dot Solar Cells. *ACS Nano* **2010,** *4* (6), 3374-3380.
4. Grätzel, M., Dye-sensitized solar cells. *Journal of Photochemistry and Photobiology C: Photochemistry Reviews* **2003,** *4* (2), 145-153.
5. Yasuo, C.; Ashraful, I.; Yuki, W.; Ryoichi, K.; Naoki, K.; Liyuan, H., Dye-Sensitized Solar Cells with Conversion Efficiency of 11.1%. *Japanese Journal of Applied Physics* **2006,** *45* (7L), L638.
6. Chung, I.; Lee, B.; He, J.; Chang, R. P. H.; Kanatzidis, M. G., All-solid-state dye-sensitized solar cells with high efficiency. *Nature* **2012,** *485* (7399), 486-489.
7. Ito, S.; Murakami, T. N.; Comte, P.; Liska, P.; Grätzel, C.; Nazeeruddin, M. K.; Grätzel, M., Fabrication of thin film dye sensitized solar cells with solar to electric power conversion efficiency over 10%. *Thin Solid Films* **2008,** *516* (14), 4613-4619.
8. Desilvestro, J.; Graetzel, M.; Kavan, L.; Moser, J.; Augustynski, J., Highly efficient sensitization of titanium dioxide. *Journal of the American Chemical Society* **1985,** *107* (10), 2988-2990.
9. Yella, A.; Lee, H.-W.; Tsao, H. N.; Yi, C.; Chandiran, A. K.; Nazeeruddin, M. K.; Diau, E. W.-G.; Yeh, C.-Y.; Zakeeruddin, S. M.; Grätzel, M., Porphyrin-Sensitized Solar Cells with Cobalt (II/III)–Based Redox Electrolyte Exceed 12 Percent Efficiency. *Science* **2011,** *334* (6056), 629-634.
10. Roy-Mayhew, J. D.; Bozym, D. J.; Punckt, C.; Aksay, I. A., Functionalized Graphene as a Catalytic Counter Electrode in Dye-Sensitized Solar Cells. *ACS Nano* **2010,** *4* (10), 6203-6211.
11. Sixto, G.; Iván, M.-S.; Lorena, M.; Nestor, G.; Teresa, L.-V.; Roberto, G.; Lina, J. D.; Qing, S.; Taro, T.; Juan, B., Improving the performance of colloidal quantum-dot-sensitized solar cells. *Nanotechnology* **2009,** *20* (29), 295204.
12. Shuqing, H.; Quanxin, Z.; Xiaoming, H.; Xiaozhi, G.; Minghui, D.; Dongmei, L.; Yanhong, L.; Qing, S.; Taro, T.; Qingbo, M., Fibrous CdS/CdSe quantum dot co-sensitized solar cells based on ordered TiO 2 nanotube arrays. *Nanotechnology* **2010,** *21* (37), 375201.
13. Lithium Fluoride. http://www.sigmaaldrich.com/MSDS/MSDS/DisplayMSDSPage.do?country=US&language=en&productNumber=237965&brand=ALDRICH&PageToGoToURL=http%3A%2F%2Fwww.sigmaaldrich.com%2Fcatalog%2Fproduct%2Faldrich%2F237965%3Flang%3Den (accessed 12-4-16).
14. Yu, J.; Ippolito, S. J.; Wlodarski, W.; Strano, M.; Kalantar-zadeh, K., Nanorod based Schottky contact gas sensors in reversed bias condition. *Nanotechnology* **2010,** *21* (26), 265502.
15. Tang, J.; Wang, X.; Brzozowski, L.; Barkhouse, D. A. R.; Debnath, R.; Levina, L.; Sargent, E. H., Schottky Quantum Dot Solar Cells Stable in Air under Solar Illumination. *Advanced Materials* **2010,** *22* (12), 1398-1402.
16. Luther, J. M.; Law, M.; Beard, M. C.; Song, Q.; Reese, M. O.; Ellingson, R. J.; Nozik, A. J., Schottky Solar Cells Based on Colloidal Nanocrystal Films. *Nano Letters* **2008,** *8* (10), 3488-3492.

17. Sargent, E. H., Colloidal quantum dot solar cells. *Nat Photon* **2012,** *6* (3), 133-135.
18. Reilly, N.; Wehrung, M.; O'Dell, R. A.; Sun, L., Ultrasmall colloidal PbS quantum dots. *Materials Chemistry and Physics* **2014,** *147* (1–2), 1-4.
19. Spin Coating: A Guide to Theory and Techniques. https://www.ossila.com/pages/spin-coating#spin-coating-general-theory (accessed 12-09-2016).
20. Peng, Z. A.; Peng, X., Formation of High-Quality CdTe, CdSe, and CdS Nanocrystals Using CdO as Precursor. *Journal of the American Chemical Society* **2001,** *123* (1), 183-184.
21. Parsi Benehkohal, N.; González-Pedro, V.; Boix, P. P.; Chavhan, S.; Tena-Zaera, R.; Demopoulos, G. P.; Mora-Seró, I., Colloidal PbS and PbSeS Quantum Dot Sensitized Solar Cells Prepared by Electrophoretic Deposition. *The Journal of Physical Chemistry C* **2012,** *116* (31), 16391-16397.
22. Islam, M. A.; Xia, Y.; Telesca, D. A.; Steigerwald, M. L.; Herman, I. P., Controlled Electrophoretic Deposition of Smooth and Robust Films of CdSe Nanocrystals. *Chemistry of Materials* **2004,** *16* (1), 49-54.
23. Jin, L.; Zhao, H.; Ma, D.; Vomiero, A.; Rosei, F., Dynamics of semiconducting nanocrystal uptake into mesoporous TiO2 thick films by electrophoretic deposition. *Journal of Materials Chemistry A* **2015,** *3* (2), 847-856.
24. Song, K. W.; Costi, R.; Bulović, V., Electrophoretic Deposition of CdSe/ZnS Quantum Dots for Light-Emitting Devices. *Advanced Materials* **2013,** *25* (10), 1420-1423.
25. Cerdan-Pasaran, A.; Lopez-Luke, T.; Esparza, D.; Zarazua, I.; De la Rosa, E.; Fuentes-Ramirez, R.; Alatorre-Ordaz, A.; Sanchez-Solis, A.; Torres-Castro, A.; Zhang, J. Z., Photovoltaic properties of multilayered quantum dot/quantum rod-sensitized TiO2 solar cells fabricated by SILAR and electrophoresis. *Physical Chemistry Chemical Physics* **2015,** *17* (28), 18590-18599.
26. Halder, G.; Bhattacharyya, S., Plight of Mn Doping in Colloidal CdS Quantum Dots To Boost the Efficiency of Solar Cells. *The Journal of Physical Chemistry C* **2015,** *119* (24), 13404-13412.

Chapter 6 Concluding Remarks

As the need for electricity increases, so does the need for clean methods of production. Currently less than 20% of this production comes from renewable sources. Of those techniques, solar harvesting provides the cleanest and most widely applicable. As these technologies progress from the bulky, high-crystalline silicone first-generation devices towards the emerging photovoltaics; there is a drive to produce smaller, higher efficiency devices. To enhance these emerging photovoltaics different components of the traditional devices have been studied. This dissertation looked at nanoarchitectures to enhance both electron transport and light absorption, along with alternate light absorbers and methods for their deposition.

The first of these studies was the enhancement of dye sensitized solar cells with plasmonic nanoparticles. Dye cells are very inexpensive to make and compatible with existing mass production techniques. With the addition of gold nanoparticles, the existing absorbance spectrum of the dye was enhanced. Using particles instead of more rigid structures maintained the ability of the devices to be flexible and mass producible. This dissertation showed that using commercial particles and incorporating them into the devices before annealing maintained the gold structure and size. The plasmonic enhancement from these particles increased the efficiency of the overall device by an average of 10%. When combined with novel sensitizers and electrolyte systems, this has the potential to make commercial dye sensitized cell efficiencies competitive with the first and second-generation devices currently in use.

To further improve upon these sensitized devices this dissertation considered the use of semiconductor nanoparticles, or quantum dots, to act as photosensitizers in place of the traditional organic dyes. This study began with the growth of semiconductor films directly onto the mesoporous TiO_2 network using a SILAR deposition process. While these devices did produce photocurrent, even the best devices only had 0.5% efficiency. To improve upon this colloidal CdSe/ZnS and PbS quantum dots were synthesized using hot-injection techniques to produce size controllable nanoparticles. These were then chemically attached to the mesoporous TiO_2 substrates using 3-mercaptopropionic acid. To find a catalytic counter-electrode that was compatible with the polysulfide electrolyte, two possible substrates were tested. The first was elemental copper sheets pre-soaked in a sample of electrolyte to produce a copper sulfide film. This was then compared to a much higher surface area electrode made of a mesoporous ITO nanoparticle film with copper

sulfide deposited using a SILAR technique. Both techniques showed promise for investigation as more stable alternatives to the platinum catalyst of dye sensitized devices.

The next study performed in the dissertation was the enhancement of Schottky type thin film devices. These are typically a semiconductor material deposited on a transparent conductive oxide ohmic contact and a metal Schottky contact. These relatively simple devices balance light absorption with electron recombination. They must be thick enough to absorb light, but not so thin as to lose photocurrent due to recombination of excitons. To reduce this effect, we studied the use of a gold nanowire array as a high surface area Schottky contact. This nanoarchitecture allowed for short lateral electron transport with interwire distances of less than 10 nm, while allowing for thicker films to increase light absorption. We studied different methods of depositing PbS quantum dots onto both Au nanowires and nanotubes.

The final investigation was into methods of assembling depleted-heterojunction devices with nanoarray substrates. These depleted-heterojunction devices are a hybrid of the dye sensitized and Schottky architectures. With a mesoporous large band-gap semiconductor, like TiO_2, film on the TCO substrate acting as a Schottky contact for the quantum dot film. These devices add more of a blocking layer between the two contacts reducing short circuits and increasing the light's path length. We worked on developing an electrophoretic technique that would allow for the even deposition of quantum dots onto a nanoarray without the shadowing of more traditional deposition methods. It was shown that even ultra-small PbS QDs could be deposited under an electric field.

Overall these techniques gave us insight into the mechanics of a few of the emerging photovoltaic devices. Through further study of both the overall device architectures, and in the methods of assembly, it will be possible to produce highly efficient solar devices at a lower cost than those currently on the market.

VITA

The author was born in Indianapolis Indiana. He obtained his Bachelor's degree in chemistry from Indiana University-Purdue University Indianapolis in 2010. He then chose to pursue his PhD in materials chemistry and attended the University of New Orleans. After which he joined Dr. Matthew A. Tarr's research group in 2010.